MODELLING THE CHARACTERISTICS OF THE BARORECEPTOR

A dissertation submitted to the Faculty of Engineering and the Built Environment, University of Witwatersrand in fulfilment of the requirements for the degree of Master of Science in Engineering.

Kirsten Taneall Smith

October, 2017

Declaration

I declare that this research is my own unaided work. It is being submitted for the Degree of Master of Science in Engineering at the University of the Witwatersrand, Johannesburg. It has not been submitted for any degree or examination to any other University.

……..

Signature

…….... day of …… year …….

Abstract

The baroreceptor is a stretch receptor which detects changes in pressure in arterial blood vessels. Baroreceptor nerves inform the brainstem of changes in blood pressure, which then influences sympathetic and parasympathetic nervous activity to counteract that change. Due to the relationship between essential hypertension, sympathetic nervous activity and the baroreflex, there is some debate in the literature about whether the baroreflex can act as a long-term controller of blood pressure. This debate has increased in recent years, due to the high prevalence of essential hypertension in all societies and the introduction of new technologies to counteract drug-resistance hypertension. The baroreflex has become a source of debate due to the complex physiological feedback control that regulates blood pressure and due to new stimulating electrical devices, which have shown promising results in reducing drug-resistant essential hypertension.

This investigation studies the baroreceptor's role as a sensor in a physiological feedback control system. This is done through a literature survey extending through experimental and modelling research, where selected mathematical models of the baroreceptor are then analysed and simulated to find the best performing model, so that they may be simulated for an extended frequency response than what would be experimentally possible. The purpose of this investigation is to determine, through simulation, what the sensor's static and dynamic characteristics are. Through this characterisation of the sensor behaviour of the baroreceptor in the baroreflex control loop, it is then possible to infer whether the baroreflex can act as a long-term controller of blood pressure.

An overview of experimental and analytical investigations on the baroreceptor over the last 70 years is summarised. This overview includes mathematical models, which predict experimental results. A subset of four models from Srinivasen et al., Bugenhagen et al., Beard et al. and Mahdi et al. are selected. These models are implemented in MATLAB and Simulink. The parameters and experimental conditions are integrated into the Simulink models, and the simulated results are compared to the reported experimental data. In this way, each mathematical model is evaluated using secondary data for its ability to simulate the expected behaviour. Thereafter, all simulated models are compared under the same input conditions (a 0-230 mmHg step input over 12 s). These results are used to select the best performing models, based on how well they were parameterised and validated for experimental tests. The best performing models are those of Beard et al. and Bugenhagen et al. They are tested for a wide range of artificial inputs at different frequencies, with sinusoidal inputs which have periods that range from 0.1 s to 10 days and have a 100 mmHg operating point with a 1 mmHg peak amplitude.

All modelling techniques studied show that the baroreceptor firing response resets due to the rate of change in strain in the visco-elastic arterial wall. Both tested model frequency responses, although parameterised for different species and for different major vessels, show high sensitivity to inputs in

the range from 1 s to 1 min 36 s (0.01 Hz – 1Hz), and very low sensitivity for changes that are longer than 16 min 36s (0.001 Hz). This extrapolated simulation suggests a zero gain near DC.

The simulated frequency response of the best performing baroreceptor models, which were validated against short-term experimental data, indicate that the baroreceptor is only able to sense changes that happen in less than 1 min 16s. The critical analysis of all the simulated baroreceptor models show that this characteristic of the baroreceptor is caused by the visco-elastic layers of the arterial wall, and is likely in all baroreceptors regardless of type or species. It also indicates that under electrical stimulation of the baroreceptor, the input signal from the electrical device bypasses the baroreceptor nerve ending (which is embedded in the arterial wall) and that the electrical signal of the baroreceptor is bypassed by the new stimulated electrical signal of the device. Furthermore, if the sensor can only detect short-term changes, then it is unlikely that the baroreceptor can inform the brainstem on long-term changes to mean arterial blood pressure. Therefore, based on the models examined in this study, this suggests that the baroreceptor is unlikely to be involved in long-term blood pressure control. This analysis of the best performing model is presented to show the limitations of the baroreflex in long term control of blood pressure. It serves as a simulated experiment to rationalise the contentious debate around the role of the baroreflex in long term blood pressure control, and to allow for future improvements that can be made on the baroreceptor model to allow for more extended modelling on the baroreceptor's sensor characteristics. An improvement that could be applied to the best performing baroreceptor models, implemented in this study, is to examine the effects of ageing and inter-species variability on carotid sinus dimensions and visco-elastic wall properties.

Acknowledgements

I would like to thank my supervisors, Martin Turner and David Rubin, for the conception of this work and their invaluable support. I would also like to thank them for their commitment to providing sound advice, feedback, and constant motivation.

I would also like to thank Opti-Num Solutions for their support and funding of this research, for the MathWorks tools to work with, as well as for the time they let me use at the office. I would like to extend my gratitude to Grant Grobbelaar and Gareth Shaw for their encouragement and ongoing support when my attention was divided at work. A special thanks to Grant, for answering so many questions and helping me get the most value from the tools.

Thank you to my husband Craig Smith for the unfailing support during my studies, for the many cups of tea, and for helping me reach my goals. Thank you to all of my family and friends for providing support, enthusiasm and encouragement throughout the course of my studies.

Finally, many thanks to Daniel Beard from the Department of Molecular and Integrative Physiology at the University of Michigan, Ann Arbor, for providing supporting insight, MATLAB models and data from his research team's mathematical model experiments.

TABLE OF CONTENTS

Declaration i

Abstract ii

Acknowledgements iv

List of Abbreviations vii

List of Figures viii

List of Tables xi

List of Symbols xii

1 Introduction and Background 1

1.1 Background 1

1.2 The Problem 4

1.3 Objectives 4

1.4 Approach 5

1.5 Overview of this Dissertation 5

2 Critical Review of Existing Models 7

2.1 Overview 7

3 Implementation and Analysis of Existing Models 23

3.1 The King Pressure-Strain Model for Arterial Walls 23

3.1.1 Model Context 23

3.1.2 Model Equations and Description 23

3.2 The Srinivasen and Nudelman Baroreceptor Model 24

3.2.1 Model Context 24

3.2.2 Model Equations and Description 24

3.2.3 Model Behaviour Compared with Published Data 28

3.3 Bugenhagen et al. Baroreceptor Model 30

3.3.1 Model Context 30

3.3.2 Model Equations and Description 31

3.3.3 Model Behaviour Compared with Published Data 35
3.4 Beard et al. Baroreceptor Model 37
3.4.1 Model Context 37
3.4.2 Model Equations and Description 38
3.4.3 Model Behaviour Compared with Published Data 41
3.5 Mahdi et al. Baroreceptor Model 46
3.5.1 Model Context 46
3.5.2 Model Equations and Description 47
3.5.3 Model Behaviour Compared with Published Data 52
4 Critical Comparison of Models 56
4.1 Model Feature Comparison 56
4.1.1 Arterial Wall Strain 56
4.1.2 Voigt Body Arterial Wall Mechanics 58
4.1.3 Signal Transmission and Firing Response 64
4.2 Frequency Response 68
4.2.1 Model Selection 68
4.2.2 Simulation Methodology 69
4.2.3 Simulation Test Results 71
5 Key Findings and Considerations for the Role of the Baroreceptor 75
5.1 Key Findings for the Role of the Baroreceptor 75
5.2 Further Considerations for the Role of the Baroreceptor 76
5.2.1 Carotid Sinus Distensibility 76
5.2.2 Age-Related Effects 77
6 Discussion and Conclusion 79
7 References 85
A. Appendix A 90
B. Appendix B 99
C. Appendix C 102

List of Abbreviations

BP	Blood Pressure
SBP	Systolic Blood Pressure
DBP	Diastolic Blood Pressure
SNA	Sympathetic Nervous Activity
SNS	Sympathetic Nervous System
PNS	Parasympathetic Nervous System
BR	Baroreceptor
BRs	Baroreceptors
CNS	Central Nervous System
SA	Sino-Atrial
BRX	Baroreflex
MAP	Mean Arterial Pressure
CS	Carotid Sinus
SAD	Sino-Atrial Denervated
PED	Post-Excitatory Depression
FBR	Baroreceptor Firing Rate
NIF	Leaky Integrate-And-Fire Model
NA	Simplified Amplifier Model
DC	Direct Current
BV	Blood Volume

List of Figures

Figure 1.1: Illustration of baroreflex pathways from the baroreceptors to the central nervous system, and from the central nervous system to target organs for regulation of arterial blood pressure. Adapted from Hirooka [19] 3

Figure 2.1: Block diagram describing the generic functional components used to model the baroreceptor. Adapted from Mahdi [2] 11

Figure 2.2: Illustration to show how pressure forces at the arterial wall through the visco-elastic layers of the arterial wll, can be described using spring-damper networks (or Voigt bodies). Adapted from Mahdi [35] 14

Figure 2.3: Illustrated dynamic Barorceptor model to further describe how spring-damper networks model strain, Adapted from Bugenhagen [22] 18

Figure 3.1: Schematic outline of subsystems in the Srinivasen and Nudelman baroreceptor model [27]..... 26

Figure 3.2: Conventional block diagram representing Srinivasen et al. baroreceptor model [27] 27

Figure 3.3: Simulink modelled states based on input pressure (A), static arterial strain (B), dynamic strain (C) and combined membrane strain (D) generated by Simulink implementation of the Srinivasen and Nudelman baroreceptor model [27] 29

Figure 3.4: Comparison between experimental and reported firing responses generated by Simulink implementation of the Srinivasen and Nudelman baroreceptor model [27] 30

Figure 3.5: Bugenhagen et al. baroreceptor model with model components shown as subsystems 33

Figure 3.6: Conventional block diagram representing the Bugenhagen et al. baroreceptor model [22]..... 34

Figure 3.7: Simulink modelled states based on input pressure (A), static arterial strain (B), dynamic strain (C) and combined membrane strain (D) with $K1(optimised)$. 36

Figure 3.8: Comparison between firing responses simulated in this study, and published experimental and simulated data (Bugenhagen et al. [22]). Model parameters as in Table 3.3 36

Figure 3.9: Comparison between firing responses simulated in this study, and published experimental and simulated data (Bugenhagen et al. [22]). Model parameters as in Table 3.3 (Optimised $K1$) 37

Figure 3.10: Beard et al. baroreceptor model with model components shown as subsystems [14] 39

Figure 3.11: Conventional block diagram representing the Beard et al. baroreceptor model [14] 40

Figure 3.12: Simulink modelled states based on pressure (A), for differential input pressure (B), total membrane strain (C) and baroreceptor afferent fibre activity (D) 42

Figure 3.13: Comparison of experimental firing from Chapleau et al. [43], reported firing from Beard et al. [14] and simulated firing following a step change of pressure. 43

Figure 3.14: Aortic volume step infusion for Guyton et al. [45] experiment 44

Figure 3.15 Firing Rates calculated by the Beard et al. MATLAB model and the Simulink model of the present study. 44

Figure 3.16: Aortic volume changes during the Quail et al. haemorrhage experiment [46] 45

Figure 3.17: Firing Rates calculated by the Beard et al. MATLAB model and the Simulink model of the present study. 46
Figure 3.18: Mahdi et al. baroreceptor model with model components shown as subsystems [2]. 50
Figure 3.19: Conventional block diagram representing the Mahdi et al. baroreceptor model [2]. 51
Figure 3.20: Firing response results for the square pulse input experiment for Mahdi et al. simplified-amplifier model. 53
Figure 3.21: Scaled and shifted firing response results for the square pulse input experiment for Mahdi et al. simplified-amplifier model. 55
Figure 4.1: Comparison of static wall strain model responses for a non-pulsatile step input pressure 57
Figure 4.2: Comparison of static wall strain model responses for a pulsatile step input pressure 58
Figure 4.3: Simulink results for the Srinivasen et al. strain model, based on a 230 mmHg step input Pressure (A), Static strain (B), Dynamic strain (C) and total strain at baroreceptor membrane (D). 60
Figure 4.4: Simulink results for the Bugenhagen et al. strain model, based on a 230 mmHg step input Pressure (A), Static wall strain (B), Dynamic strain (C) and total strain at baroreceptor membrane (D). 60
Figure 4.5: Results from simulation of the Beard et al baroreceptor model, based on a pulsatile step input pressure. 62
Figure 4.6: Results from simulation of the Mahdi et al baroreceptor model, based on a pulsatile step input pressure. 63
Figure 4.7: Step input firing rates for different baroreceptor modelling techniques 66
Figure 4.8: Pulsatile step input firing rates for different baroreceptor modelling techniques 66
Figure 4.9: Step input firing rates for different baroreceptor modelling techniques, as compared with experimental data from Bugenhagen et al. [22] 67
Figure 4.10: Example of input sinusoidal pressure used to test frequency response 70
Figure 4.11: Input to Output Comparison for the Beard et al. model at Test Frequency 100 Hz, with portion of the last 0.04 s of the signals highlighted to show their sinusoidal nature 71
Figure 4.12: Frequency Response for the Beard et al. Baroreceptor Model [14]. 72
Figure 4.13: Frequency Response for the Bugenhagen et al. Baroreceptor Model [22] 73
Figure C.7.1: Simulink block diagram representing Srinivasen et al Baroreceptor Model. 102
Figure C.7.2: Simulink block diagram representing Bugenhagen et al arterial wall strain model. 103
Figure C.7.3: Simulink block diagram representing Bugenhagen et al dynamic strain model. 104
Figure C.7.4: Simulink block diagram representing Bugenhagen et al simplified integrate-and-fire model. 105
Figure C.7.5: Simulink block diagram representing Vessel Mechanics Subsystem for the Beard et al Baroreceptor Model. 106
Figure C.7.6: Simulink block diagram representing Strain Dynamics Subsystem for the Beard et al Baroreceptor Model. 106
Figure C.7.7: Simulink block diagram representing Afferent Nerve Fibre Recruitment Subsystem for the Beard et al Baroreceptor Model. 107

Figure C.7.8: Simulink block diagram representing Firing Response Subsystem for the Beard et al Baroreceptor Model..... 107
Figure C.7.9: Simulink Block Diagram representing Arterial Wall Subsystem for the Mahdi et al. Baroreceptor Model. 108
Figure C.7.10: Simulink Block Diagram representing Strain Dynamics Subsystem for the Mahdi et al. Baroreceptor Model..... 108
Figure C.7.11: Simulink Block Diagram representing Simplified Amplifier Response Subsystem for the Mahdi et al. Baroreceptor Model. 109
Figure C.7.12: Simulink Block Diagram representing Leaky Integrate-and-Fire Response Subsystem for the Mahdi et al. Baroreceptor Model. 109

List of Tables

Table 2.1: Summary for historical overview of baroreceptor research 8

Table 3.1: Experimental and calculated values for human aortas of different ages [24]. 24

Table 3.2: Parameter-Value pairs for Step Input (46 – 202 mmHg) Pressure Experiment [27] 28

Table 3.3: Parameters for Step Input (0 – 230 mmHg) Pressure Experiment..... 35

Table 3.4: Parameters used to simulate the experiment of Chapleau et al. [14]..... 41

Table 3.5: Initial conditions required to model the Chapleau et al experiment 42

Table 3.6: Parameters as per Table 6 for Figure 8 of the Mahdi et al. paper [2]..... 52

Table A.1: Historical Overview of Baroreceptor Research 90

List of Symbols

Srinivasen et al. Model Symbols

r_0	Unconstrained radius
A_r	Factor dependent on the arterial wall thickness
β	Factor for the unconstrained surface area of a cylinder
ε	Static arterial wall strain
P	Input pressure
A	Resting mean pressure
ε_d	Dynamic wall strain
ε	The static wall strain
δ	Membrane strain
x	Transduced membrane signal
y	Nerve discharge signal,
δ_{th}	Membrain strain threshold
C_D	Dynamic viscosity coefficient
C	Viscosity coefficient
τ	Time constant

Bugenhagen et al. Model Symbols

ε_{wall}	Arterial wall strain
P	Pressure
C_{wall}	Wall compliance
R_0	Unstressed aorta radius
B_{wall}	Viscosity of the artery wall
$\varepsilon_1, \varepsilon_2, \varepsilon_3$	Strain elements

K_1, K_2, K_3	Elastic constants
B_1, B_2, B_3	Viscous constants
K_{ne}	Elasticity of the baroreceptor nerve ending
δ	Dynamic strain
n	Firing response
δ_{th}	Baroreceptor threshold strain
S	Strain sensitivity
ζ	Jump frequency parameter
$K_{1(optimised)}$	Optimised elasticity constant

Beard et al. Model Symbols

V_{Ao}	Aortic volume
C_{Ao}	Aortic compliance
V_{SAo}	Creep stress volume of the aorta
τ_{CAo}	Time constant of stress relaxation
$V_{SAo}{}^{\infty}$	Long-term/chronic creep stress volume
γ_{Ao}	Ratio of the acute to the effective long-term compliance factor
δ_{ε}	Strain at the baroreceptor nerve ending
ε	Strain at the arterial wall
V_0	Unstressed volume
$\dot{\bar{\varepsilon}}$	Average rate of change in strain
τ_s	Time constant
s	Fraction baroreceptor afferent fibres in an active state for discharge
a	Adjustable parameter
b	Adjustable parameter

d_0	Unstressed diameter
f_0	Resting firing rate

Mahdi et al. Model Symbols

A	Area of the artery
A_0	Unstressed area
A_m	Maximum area
α	Saturation pressure
k	Vessel distensibility
p	Pressure
α_1, α_2, and α_3	Nerve ending constants
β_1, β_2, and β_3	Nerve ending relaxation rates
ε_w	Strain directly applied to the inner side of the wall
$\varepsilon_1, \varepsilon_2, \varepsilon_3$	Tissue strain between arterial wall and nerve ending membrane
ε_{ne}	Strain at the nerve ending
f_{N_a}	Frequency of the baroreceptor firing rate for simplified-amplifier model
s_1	Constant for a baroreceptor gain
s_2	Baroreceptor shift
g_{leak}	Leakage conductance of the membrane
V_{th}	Threshold voltage
$\bar{s_1}$	Constant for gain of the stimulus
$\bar{s_2}$	Constant for shift of the stimulus
V_m	Voltage in the membrane
I_{ne}	Generated current

C_m	Capacitance of the membrane
$f_{N_{IF}}$	Frequency of the BR firing rate of the action potential for leaky integrate-and-fire model
t_{ref}	Time taken for the membrane voltage to discharge and to recover
$W_{ne}V_2N_a$	Non-linear elastic arterial wall, two-Voigt body, simplified amplifier model
$W_{ne}V_2N_{IF}$	Non-linear elastic arterial wall, two-Voigt body, integrate and fire model
$W_eV_2N_a$	Elastic arterial wall, two-Voigt body, simplified amplifier model

1 Introduction and Background

In healthy individuals “normal” resting systolic and diastolic arterial blood pressures (SBP and DBP) are usually considered to be 100–120 and 60–80 mm Hg respectively [1], although both SBP and DBP vary substantially both within and between individuals [1]. Hypertension, in which an individual’s usual blood pressure (BP) is above normal, is associated with increased risk of stroke and other cardiovascular diseases [2]. Hypertension that has no identifiable cause is termed “essential hypertension”. Many researchers suggest that increased sympathetic nervous activity (SNA) may play a role in essential hypertension [2], [3]. One mechanism which increases SNA is the baroreflex, which has been shown to adapt its firing rate to long-term stimuli [4].The baroreflex is a physiological feedback system which contributes to BP regulation [3]. The baroreceptors (BRs), which are transducers in the baroreflex, are stretch receptors that detect changes in arterial BP through deformation of the arterial wall [3]. Due to the relationships between essential hypertension, sympathetic nervous activity, and the baroreflex, baroreceptors have come under recent investigation [5]. Baroreceptors have been proven experimentally in a wide range of investigations to sense short-term changes in BP but not respond well to long-term changes (ten minutes or longer [5]) a behaviour termed adaptation or resetting [4], [6]–[11].

Baroreflex adaptation or resetting is evident in animals and humans, including patients with essential hypertension [3], [4], [12]. There is some disagreement in the literature as to whether adaptation occurs in the brainstem, or in the baroreceptor itself which, under prolonged increased strain, adapts its tonic firing rate to the new strain reference, or whether adaptation is related to the visco-elastic properties of the arterial wall [5], [9], [13]–[15].

1.1 Background

Compliant arterial blood vessels create resistance to the pulsatile flow of blood, and generate BP. Pressure in the arterial vessels is maintained through neuro-humoral mechanisms which vary the intravascular fluid volume and cardiac output, as well as the compliance and resistance of the vessels [16]. The pressure is maintained for delivery of nutrients to all parts of the body, and for the removal of metabolic waste products.

Sympathetic nerve activity is maintained by the central nervous system through the cardio-pulmonary centres and other regulatory centres in the thoracolumbar spinal cord [17]. These cardio-pulmonary centres are influenced by the baroreceptor (BR) afferent nerves that transmit BR responses. The BRs are stretch receptors embedded in the compliant walls of the carotid artery and aorta. They transmit information associated with changes in arterial pressure to the central nervous system (CNS) [2]. These stretch receptors are nerve fibres that generate an electrical signal (action potential) at a firing

rate that increases with increasing pressure and rate of change of pressure across the arterial wall [18]. [3]. The firing rate is relayed to the medulla oblongata in the brainstem (cardio-regulatory and vasomotor centres), where under normal resting conditions it inhibits the sympathetic nervous system [3]. [19], [20].

The baroreflex is made up of two arcs, namely the neural and the peripheral arc [2]. The neural arc transmits baroreceptor firing rate to the cardio-pulmonary centres in the brainstem [2]. The peripheral arc transmits sympathetic nervous activity to target organs and tissues to regulate BP based on changes in SNA [2].

Increased firing rate of baroreceptors is translated in the brainstem, and leads to a decreased stimulation of the sympathetic nervous system (SNS) and an increased stimulation of the parasympathetic nervous system (PNS) [20]. Decreased SNS activity reduces BP through vasodilation, decreasing heart rate and stroke volume, and also reduces production of renin which increases excretion of sodium by the kidneys [19], [20]. This is the peripheral arc of the baroreflex. Decreased baroreceptor firing rate results in an increase in sympathetic nervous activity, and a decrease in vagal tone at the sino-atrial (SA) node, so that heart rate is increased [19], [20]. The interaction between these different nervous systems and their target organs, is summarised in Figure 1.1.

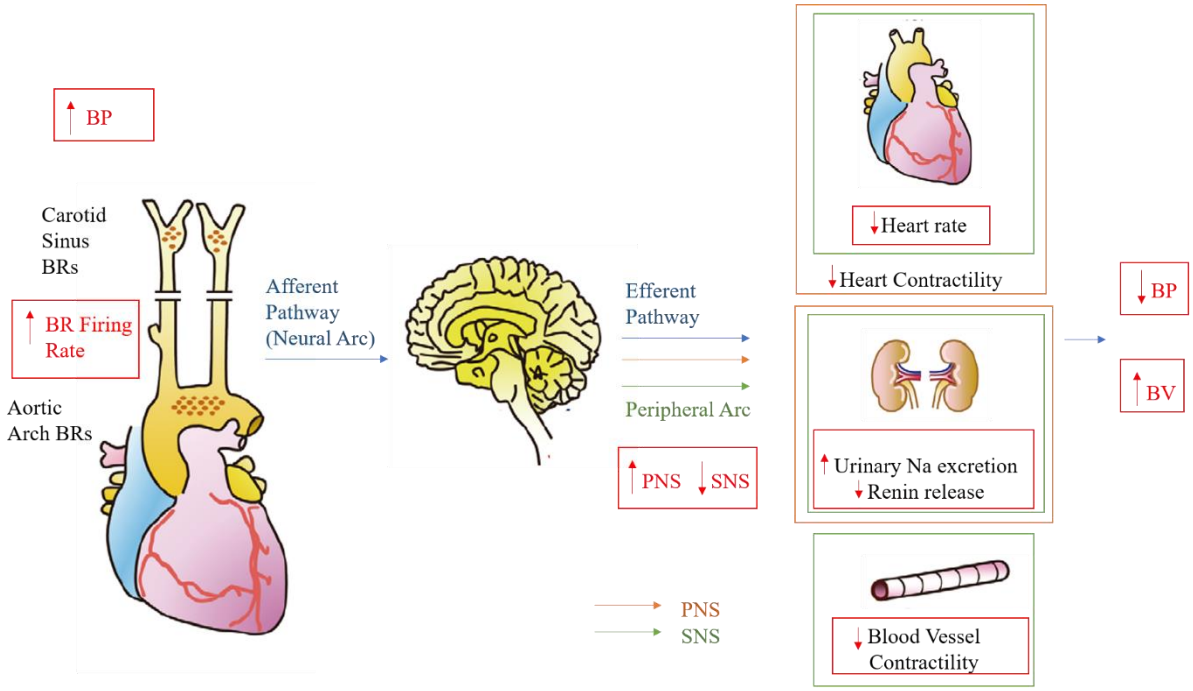

Figure 1.1: Illustration of baroreflex pathways from the baroreceptors to the central nervous system, and from the central nervous system to target organs for regulation of arterial blood pressure. Adapted from Hirooka [19]

The baroreceptor forms part of a feedback system for the regulation of BP, in which baroreceptors are the sensors, the brainstem is the controller, and the sympathetic and parasympathetic responses are the effectors [7]. These effectors act on the regulated variable which is BP or some function of BP [7]. This feedback is referred to as the baroreflex.

Feedback systems for engineering applications have been modelled for a number of different fields, which range from hydraulic to chemical. The purpose of modelling such systems is to be able to gain insight into how all the components of a system operate, and how each component affects the regulated variable [21]. Such modelling can also be used for design in selecting sensors for regulated variables, such that the variable is measured accurately and with sufficient precision to achieve the frequency response of the system required [21]. By modelling the sensor characteristics of the baroreceptor, I hope to gain insight into the ability of the baroreflex to regulate pressure in the long-term.

Blood circulation and the physiological homeostasis of blood pressure and heart rate have been the subject of investigation since the 17th century [18]. According to Ottesen et al. [18, pp. 140–156], the baroreceptor response is divided into separate elements of response:

- Sensitivity to pressure of receptors across a frequency band of interest is based on the superposition of signals from the high-pressure receptors in the aortic arch and from the carotid sinus.
- Sensitivity through 'low-pressure receptors' found in the heart and pulmonary veins.
- Resultant control of heart rate through the 'sympatho-vagal balance' which is a combination of sympathetic and parasympathetic actions on the heart and vessels

Historically, the adaptation/resetting property was used to exclude the baroreflex from being one of the possible mechanisms which may influence long-term control of blood pressure [9], [13]. However, recent research has shown that different baroreceptors have different thresholds, and different adaptation ranges, and that electrical stimulation of baroreceptors can lower BP in hypertensive patients [5], [14]. For these reasons, some researchers argue that the baroreflex is capable of participating in long-term control of blood pressure [5], [14], [22].

1.2 The Problem

For the baroreceptor to act as a primary sensor in a feedback loop controlling long-term BP, it is required to exhibit an adequate frequency response, particularly at very low frequencies [21]. The resetting behaviour of baroreceptors is not consistent with these structures playing a significant role in long-term BP regulation. However, recent studies suggest that there may be more subtle aspects of baroreceptor resetting. Resetting of different components of the baroreceptor (such as different fibres which detect absolute and relative pressure changes) may occur at different thresholds and at different resting pressures, and different baroreceptors fibres may terminate in different regions of the brainstem and control different reflex pathways [5]. Also, in-vivo findings show that although baroreceptors reset when exposed to prolonged BP changes, they appear not to reset when they are electrically stimulated [23]. Hence some researchers have suggested that because no resetting occurs during electrical stimulation, and baroreceptors affect blood pressure through sympathetic tone, baroreceptors may play a significant part in the long-term regulation of blood pressure.

The issues investigated in this dissertation by mathematical modelling are the mechanisms whereby baroreceptors reset, and the frequency response of baroreceptors as transducers in a feedback control loop.

1.3 Objectives

The objectives of this research are to review published mathematical models of baroreceptors, and use selected models to investigate mechanisms of baroreceptor resetting, investigate baroreceptor responses to long-term inputs, and hence draw insights as to how the baroreceptor may affect long-

term blood pressure regulation. The models are also used to investigate the frequency response of baroreceptors, particularly at very low frequencies.

1.4 Approach

Stages involved:

1. Critically review how understanding in the field of the baroreceptor for long-term blood pressure control has developed.
2. Implement key existing models of baroreceptor function in MATLAB and Simulink.
3. Test these models against available data in the literature and assess their performance.
4. Compare the different modelling techniques for the separate components in the mathematical models.
5. Analyse the performance of different components of all the models to the same input.
6. Test selected models using a range of artificial inputs to characterize their dynamic performance, particularly at low frequencies

1.5 Overview of this Dissertation

Chapter 1 provides the background to the subject of this study. This chapter contextualises the understanding of the baroreceptor, how it interacts with the CNS, as well as the physiology involved in the autonomic nervous systems actions on BP.

Chapter 2 critically reviews published mathematical baroreceptor models used to investigate baroreceptor behaviour. The review covers the progress of research surrounding BR experimentation and modelling, as well as other BR literature reviews. This critical review is summarised to show how understanding developed over the last 70 years. The review shows how researchers grapple with the complexity around blood pressure regulation, how they have different views around long-term regulation, and how certain experiments have impacted the research.

In Chapter 3, I simulate selected, published baroreceptor models according to the experiments which were used to validate them. I implement the BR models in MATLAB & Simulink, and evaluate them for different parameter values. I find parameter values that match the model data in the published findings, such that the model output result in Simulink reflects the model results reported by the researchers. I then compare the reported results to the simulated results (under the same parameterisation and input conditions).

Chapter 4 compares models by running simulations with the same inputs. Furthermore, I evaluate a subset of the investigated baroreceptor models (in the time domain) to estimate behaviour (in the frequency domain). The technique uses two of the best performing simulated models, based on the results shown in Chapter 3, for frequency response tests at linearised operating points along the entire

frequency range. These models are tested with artificial long-term inputs in order to characterise how the baroreceptor models behave in the long-term. This allows me to draw some insight into what the baroreceptor's dynamic characteristics are, based on the modelled dynamic characteristics.

In Chapter 5 I describe recommendations for further investigation into the dynamic characteristics of the baroreceptor, through experimentation and modelling. These recommendations cover further modelling work which could potentially improve the models. Carotid sinus dispensability is the first model adaption, while the age-related effects of the arterial wall is the second adaption. These changes to the BR model will include features known to affect the physiology of blood pressure, and subsequently clarify how the BR dynamics are affected by them

Chapter 6 covers a discussion on the critical review, and clarifies the understanding around the long-term controller capabilities of the baroreflex (BRX). I also discuss the characteristics identified through the critical analysis of the modelling research, as well as some extrapolative insights into the response of baroreceptors at low frequencies. In this chapter, I discuss how some of the contention in the literature can be clarified by understanding the difference between a BP controller and a sensor that can affect BP. Furthermore, the critical evaluation of all the BR models, even when they come from researchers with different opinions, show a definitive explanation for BR resetting. I underline this reasoning by drawing on the low frequency response of the BR models.

I then conclude this dissertation, by wrapping up the outcomes of the critical review of the literature with the insight from the critical analysis of the BR modelling. My conclusion points out some of the potential shortfalls of my research, and I make some recommendations for improving the modelling.

2 Critical Review of Existing Models

2.1 Overview

The role of the baroreceptor in detecting changes in arterial BP has been investigated for decades, however its role in long term regulation is still widely debated. Resetting of the baroreceptor has been investigated through a wide range of experimental techniques, and on a wide variety of species. Investigations have shown that the baroreceptor does reset under prolonged elevated BP. Experiments to investigate the extent of this resetting, as well as to what extent baroreceptors regulate BP through the CNS, have been widely modelled and discussed.

Table 2.1 gives a summary of a historical overview of the research which has been conducted in this field over the past four decades. The full overview is available in Appendix A, Table A.1.

The following points describe the development of understanding around BP regulation, the role of the baroreflex, and the dynamic behaviour of the baroreceptor. The overview covers the following main topics:

- Experimental research, which investigates how the baroreceptor behaves
- Physiology reviews, which discuss the understanding in the field and make assumptions about the role of the baroreflex
- Modelling research, which tries to explain experimental behaviour in order to validate or clarify understanding around the role of the baroreceptor.

The overview covers these topics, as investigated by a wide range of research, across the historical period since 1945. This overview does not presume to cover all research in this field, but rather to highlight specific examples from the literature which have made a significant contribution to understanding of the sensor characteristics of the baroreceptor and the role it may play in long-term arterial BP control.

Table 2.1: Summary for historical overview of baroreceptor research

Year	Authors	Title	
1945	A.L King	Pressure-Volume Relation for Cylindrical Tubes with Elastomeric Walls: The Human Aorta	[24]
1952	S. Landgren	On the Excitation Mechanism of the Carotid Baroreceptors	[6]
1968	W.B. Clarke	Static and Dynamic Characteristics of Carotid Sinus Baroreceptors	[7]
1970	E.M. Krieger	Time Course of baroreceptor resetting in acute hypertension	[8]
1972	B.W. Knight	Dynamics of Encoding in a Population of Neurons.	[25]
1972	A.C. Guyton	Circulation: Overall Regulation	[9]
1972	R. Srinivasan et al.	Modelling the Carotid Sinus	[26]
1973	R.Srinivasan et al.	Theoretical Studies on the Behaviour of Carotid Sinus Baroreceptors	[27]
1978	A.M. Brown et al.	Baroreceptor Dynamics and Their Relationship to Afferent Fiber Type and Hypertension	[10]
1980	H.M. Coleridge et al.	Operational Sensitivity and Acute Resetting of Aortic Baroreceptors in Dogs	[11]
1983	P.A Munch et al.	Rapid Resetting of Aortic Baroreceptors In Vitro	[4]
1990	A.C. Guyton	The Surprising Kidney-Fluid Mechanism for Pressure Control – Its Infinite Gain!	[28]
1992	A.W Cowley Jr	Long-Term Control of Arterial Blood Pressure	[13]

1996	J.E. Hall et al.	Pressure-Volume Regulation in Hypertension	[29]
1999	M. Ursino	A Mathematical Model of the Carotid Baroregulation in pulsating conditions	[30]
2001	G.A. Head et al.	Comparing Spectral and Invasive Estimates of Baroreflex Gain	[31]
2001	E. Petiot et al.	Frequency Response of Renal Sympathetic Nervous Activity to Aortic Depressor Nerve Stimulation in the Anaesthetized Rat	[32]
2004	C.J. Barret et al.	Problems, possibilities, and pitfalls in studying the arterial baroreflexes' influence over long-term control of blood pressure.	[5]
2005	J.W. Osborn et al.	A neural set point for the long-term control of arterial pressure: beyond the arterial baroreceptor reflex	[33]
2010	S.M. Bugenhagen et al.	Identifying physiological origins of baroreflex dysfunction in salt-sensitive hypertension in the Dahl SS rat.	[22]
2013	D.A. Beard et al.	A Computational Analysis of the Long-term Regulation of Arterial Pressure	[14]
2013	A. Mahdi et al.	Modelling the Afferent Dynamics of the Baroreflex Control System	[2]
2014	H.M. Horsman et al.	Cardiac baroreflex gain is frequency dependent: insights from repeated sit-to-stand manoeuvres and the modified Oxford method	[12]
2014	K.H. Pettersen et al.	Arterial Stiffening Provides Sufficient Explanation for Primary Hypertension.	[15]

In 1952 Landgren performed experiments on single fibre preparations of cat carotid sinuses [6]. By investigating the responses of the baroreceptor fibres, he aimed to contribute to the analysis of the discharge of the carotid sinus nerve, which had been found in previous studies to be affected by the vasocontraction of arterial walls under the influence of adrenalin [6]. His interest was also sparked by the differences in impulse discharge of the different fibres contained in the carotid sinus nerve. In his experiment on the baroreceptor fibres, he showed that larger fibres have higher firing rates, that different fibres have different sensitivities to inputs, and that the adaptation of the firing rate is strongly related to the rate of change of the pressure input [6]. In his discussion he noted that all fibres have a similar reaction to constant pressure or to pressure changes.

Landgren also showed that baroreceptor fibres have a limited operating region in which the BR can respond to pressure changes. The lower bound of this operating region is explained to be the threshold pressure of the BR, and the upper bound is determined from the pressure where the firing response is within 10 % of its maximum value [6]. Based on these experiments from Landgren, an overview of the behaviour of the baroreceptor fibres under a wide range of input types is available [6]. Landgren concluded from his work that at pressures above the upper bound of the BR operating region, the firing response ‘asymptotically adapts’ towards a steady state discharge frequency [6]. At this point it was relevant for researchers to further their understanding about how this baroreceptor operating region could affect, and be affected by, hypertension.

In 1968 Clarke prepared a mathematical model of the behaviour of the BR, based on experiments on dog carotid sinuses [7]. The model was prepared to reproduce the behaviour discovered through his experiments with step input, ramp input and triangular input waveforms. These experiments were able to show the characteristics of the baroreceptor when pressure increases and when pressure decreases [7]. His results and analysis clearly show that increase in pressure increases the firing rate of the BR, and decrease in pressure decreases the firing rate, but that the rates of change of firing rate are not the same for increasing and decreasing pressures. Clarke’s model introduced a previously unpublished feature, viz. that the sensitivity of the baroreceptor changes depending on the direction of change of the BP. Clarke mentions in his paper that his aim is to define the relationship of the firing response to pressure. His model is made up of three components, namely the relationships between intra-sinus pressure and receptor membrane strain, receptor membrane strain and generator potential, and the generator potential to the discharge frequency of the nerve [7]. These three components form the foundation of how researchers have mathematically modelled the baroreceptor. The interaction between these components on a fundamental level, is illustrated with the block diagram in Figure 2.1. A key observation made by Clarke is that the positive sensitivity of the BR is a non-linear function of strain. BR output is proportional to strain at low pressures but the relationship is non-linear at higher pressures. He makes the assumption that such behaviour is due to the visco-elastic coupling between the receptor terminal and the connective tissue in the vessel wall. This assumption is

also made by Coleridge et al., based on experiments involving short-term resetting and hysteresis. Coleridge et al. claim that the non-linear relationship between BR output and strain, at high pressures, is most likely caused by 'visco-elastic relaxation and creep' [11]. Clarke also discusses the role of the baroreceptor as a sensor in a feedback control system, in which the central nervous system acts as the controller but the regulated variable may be pressure or some function of pressure [7]. An important comment related to this is that the regulated variable is not the mean arterial pressure (MAP) as modelled by investigators before him, but rather an unknown function of pressure. He notes the work of other researchers which showed baroreceptor discharge to be a function of the sinus wall deformation and not the pressure itself. This proposed model is referenced and used as a basis for a number of more recent baroreceptor models, from authors such as Srinivasen and Nudelman, as well as Bugenhagen et al. [22], [26], [27].

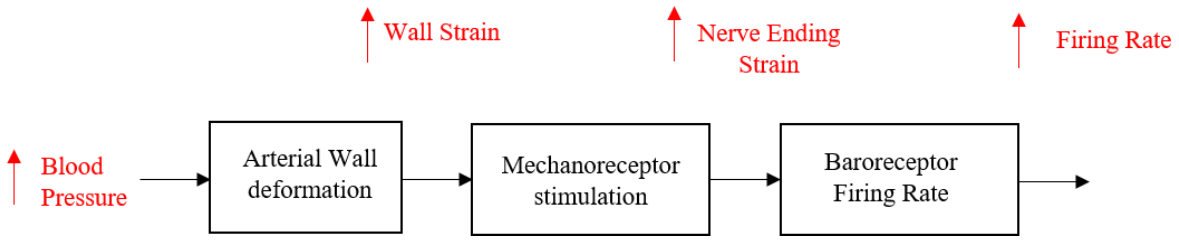

Figure 2.1: Block diagram describing the generic functional components used to model the baroreceptor. Adapted from Mahdi [2]

The Guyton et al. 1972 paper [9] describes a model of the overall regulation of circulatory physiology and highlights three main factors which regulate pressure. These are autonomic reflexes, changes in body fluid volumes and electrolytes, and the renin-angiotensin system [9]. These autonomic reflexes and their interaction with the baroreceptors, are illustrated in Figure 1.1. Guyton et al. mention the role of autonomic mechanisms in arterial pressure regulation, which they says seem to operate only in the short-term (from seconds to hours), can have an effect on the long-term mechanisms [9]. Two controversial statements made in this paper are that 1) the 'total peripheral resistance' plays no role in regulating arterial pressure in the long-term, and 2) that chronic changes to BP can only be through changes to kidney function or fluid balance. This circulatory model and stand-point have been the source of wide debate and research around the role of the baroreflex in long-term BP control [5], [9], [13], [14].

Some key contradictions to these statements are that increased peripheral resistance can affect the tonic firing rate of the baroreceptors in the aorta and carotid sinus walls, which does affect the sympathetic nervous system regulation of chronic BP [13], [34], and secondly that the electrical stimulation of the baroreceptor has been shown to affect chronic BP [5], [14], [15], [34]. A discussion of the problems in studying this reflex was published by Barret and Malpas in 2011 [5]. Guyton et al. note that, although carotid sinus and aortic baroreceptors behave similarly, aortic baroreceptors have a

higher pressure threshold above which firing starts [9]. In addition, Guyton et al. describe findings by Krieger [8], which suggest that the baroreceptor is a volume sensor and not a pressure sensor. The descriptions and assumptions made about what causes the baroreceptor to fire, reiterates the comments of many researchers [7], [14], [27] who have described the baroreceptor as interpreting a signal based on strain. Many of them consider the firing rate to be initiated by pressure through a change in strain, based on factors such as a change in compliance of the vessel wall or creep stress in the vessel wall [14].

Cowley discusses a number of theories and experiments regarding the long term control of BP in his physiology 1992 review [13]. In this review he highlights how mechanisms which can detect short term changes in BP may not have the ability to regulate BP in the long term. He tries to clarify the roles played by the nervous system in adjusting sympathetic tone, and the kidneys through fluid volume control. He notes that there is an interdependence between these systems, but that long-term BP must be regulated through some measurement and adjustment mechanism that can operate over a time-span of years. Cowley's argument is that the baroreceptors cannot regulate BP in the long-term because they adapt, much like previously studied mechanoreceptors adapt to a constant stimulus [13]. Several experiments are highlighted in order to illustrate this point, where the MAP is found to be unchanged in the long-term when the baroreceptor afferent nerve fibres are removed [13]. Cowley also states that it is possible for the brain to change the long term operating point for arterial pressure control, but that there is not much evidence that the CNS can act as a long-term arterial pressure controller. Based on this the CNS seems to rely solely on the baroreceptor for detecting changes and so it cannot independently adapt to long term changes. His review is an extensive study on experiments surrounding BP control, in many different species, under a wide range of experimental conditions. He presents four main points of evidence for why the pressure-natriuresis mechanism is the main long-term controller of BP:

- Chronically elevated BP can only be sustained by reducing the excretory ability of the kidney
- Increased total peripheral resistance, such as in limb amputees, does not lead to a chronically elevated BP
- The gain of the baroreceptor at very low frequencies is insufficient to reduce long-term increases in BP
- The role of the brain in releasing factors which increase vascular tone and elevate BP ('ouabain-like factors'), and the role of those factors, has not been shown to have any measurable natriuretic properties [13].

Based on his investigation, Cowley explains that although the baroreceptors don't have a sustained signal to match a sustained input, the changes to their firing rate needs to be investigated further. He makes the careful observation, that although the nervous system doesn't regulate BP it still does influence BP through the compliance and hormonal effects of the sympathetic nervous system. In this

way, although the sensitivity of the pressure-diuresis mechanism is affected by neural and hormonal influences, it is still the primary regulator for maintaining BP within a sufficient range, and that it seems to have an infinite gain for long term control. Cowley also points out that, at that time, the long-term changes to the compliance of arterial vessels under chronic hypertension were known only to be due to the signal transduction pathways which control vascular tone. This review by Cowley draws a number of insights into the complex systems of cardiovascular function, and is a useful overview of a number of opinions and experimental investigations in the field. He draws convincing conclusions based on a wide collection of studies, and notes areas of experimentation which are lacking or flawed. Some of his key findings are how investigation of long-term BP regulation is difficult as most methods compromise the interacting mechanisms of control. An example of this is the use of anaesthesia which alters sympathetic tone and subsequently changes vessel compliance and angiotensin levels. His review is a strong argument for pressure-natriuresis as the long-term controller of BP.

In 1972 Srinivasen and Nudelman developed a mathematical model to describe how the carotid sinus (CS) BR discharge frequency is a result of change in intra-sinus pressure, with specific emphasis on the sensor characteristics of the BR. Their model is based on the visco-elastic properties due to the elastin and collagen of the arterial wall, and an encoding of the transduced signal into a firing rate [26]. The visco-elastic properties of the arterial wall are modelled using spring-damper networks (also referred to as Voigt bodies). The modelling of these properties is illustrated in Figure 2.2 below. These linear viscous strain and non-linear elastic strain properties are modelled with a spring damper system [26]. One key feature of this model is how they used linear regression techniques to fit a curve to the relationship between the pressure and non-linear strain. This curve is based on King's model for strain in elastomeric cylindrical walls, where the compliance of the wall is affected by age [24]. Their model was validated experimentally with data from Clarke, Landgren, and their own data [6], [7], [26], [27]. This model is discussed more thoroughly in Section 3.2 below, along with the modelling work from King which preceded it, and from Bugenhagen et al. who extended it [22], [24].

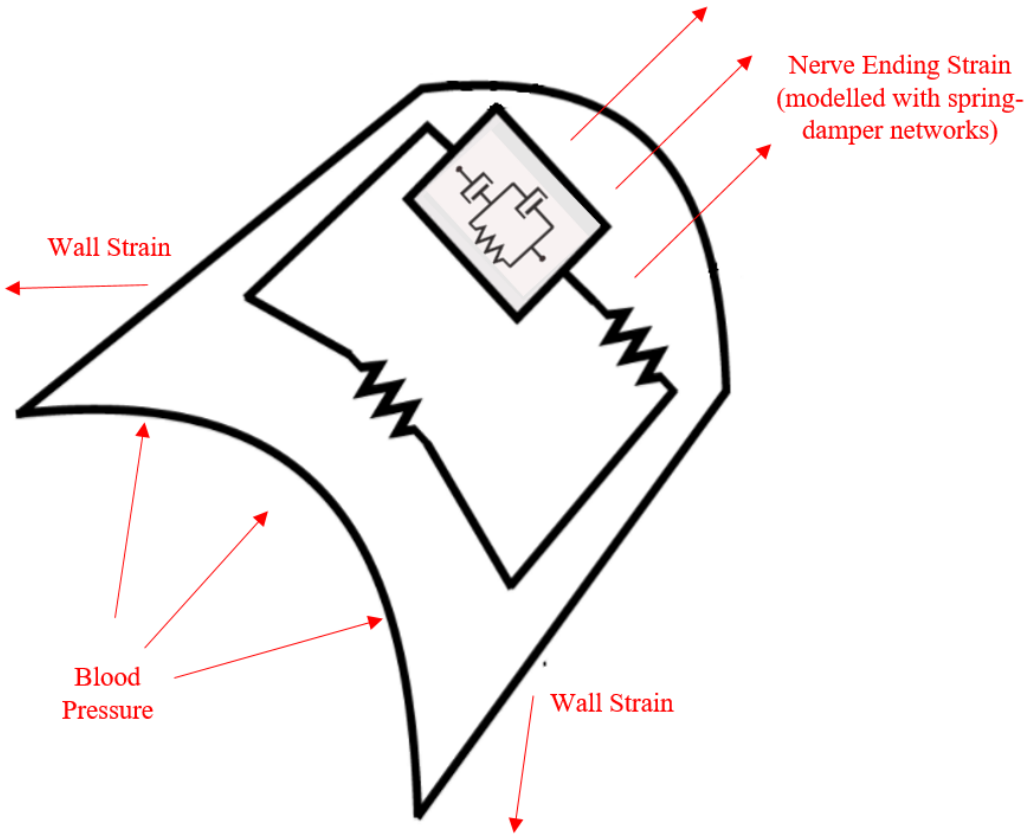

Figure 2.2: Illustration to show how pressure forces at the arterial wall through the visco-elastic layers of the arterial wll, can be described using spring-damper networks (or Voigt bodies). Adapted from Mahdi [35]

Experiments were conducted by Munch, Andresen and Brown [4], as well as by Krieger [8], with mechanically adjusted ramp pressure inputs (non-pulsatile) applied to in-vivo rat aortic arch baroreceptor nerves. These were slow pressure ramps, which were conditioned with 5-15 min of MAP before the ramps were applied [4]. Their findings show that the pressure response curve shifts along the pressure axis in the direction of the change, with hardly any change to the pressure-sensitivity (gain). Munch compares his findings with the results of a number of different experiments performed by a range of authors, in which BP is raised using different means in different species and in different time frames. He mentions that direct comparability is difficult based on all these factors. Their hypothesis is that the resetting may be due to decreases in vessel dispensability, changes in the receptor membrane characteristics as well as age-related effects on mechanical transduction properties. This 1985 paper provides a good description of in-vivo experimentation and comparative study results on baroreceptor firing rates. They note that: ‘the conditioning pressure is the primary if not sole determinant of resetting’, and that ‘efferent neural or hormonal influences on the baroreceptors are not

required for resetting' [4]. In this way, the paper provides a thorough investigation into experimental findings and compares their results to other similar experiments, all without hypothesizing how resetting affects blood-pressure control. Munch et al. conclude that, according to their results, they cannot show that the baroreceptor ever completely resets.

Guyton published a paper explaining his hypothesis around the infinite gain of the kidney-fluid mechanism of BP control, which re-iterates that in the long-term, BP can only be regulated by changes in sodium and water levels [28]. In this paper Guyton describes the many experiments and conclusions which show that BP can only be regulated by the kidneys, because in their model, and in other supporting experiments, they found that when they increase the total peripheral resistance, pressure returns to a baseline after a few days. After publication of this model of long-term pressure control, and Munch's baroreceptor resetting results, it became generally accepted that the baroreceptor could in no way play a role in regulating BP in the long term. Guyton also argues that total peripheral resistance is shown to increase after volume-induced BP increases, and that the infinite gain of the kidney-fluid mechanism cannot be by-passed by any other controlling mechanism [28]. This is evident where other mechanisms which affect BP, such as sodium loading and angiotensin levels, shift the renal function curve. The work from Guyton and colleagues initiated much research into the dynamic characteristics of the baroreceptor; the role of the baroreflex in essential hypertension, and the role of the baroreceptor in affecting sympathetic control during hypertension [5], [22], [32].

Petiot et al. studied the neural and peripheral arcs of the baroreflex to characterise their dynamic behaviour at different frequencies. For the neural arc, which they define as being from arterial pressure to sympathetic nervous activity, they found the transfer gain to have high-pass filter properties [32]. This observation indicates that the baroreceptor firing rate, which relates BP to SNA, increases as the frequency of the pressure variation increase. This finding ties in with those of Franz et al.[36] and Brown et al. [37]. Franz et al show that the baroreceptor exhibits a high-pass dynamic response that amplifies inputs at frequencies above 0.1 Hz, and attenuates inputs between 0.01 Hz and 0.1 Hz [36]. More recently Sato et al. also showed that baroreceptor sensitivity increased by a factor of between two and three in the frequency range 0.01–1 Hz [10], [32], [36], [38]. Sato's experiments also show that the sensitivity (or gain) decreases above 2 Hz [38]. Franz suggests that because the step response contains many time-constants, there must be 'viscoelastic relaxation and creep processes' which cause the adaptation feature of the baroreceptor response [36].

In 2004 Barret and Malpas published a review article regarding the influence of the baroreceptor on long-term BP control [5]. They discuss the different studies and findings around the functionality of the baroreceptor for long-term control, and highlight the two main arguments that suggest that the baroreflex cannot play a role in long-term control of BP. They discuss the reasoning and pitfalls behind some of the assumptions that have been made about the baroreceptor. Their review is valuable because it introduces the reasoning that the baroreceptor may be made up of many different

parts and functions, which may have different thresholds and frequency responses under different situations. An example is where the baroreceptor afferent fibres are made up of A-fibre and C-fibres. A-fibres have a high firing rate and low pressure threshold, while C-fibres have a low firing rate and a high pressure threshold [5]. This collection of different fibres lends itself to a possible physiological function where the A-fibres can buffer quick changes in pressure and reset readily, while the C-fibres are more likely to act in the case of high pressures and are reset less readily. These different fibres could act as different triggers to the BR sensor transfer function, or the various fibres could control different feedback mechanisms at the brainstem [5].

The first argument suggesting that baroreceptors can't contribute to long-term control is based on their resetting behaviour, in which baroreceptors are known to shift their operating range in the direction of the prevailing pressure change. Although this behaviour, experimentally reported by Munch et al. [4], is widely accepted, Barret and Malpas note that baroreceptors are composed of many different fibres which are known to have different operating regions and that it cannot be conclusively stated that all baroreceptor fibres reset at the same rate [5]. This observation is based on the A-fibre and C-fibre components of the baroreceptors, as well as in the characteristics of the terminal endings themselves, which suggest that the baroreceptor is capable of interpreting both absolute and relative pressure [5]. They note that findings have shown that even in established hypertension, the baroreceptors may still contribute to decreasing pressure [5].

The second argument against the baroreceptor's ability to control arterial pressure in the long-term, is based on experimental findings on sinoatrial denervated (SAD) rats and dogs. The interpretation of the results is that although there is generally an increased pressure variability at the onset, the long-term averaged MAP of the SAD subjects is relatively similar to the MAP of the intact subjects. Based on this result, many researchers such as Cowley [13]and Guyton [28] maintain that this is why the baroreceptor cannot set long term BP. According to these researchers, such a recovery in average mean arterial pressure implies a 'resetting of central control' of SNA when the high pressure spike settles over a period of days. Barret and Malpas's response to this argument is that subjects with intact baroreceptors have less pressure variability, and lower maximum pressure spikes, factors that significantly affect organs and tissue function, therefore the baroreceptors must play some role in maintaining absolute and relative pressure [5]. Barret and Malpas state that because of the other neuronal and hormonal players which are capable of compensating for the loss of baroreceptor function, baroreceptor denervation is not an adequate experimental investigation to understand chronic MAP change [5].

The roles played by the different types of fibres must affect the analysis of the baroreceptor characteristics deeply, as the frequency response depends on the type of receptors and the type of fibres which are built into the model. The variable threshold differential pressure, which affects the baroreceptor's firing rate, shows that this system in non-linear. This property is based on the fact that

superposition does not hold, because a linear increase in pressure won't result in the same linear increase in firing rate for the baroreceptor. It also implies that this system will be time-varying, based on the implication that the frequency of the change being applied affects the output. In order to investigate the role these fibres might play, and better understand the comments from Barret et al. [5], models will be investigated with simulated frequency response tests in section 4.2.

In 2010, Bugenhagen et al. developed a model to describe the physiological behaviour of the baroreflex and how its dysfunction seems to be tied to hypertension [22]. By using experimental results from spontaneously hypertensive rats and Dahl salt sensitive rats, they parameterise a baroreflex model to draw conclusions about the relationships between salt sensitive hypertension and the baroreceptors. Their model describes the baroreflex, from an input aortic BP transduced by the baroreceptors into a signal which is interpreted by the central nervous system to regulate heart rate at the SA node via the SNS and PNS [22]. The mathematical model of the transduction of aortic BP into a firing rate is of particular interest for this research, and is discussed more thoroughly in section 3.3 below. This baroreceptor part of the model is an extension of the model from Srinivasen and Nudelman [26], [27], and was further investigated more recently by Mahdi [2]. Differences in fibre types, such as myelinated and unmyelinated fibres (Type I and Type II) are not accounted for in this model, nor is the effect of carotid sinus baroreceptors. Particular features of the model involve strain detection based on the rate of change of the vessel wall dimensions, under a non-linear function of compliance. The junction between the aortic wall and the baroreceptor nerve ending is modelled using a series of Voigt bodies [22], which are used to represent the different time constants at which the baroreceptor is known to reach steady-state after reaching its maximum firing rate (adaptation) [22]. This baroreceptor nerve ending strain, along with a strain sensitivity parameter and strain threshold parameter, results in an afferent baroreceptor firing rate. The method of modelling the junction between the strain at the arterial wall, and the strain at the nerve ending, was illustrated in Figure 2.2. This is further expanded in Figure 2.3 to show the mechanical model for the visco-elastic layers in a series of spring-damper systems (or Voigt bodies). Importantly, the authors point out that although this is the most mechanistically detailed available model, it has only been implemented and tested at constant heart rate and not with a fluctuating heart rate. Hence it is possible that this model may be further improved for simulating dynamic changes, by improving the model parameters [22]. The main value in this paper is their adaptation of the mechanical modelling of the pressure-response behaviour of the baroreceptor performed by Srinivasan and Nudelman [27], and their attempt to fit their model to datasets from rats.

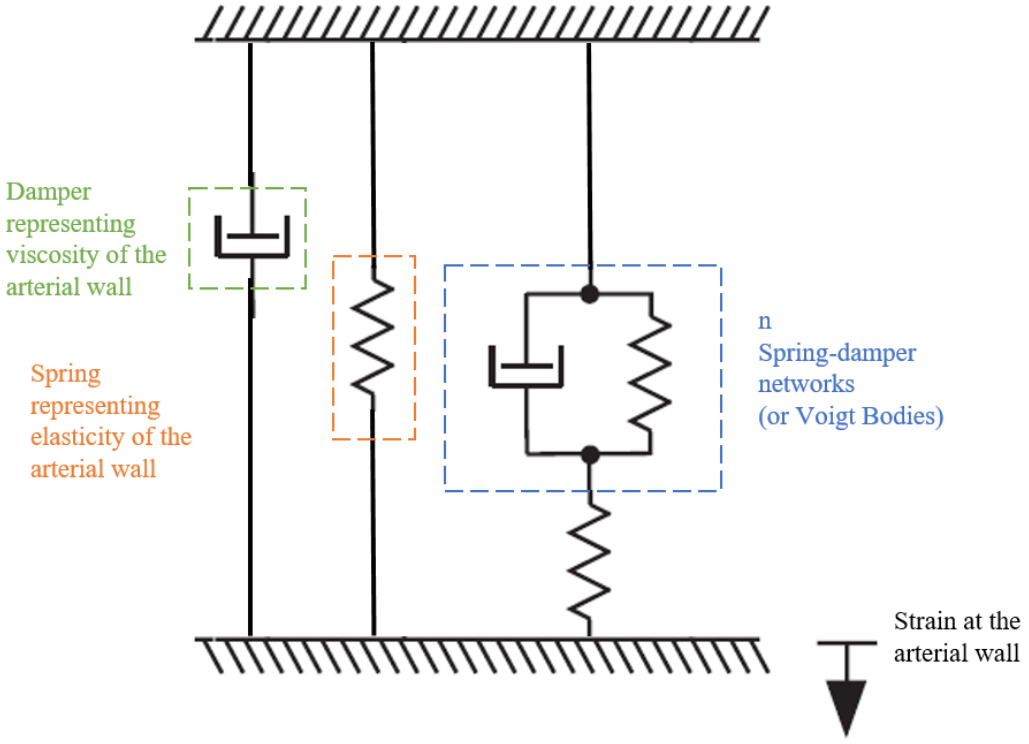

Figure 2.3: Illustrated dynamic Barorceptor model to further describe how spring-damper networks model strain, Adapted from Bugenhagen [22]

Beard et al. [14] expands on the models presented by Srinivasen et al. [27] and Bugenhagen et al. [22] to present an alternative to Guyton-based models [9] for arterial pressure regulation. Beard et al. argue that because the Guyton models assume that arterial pressure is regulated only by the kidneys, they cannot be used to investigate alternatives [14]. These alternatives include other complex relationships between neuronal and hormonal systems that are affected by the baroreceptors [14]. Their argument also highlights that there is no formal description or parametrisation of the Guyton models [14]. Based on these limitations, the Beard et al. model is presented as a "phenomenological" model of physiological interactions between components [14]. Beard's goal is to present a practical model which relates the input-output behaviour of selected BP controller variables, based on general physiological principles which are supported by experimental data. In this way, he confirms that his model is a "data-driven phenomenological representation" of the physiology rather than a fundamental representation based on mechanical and physical relationships [14].

The components in the Beard et al. model include large artery mechanics for the baroreceptor [14], the dynamics of the baroreceptor firing rate, mechanics of the heart, the autonomic system as well as the renin-angiotensin system. It is interesting to note that their model relates the changes in sympathetic tone to changes in aortic compliance, as well as long-term mechanical creep volume, which are not accounted for in other open loop baroreceptor models. I investigate and analyse this closed loop model

for dynamic characteristics using open-loop Simulink modelling techniques in section 3.4 below. Beard et al. concluded the following [14]: the baroreflex arc and the renin-angiotensin system may interact in order to regulate long term BP; renal function (or dysfunction) is not the main determinant of long-term arterial pressure according to their model; chronic stimulation of the baroreflex can regulate BP through the baroreflex and the renin-angiotensin system; arterial stiffening contributes to long-term changes in arterial pressure that is related to aging [14]. Some of these conclusions directly contradict other researchers' views on the reno-centric role of arterial BP regulation. One important distinction, which is not clearly discussed by Beard, is the difference between the normal physiological role of the baroreflex during long-term BP regulation and its role in the increase of BP with age and the development of hypertension. The ability of the baroreflex to adapt under chronic changes in compliance may affect sympathetic tone and renin-angiotensin levels and lead to essential hypertension [5], [13]. This observation is further investigated in section 4.2, when the frequency response of the Bugenhagen et al. and Beard et al. baroreceptor models are tested.

The phenomenological model by Beard et al. [14] is very clearly described, along with clear parameterisation and experimental results, and compared against existing data from reliable sources. Interestingly Cowley [13] described the baroreceptor as incapable of acting as a sensor for long term control because of its frequency response and low gain (sensitivity), whereas Beard et al. [14] showed that electrical stimulation of the baroreceptor can affect the sympathetic nervous system when the arterial pressure baseline changes. One may argue that the contention in the literature can be clarified by separating the sensor characteristics of the baroreceptor from the ability of a system to control/regulate the measured variable (in this case some function of pressure). The difference between these two viewpoints is that although the baroreceptor can affect blood pressure over longer time periods (through stiffening walls or electrical stimulation), that does not infer that the baroreceptor can detect long-term changes or regulate blood pressure.

Mahdi et al. presented a comparative analysis of baroreceptor models in their 2013 paper [2]**.** This study shows how different types of models perform according to the known features of baroreceptor dynamics. The afferent dynamics of the baroreflex are modelled in three stages:

1. The arterial wall deforms to convert pressure inputs into an arterial wall strain [2]
2. Arterial wall strain stimulates the mechanoreceptor nerve ending [2]
3. Baroreceptor firing rate is encoded as a function of the mechanoreceptor nerve ending activity [2].

Mahdi et al compares three types of models for arterial wall deformation, based on whether the wall is modelled as linearly-elastic, nonlinearly-elastic or visco-elastic [2]. Three different conditions are compared for the pairing of the strain at the arterial wall and the strain at the receptor nerve ending. These conditions are for modelling the coupling through different amounts of elastic and damping

elements (Voigt body elements). Thereafter Mahdi et al compares in two models the translation from a nerve ending strain to a firing rate, viz. the simple amplifier model and the leaky integrate-and-fire model.

The features of these different types of models are compared for their ability to fit a range of experimental results based on sinusoidal and step inputs. These results are based on experiments from Brown et al. on rat aortas for baroreceptor firing rates [2], [10]. Features which are used to test the behaviour of the models under these different conditions are saturation and threshold, adaptation and overshoot; as well as post-excitatory depression (PED) and rectification. Using these methods, Mahdi at al. are able to compare a variety of different models by examining each of the components that describe the behaviour of the baroreceptor [2]. They first quantitatively evaluate the different models' ability to fit experimental data, and then qualitatively investigates which combinations of models are capable of showing the features (saturation, threshold, and rectification) of the baroreceptor under different inputs [2]. In the quantitative analysis he optimises the model parameters for arterial wall deformation in order to reduce the error between the model output and the expected result. Using the model which performs the best with optimised parameters, he then qualitatively investigates the performance of the mechanoreceptor stimulation [2].

Mahdi et al's qualitative comparisons [2] show that the non-linear arterial wall, two Voigt body, integrate-and-fire collection of models result in the best alignment between responses and data [2]. This preferred model shows response sufficiently in line with the expected behavioural properties for rectification, threshold and saturation, adaptation as well as asymmetry [2]. A more extensive description and analysis of this model is outlined in section 3.5 below. A far more elaborate discussion on models which discern between A-fibre and C-fibre baroreceptors is available in the work from Sturdy et al. [39].

Mahdi et al. [2] mention that to his knowledge this is the first comparative study that tries to identify a simple collection of generic BR models that characterise the features of the BR [2]. Their results show that linear wall models are insufficient for describing a BR response when the input has 'multiple step-pressure inputs'[2]. Furthermore, the use of two Voigt bodies to describe the mechanoreceptor stimulation is sufficient to describe the adaptation on multiple time scales [2]. They say that the reason this may be sufficient is because the first Voigt body describes the time constant responsible for the deformation at the arterial wall, and that the second time constant is responsible for the deformation at the receptor nerve ending [2]. Importantly, he notes that based on his knowledge this is the first study to show the importance of different time constants in BR models, and that more careful tests with data over longer time periods would be invaluable for such an analysis [2].

In 2014, Petterson et al. [15] **combined the age-related strain component from King** [24]**, with the firing** response component of the baroreceptor from Bugenhagen et al. [22] along with the

circulatory model from Smith [40] in order to 'mechanogenically' understand the physiology behind essential hypertension [15], [22], [24]. This model is similar to Beard et al.'s model [14], only with a more simplistic baroreceptor model and an updated model of the closed loop effects on the kidney. Petterson et al.'s model [15] shows how when the arterial wall stiffens over long periods of time, the baroreceptor has a diminished response. They discuss how the natural process of age-related arterial wall stiffening will gradually affect the strain interpreted by the baroreceptor, which means the baroreceptor receives inaccurate information about the pressure and responds inadequately [15]. Hence they hypothesise that the kidneys fail to restore BP to normal as arterial stiffening progresses, which could lead to essential hypertension [15]. By using Bugenhagen et al.'s model for central nervous system responses [22], and Smith et al.'s model for the renal changes to the pressure-natriuresis curve [40], they present a closed loop model of an aging aorta [15]. They are able to show that as time progresses, and without any other pathological effects, BR sensitivity decreases over time [15]. This relates to the stiffening of the aorta in aging, and a decreased short term peak BR response [15]. This paper is interesting as it pulls in a number of different recognized models in order to achieve a result that does not contradict Guyton's theory that the renal curve is the only controller of BP over time, but supports a different perspective on why the renal curve would shift without an observed renal pathology. Although the Bugenhagen model is available through virtualrat.org [22], it is described in the paper only by the governing mathematical equations [15], [22]. Pettersen et al. claim that their model is the first qualitative example to show that arterial stiffening sufficiently explains essential hypertension [15]. This is in contrast to Beard et al.'s similar statement [14] that the model from Averina et al. [41] was the only model known to show how the renal pressure-natriuresis curve adapts under long-term pressure changes [14]. One key distinction between all these models and their corresponding papers, is that they are used to analyse different topics. The models of the closed loop baroreflex, whether they include models of the kidney and the renin-angiotensin system or not, can be used to understand the effect of the baroreceptor in chronic hypertension as well as to understand the regulatory control mechanisms for arterial pressure.

Another interesting note is that all the authors of this group (Beard [14], Pettersen [15] and Bugenhagen [22]) indicate that the mechanical suppression of arterial wall strain can lead to a sustained elevation in arterial BP, but that they do not all seem to state clearly whether this is directly in opposition to Guyton's theory that the renal function curve and the salt-volume uptake rates are the only controllers of BP. Pettersen et al. state that their findings do not contradict Guyton's view, but rather support a mechanism which affects the renal curve in the long-term [15]. Whereas Beard et al. [14] state that because the arterial stiffening can contribute substantially to the long-term control of BP, it contradicts the 'renocentric' Guyton view [14], [15]. Pettersen et al. [15] state in their paper that the dysfunction of the baroreceptor is not really a dysfunction at all, but really a misrepresentation of the arterial pressure through strain in a vessel with lower compliance[15].

Guyton's model analyses BP regulation for mean BP only [9], where Clarke and others [7], [15] have shown that BRs are more sensitive to systolic BP peaks. Based on the physiology assumed by most authors that the BRs supress SNA to some extent [14], [15], [20], [22], Petterson et al. have shown how arterial stiffening can affect BR firing and subsequently decrease SNA suppression [15]. Based on these observations some further investigation is necessary. This investigation would be on the effect of intermittent stimulation of the BRs, preferably synchronised with systolic pressure, on suppression of SNA. This could help highlight new ways of resolving isolated systolic hypertension in aging subjects.

3 Implementation and Analysis of Existing Models

This chapter discusses my implementation of four different models for the baroreceptor. In each section I give a short contextual background into each model, along with a description of the modelling equations. All modelling equations are also presented in Appendix B for review. The models are implemented in Simulink R2016b (The MathWorks Inc, © 1994-2017, USA) and are validated with data from the experiments described by the model authors. All Simulink modelling diagrams are presented in Appendix C for review. The outputs of the models are compared with the reported model outputs, and with corresponding published experimental data. A critical comparison of how the different components of the models behave under the same input conditions is also discussed. This comparison elaborates on the strengths and limitations of different ways of modelling the main features of the baroreceptor.

3.1 The King Pressure-Strain Model for Arterial Walls

3.1.1 Model Context

King developed a model of the pressure-strain relationship in elastomeric arteries [24]. This model was expanded by Srinivasen et al. [27]. Srinivasen extended King's arterial wall model for the baroreceptor by including a dynamic strain model component. Later, Bugenhagen et al. developed a model of the complete baroreflex to study the physiology behind salt sensitive hypertension in rats [22]. Bugenhagen et al. also used the elastomeric model of the arterial wall, but adapted and linearised his model of the wall strain using a curve fitted across experimental results for a rat aorta pressure-radius relationship.

King's model of cylindrical tubes of elastomeric materials is described briefly in the next section, to provide context for the baroreceptor models described later in this chapter. Simulation of this model's behaviour is not presented here, as it is simulated in the model from Srinivasen et al.

3.1.2 Model Equations and Description

King investigates and describes the visco-elastic properties of the arterial wall to find out how large systemic arteries might be able to regulate pulsatile blood flow. Based on his investigations, he models the arterial wall as a uniform elastomeric cylinder. In this way the strain experienced by the arterial wall is determined using the non-linear sigmoidal Langevin function [24]. This function approximates rubber-like stress-strain behaviour as a function of variables such as age, arterial wall thickness and arterial wall radius. This model of the pressure to strain relationship is known as a non-linear elastic wall model, and a similar model with a non-linear sigmoidal pressure response curve is extensively tested and compared to other wall models by Mahdi et al. [2].

King's paper gives a number of useful parameters for the human aorta, under different pressures and at different ages [24]. Table 3.1 below is based on the data reported by King, for the ranges of

parameters β, A and the unconstrained radius (r_0) [24]. A is a factor dependent on the arterial wall thickness, undistorted radius and initial pressure. β is a factor for the unconstrained surface area of the cylinder, which represents the level of twisting of the molecular chains at the periphery of the arterial wall.

Table 3.1: Experimental and calculated values for human aortas of different ages [24].

Age (years)	β	A (mmHg)	r_0 (mm)
20-24	0.302	88	5.8
36-42	0.462	70	6.4
71-78	0.640	44.5	7.9

3.2 The Srinivasen and Nudelman Baroreceptor Model

3.2.1 Model Context

Srinivasen and Nudelman base their baroreceptor model on the transmission from pressure to strain at the arterial wall [27]. The model is comprised of an arterial wall strain based on the non-linear strain characteristics of elastomeric cylinders (as adapted from King) [24], [26]. King's model parameters are based on experimental data collected from human aortas, whereas Srinivasen et al. model parameters are fitted for cat and dog carotid sinus experimental data. This strain model at the arterial wall is further extended to include a dynamic strain component, based on the coupling between the membranes and connective tissue layered between the arterial wall and the baroreceptor nerve ending membrane.

3.2.2 Model Equations and Description

This section describes the model presented by Srinivasen and Nudelman, which relates changes in pressure at the carotid sinus arterial wall to the baroreceptor firing response [27]. The dynamic strain model includes the frictional coupling between the arterial wall and the baroreceptor nerve ending membrane. Together, the combined static and dynamic strains are transduced into a combined strain signal, which is only propagated to the output if the combined signal exceeds a threshold. Thereafter the strain signal is transduced into firing response based on an integrate-and-fire model of the nerve discharge firing pattern.

The following set of equations summarises the model presented by Srinivasen and Nudelman [26], [27].

The Langevin function (Eq. 3.1), used to model the non-linear elastomeric behaviour of the arterial wall, is included in the model of the static arterial wall strain (ε) in Eq. (3.2) [24]. In Eq 3.2 the rate of change of the static wall strain is a function of the input pressure (P) [26]. The elastomeric behaviour of the strain depends on resting mean pressure (A) and a factor for unconstrained surface area (β) [26].

$$\mathcal{L}(z) = \coth z - \frac{1}{z} \tag{3.1}$$

$$\dot{\varepsilon} = \frac{P}{C} - \frac{A}{C\sqrt{(\varepsilon+1)}}\left[\frac{\mathcal{L}^{-1}\{\beta(\varepsilon-1)\}}{\mathcal{L}^{-1}(\beta)} - \frac{1}{\varepsilon+1}\right] \tag{3.2}$$

The dynamic strain (ε_d) is modelled with a single Voigt body (a nonlinear spring in parallell with a linear damping element for viscosity).

$$\dot{\varepsilon}_d = \frac{\sigma}{C_D}\left|\dot{P}\right| - \frac{1}{C_D}(\varepsilon_d)^2 \tag{3.3}$$

Note that the static wall strain (ε) is the series viscoelastic coupling of the nerve terminal to the arterial vessel wall, whereas the dynamic wall strain (ε_d) is the coupling caused by the different layers of the arterial wall around the nerve ending which slip past each other and cause friction. These two types of strain are combined into a membrane strain (δ in Eq. (3.4)). The membrane strain is then transformed into a transduced signal (x), which is generated if the combined membrane strain exceeds the strain threshold for the baroreceptor (Eq 3.5). The response signal generated is a nerve discharge signal, y (firing response in Figure 3.2). The firing response is modelled using a simple integrate-and-fire model, which triggers a depolarisation as soon as the threshold is reached, resets the transduced signal, and whose response slowly decays as the transduced signal is maintained. In this way, Eq. (3.5 – 3.6) model a response which is initiated for transduced strains that exceed the minimum threshold, for changes to the arterial pressure.

$$\delta = \varepsilon + \varepsilon_d \tag{3.4}$$

$$x = \begin{cases} 0 \; if \; \delta < \delta_{th} \\ \delta \; if \; \delta \geq \delta_{th} \end{cases} \tag{3.5}$$

$$if \; y > y_{th}, \tag{3.6}$$

$$then \int_{t_i}^{t_{i+1}} y(t)dt = A_r$$

In this model, the authors introduced a function h(x) (Eqs. 3.7 – 3.8) to relate the transducer signal to the response signal, which is not a physical model but rather a fitted model for different trapezoidal input pressures so that the modelled firing response matches the expected experimental firing response [27]. In this way the transduction mechanism of the actual baroreceptor is not physically modelled.

$$\tau\dot{y} + y = g(x, \dot{x}) \tag{3.7}$$

$$g(x, \dot{x}) = x + h(x)\dot{x} \tag{3.8}$$

$$h(x) = w_1 + w_2 x \tag{3.9}$$

Figure 3.1 shows how each of the model components relate the pressure to the baroreceptor firing response.

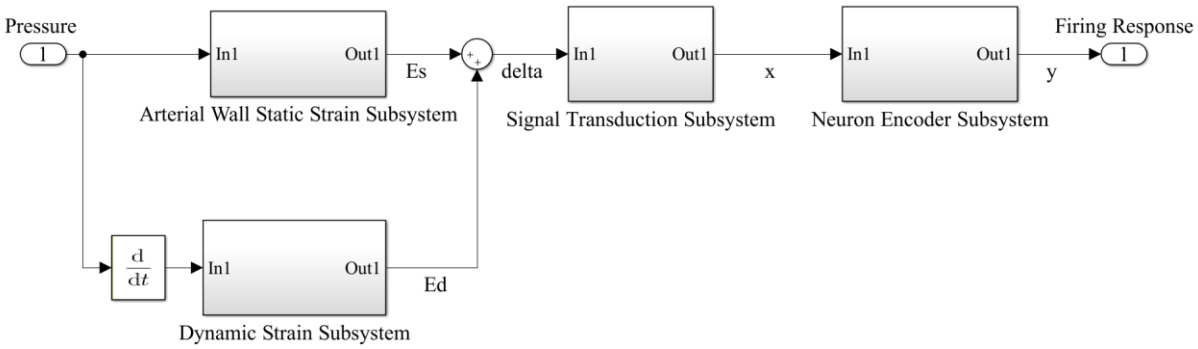

Figure 3.1: Schematic outline of subsystems in the Srinivasen and Nudelman baroreceptor model [27].

The conventional block diagram representation of the Srinivasen and Nudelman model is shown in Figure 3.2. The conventional block diagram represented in Figure 3.2, is modelled in Simulink. The Simulink block diagram is available in Appendix C, Figure C.7.1.

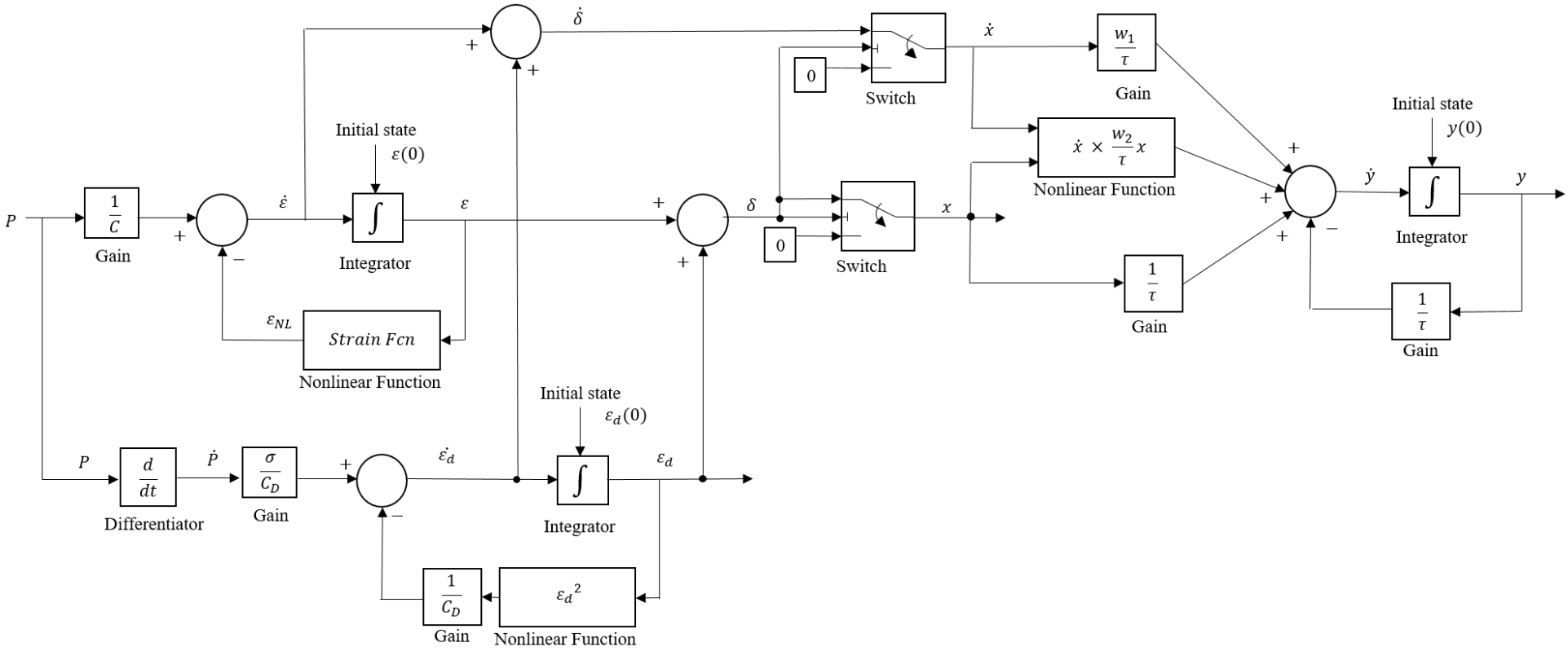

Figure 3.2: Conventional block diagram representing Srinivasen et al. baroreceptor model [27]

3.2.3 Model Behaviour Compared with Published Data

I implement this model in Simulink to assess its performance according to the reported behaviour. I then compare the Simulink outputs to results reported by Srinivasen et al. [26], [27]. The parameters used in the experiment described in their 1973 paper [27] are outlined in Table 3.2, and simulation outputs are shown in Figure 3.3 and Figure 3.4 below. The input pressure is a step at 0.01s from 46 mmHg to 202 mmHg at a rate of 1730 mmHg/sec. The initial conditions for this simulated experiment are as per the reported experiment in the Srinivasen et al. 1973 paper [27]. Note that I scaled the simulated firing response plotted in Figure 3.4 to show the maximum expected firing response, as per the reported results. In the Srinivasen et al. model, the firing response of the BR is highly sensitive to the rate of change of the step increase in pressure. Review of figure 5 in Srinivasen and Nudelman's experimental tests shows this feature of the model clearly [27]. Due to the nature of the model implementation in Simulink, each pressure change is implemented based on a defined time step. Based on the differential solver used to evaluate the model output at each time step, the rate of change of the pressure is averaged over time steps which are more granular than one second. This results in a small artifact in the summed number of pulses per second. In this way, scaling is necessary to remove the slight difference in the sum of BR pulses per second (simulated response for firing rate), caused by the simulated time steps for the experiment.

Table 3.2: Parameter-Value pairs for Step Input (46 – 202 mmHg) Pressure Experiment [27]

Parameter	Value	Units	Parameter	Value	Units
A	195.5000	mmHg	w_1	-0.0660	unitless
β	0.4000	unitless	w_2	0.2600	unitless
A_r	0.0072	unitless	σ	0.0004	N/m^2
δ_{th}	0.1210	unitless	C_D	0.1100	unitless
C	2.0000	unitless	τ	0.0400	s

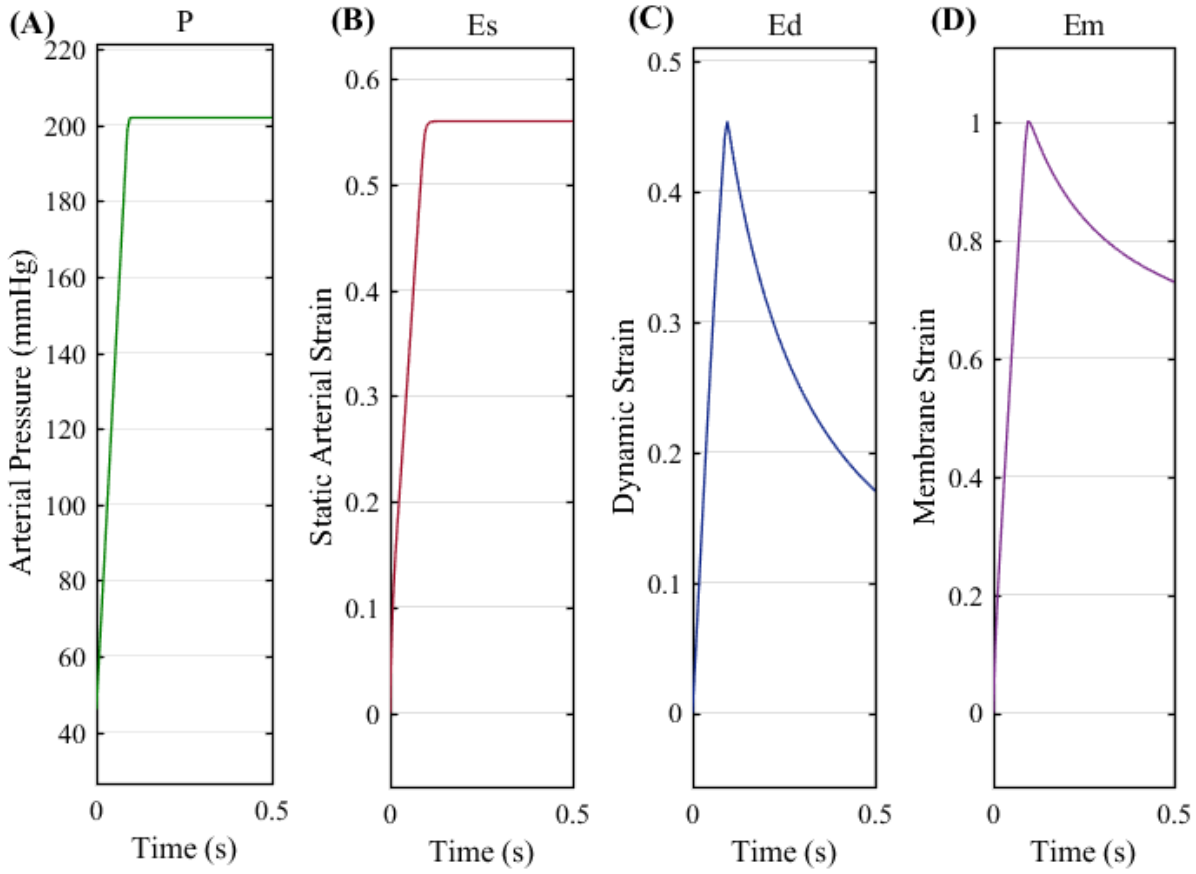

Figure 3.3: Simulink modelled states based on input pressure (A), static arterial strain (B), dynamic strain (C) and combined membrane strain (D) generated by Simulink implementation of the Srinivasen and Nudelman baroreceptor model [27]

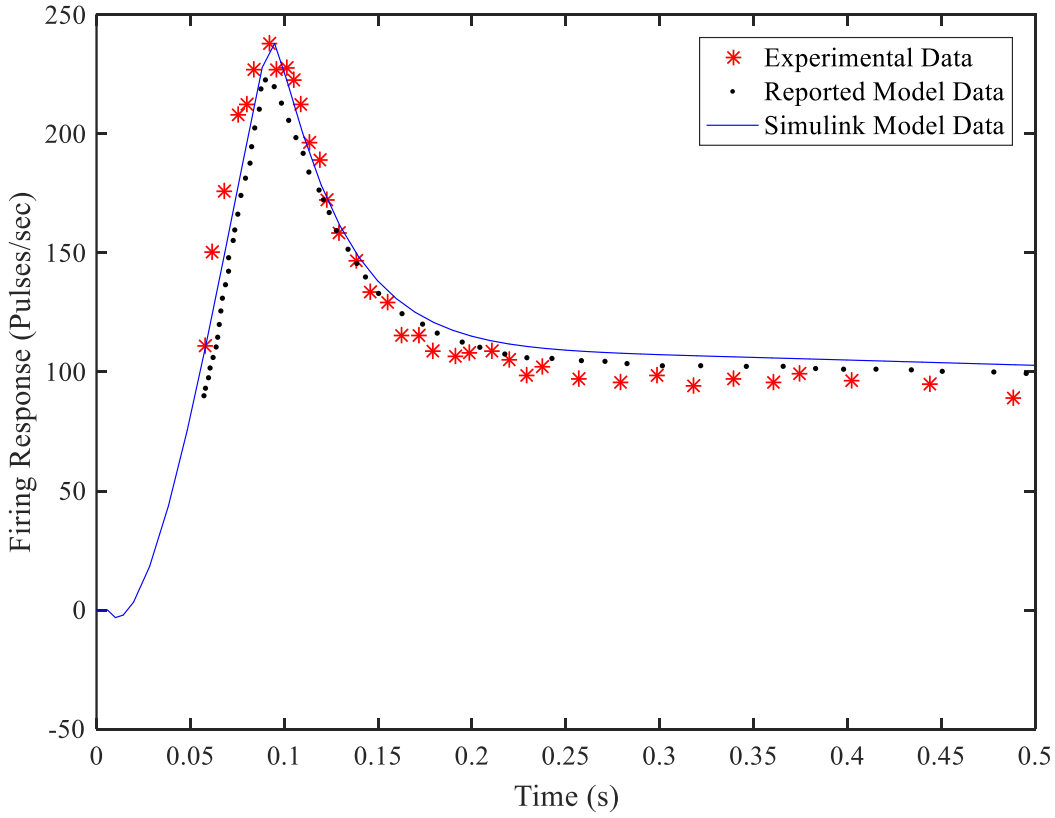

Figure 3.4: Comparison between experimental and reported firing responses generated by Simulink implementation of the Srinivasen and Nudelman baroreceptor model [27]

3.3 Bugenhagen et al. Baroreceptor Model

3.3.1 Model Context

Bugenhagen et al. adapted their non-linear elastomeric model of the strain in the arterial wall from a similar model based on a pressure-area relationship [22]. This similar model is a 3-parameter empirical model, which Bugenhagen explains is from the pressure-area relationship proposed by Langewouters et al. [22]. In this model the non-linearity is modelled with an inverse tangent curve, whereas Srinivasen et al used the functional inverse of the hyperbolic cotangent. Bugenhagen linearises the 3-parameter model into a 2-parameter model, using a fitted curve which approximates rat experimental data. Using this method, he shows that a linearised relationship between pressure and strain is adequate in the normal pressure range, but inadequate at extreme pressure ranges.

Bugenhagen also extends the dynamic strain model from Srinivasen's single Voigt body to three Voigt bodies for modelling viscoelastic coupling between the arterial wall and the baroreceptor nerve ending membrane. Mahdi et al. evaluates the effect of using different numbers of Voigt bodies in a

baroreceptor model based on its dynamic strain response to pressure [2] (discussed further in section 4.1.2).

The firing response generated by Bugenhagen et al.'s model is not a fitted response, but is the output of a physiological model based on the membrane strain, by adapting and simplifying Srinivasen's 'integrate and fire' model [22], [27]. This firing rate is the baroreceptor nerve discharge which is a function of the transduced strain at the baroreceptor nerve ending.

3.3.2 Model Equations and Description

This section describes the components of the model from Bugenhagen et al. of the baroreceptor response to pressure changes [22]. The model relates changes in pressure to the baroreceptor nerve through a static (elastomeric) strain and a dynamic strain (frictional coupling between arterial wall membranes). The total strain in the wall is transduced at the baroreceptor nerve ending using a specific sensitivity and pressure threshold, which initiates a firing response from the baroreceptor [22].

The model used for the strain at the arterial wall is altered from Srinivasen's more complex non-linear elastomeric model, to rather be represented by a three-parameter 'static empirical pressure-area relationship' based on experimental data [22]. Thereafter a dynamic strain model is included, based on the rate of change of that area. Although the three parameter non-linear model is shown by Bugenhagen et al. to compare well with experimental data from Andresen et al. [42], they further confirm that a two-parameter linearized model of the pressure-area relationship performs suitably well within the physiological range [22]. It is this linearised model that is used in this analysis, and presented here. Equations (3.10-3.12) show how arterial wall strain (ε_{wall}) is related to pressure (P), through wall compliance (C_{wall}) and the unstressed aorta radius (R_0), as well as the viscosity of the artery wall (B_{wall}).

$$A = \pi(R_0 + C_{wall}P)^2 \tag{3.10}$$

$$\dot{A} = \left(\frac{-\sqrt{\frac{A}{\pi}} + R_0}{B_{wall}C_{wall}}\right) + \frac{P}{B_{wall}} \tag{3.11}$$

$$\varepsilon_{wall} = \frac{\sqrt{\frac{A}{\pi}} - R_0}{R_0} \tag{3.12}$$

The dynamic model of the artery mechanics due to the frictional coupling of the arterial wall membrane is comprised of Voigt bodies. According to Bugenhagen et al., Voigt bodies model the different time constants of the resetting phases in the transduced strain. Physiologically, each element represents the mechanics associated with elasticity and viscosity in the arterial wall, the baroreceptor nerve ending, as well as in the connective tissue surrounding that nerve ending [22]. These elements are modelled by Eq. (3.13 – 3.16) in which the strain elements (ε_1, ε_2, ε_3) are functions of the respective elastic (K_1, K_2, K_3) and viscous (B_1, B_2, B_3) constants, and in which the elasticity of the baroreceptor nerve ending is represented as K_{ne} [22]. In this way the dynamic strain (δ) detected at the baroreceptor nerve ending is a function of the difference between the strain at the arterial wall (ε_{wall}) and the strain from the coupling across the different tissues and membranes.

$$\dot{\varepsilon_1} = \left(\frac{K_{ne}}{B_1}\right)\varepsilon_{wall} - \left(\frac{K_{ne} + K_1}{B_1}\right)\varepsilon_1 + \frac{K_1}{B_1}\varepsilon_2 + \dot{\varepsilon_2} \tag{3.13}$$

$$\dot{\varepsilon_2} = \left(\frac{K_1}{B_1 + B_2}\right)\varepsilon_1 - \left(\frac{K_1 + K_2}{B_1 + B_2}\right)\varepsilon_2 + \left(\frac{K_2}{B_1 + B_2}\right)\varepsilon_3 + \left(\frac{B_1}{B_1 + B_2}\right)\dot{\varepsilon_1} + \left(\frac{B_2}{B_1 + B_2}\right)\dot{\varepsilon_3} \tag{3.14}$$

$$\dot{\varepsilon_3} = \left(\frac{K_2}{B_2 + B_3}\right)\varepsilon_2 - \left(\frac{K_2 + K_3}{B_2 + B_3}\right)\varepsilon_3 + \left(\frac{B_2}{B_2 + B_3}\right)\dot{\varepsilon_2} \tag{3.15}$$

$$\delta = \varepsilon_{wall} - \varepsilon_1 \tag{3.16}$$

Thereafter the firing response of the baroreceptor nerve is modelled with a simplified integrate and fire model, as seen in Eq. (3.17). The firing response (n) initiated if the strain at the baroreceptor nerve ending (δ) exceeds the baroreceptor threshold strain (δ_{th}), is a function of the strain sensitivity (S) and the jump frequency parameter (ζ) [22].

$$n = \begin{cases} 0\,, if\ \delta < \delta_{th} \\ S(\delta - \zeta\delta_{th})\,, if\ \delta \geq\ \delta_{th} \end{cases} \tag{3.17}$$

The subsystems shown below in Figure 3.5 show the relationships between the model subsystems. The block diagram for the expanded subsections of the model is shown in Figure 3.6, where the colours highlight the separate subsystems. The equations above are described with reference to the variables in Figure 3.6.

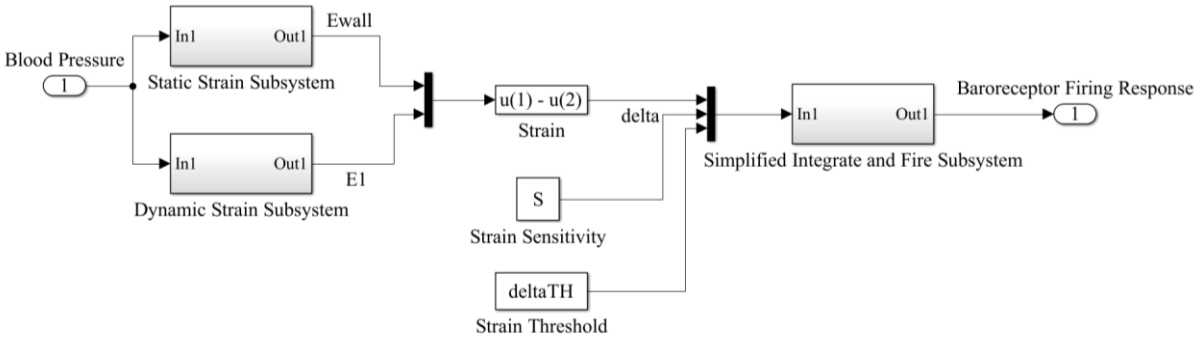

Figure 3.5: Bugenhagen et al. baroreceptor model with model components shown as subsystems [22]

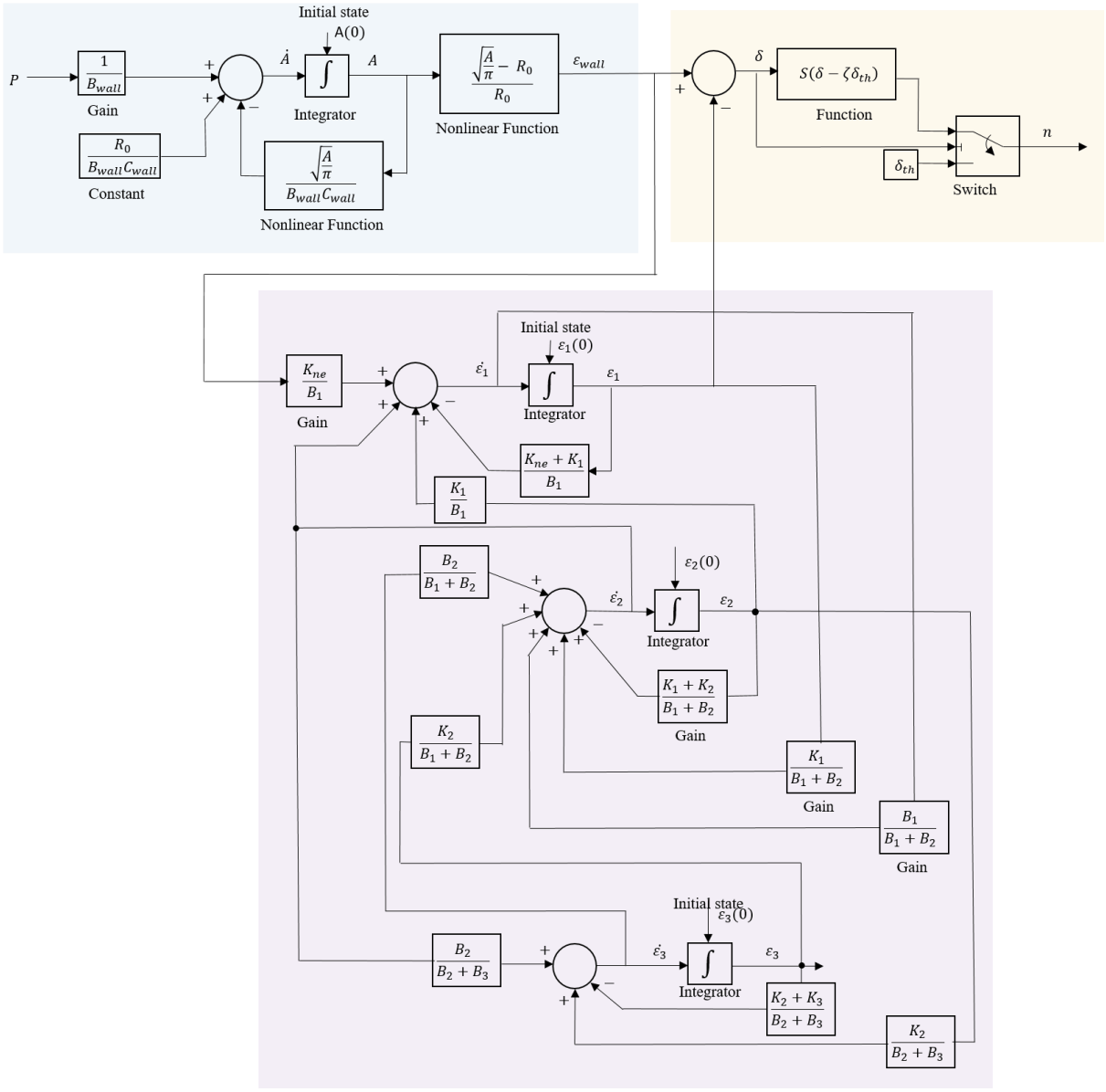

Figure 3.6: Conventional block diagram representing the Bugenhagen et al. baroreceptor model [22].

The block diagram of the implementation of the model components in Simulink, as per the subsystems shown in Figure 3.6 are available in Appendix C, Figure C.7.2 to Figure C.7.4.

3.3.3 Model Behaviour Compared with Published Data

I implement this model in Simulink and compare its performance with simulated and experimental data from WKY rats published by Bugenhagen et al. [22].

The parameters for one of the experiments described in the Bugenhagen paper [22] are presented in Table 3.3. Plots of simulated static arterial strain, dynamic strain and membrane (combined) strain are presented in Figure 3.7. Simulated firing response based on the parameters as reported by Bugenhagen is shown in Figure 3.8, while the result after optimising one parameter ($K_{1(optimised)}$) is shown in Figure 3.9. The input is a step in pressure from 0 mmHg to 230 mmHg at 3.0 s. The initial conditions for the differential states in this simulation are determined from simulating the model at 0 mmHg for 3 s.

Note that I have scaled the magnitude of the firing response in Figure 3.8 and Figure 3.9 to remove the slight difference in the sum of BR pulses per second (simulated response for firing rate), caused by the simulated time steps for the experiment.

Table 3.3: Parameters for Step Input (0 – 230 mmHg) Pressure Experiment

Parameter	Value	Units	Parameter	Value	Units
K_{ne}	1.000	mmHg/mm	S	255.000	Hz
K_1	1.500	mmHg/mm	δ_{th}	0.200	unitless
K_2	3.750	mmHg/mm	ζ	1.000	unitless
K_3	1.050	mmHg/mm	$\varepsilon_{1_{initial}}$	0.204	unitless
B_1	1.000	mmHg x s/mm	$\varepsilon_{2_{initial}}$	0.232	unitless
B_2	10.000	mmHg x s/mm	$\varepsilon_{3_{initial}}$	0.149	unitless
B_3	300.000	mmHg x s/mm	R_0	1.600	mm
B_{wall}	1.000	mmHg x s/mm	$K_{1(optimised)}$	1.950	mmHg/mm
C_{wall}	0.006	mm/mmHg			

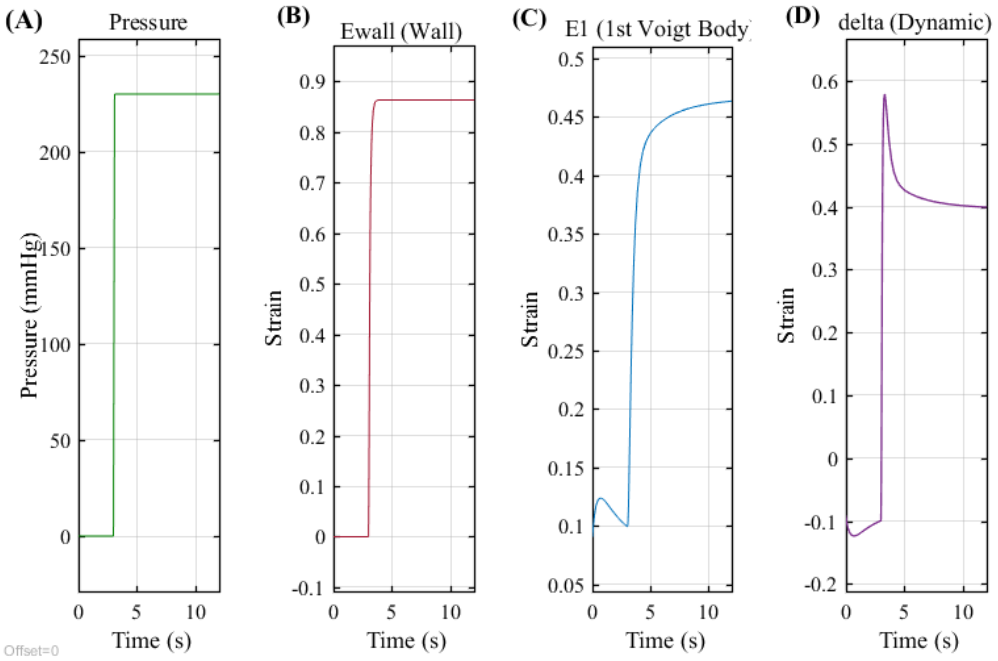

Figure 3.7: Simulink modelled states based on input pressure (A), static arterial strain (B), dynamic strain (C) and combined membrane strain (D) with $K_{1(optimised)}$.

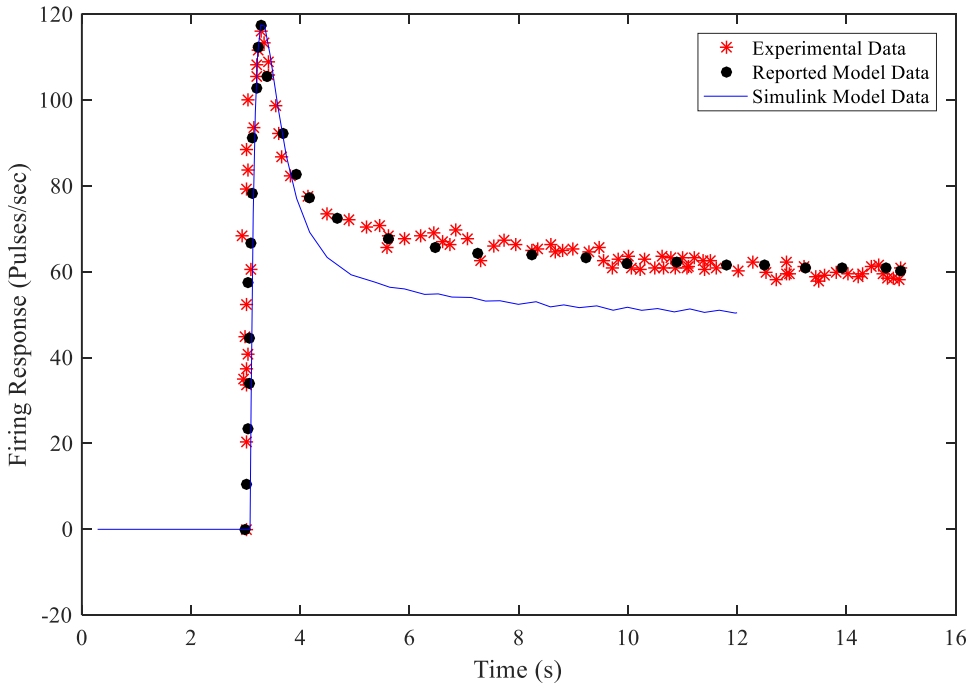

Figure 3.8: Comparison between firing responses simulated in this study, and published experimental and simulated data (Bugenhagen et al. [22]). Model parameters as in Table 3.3

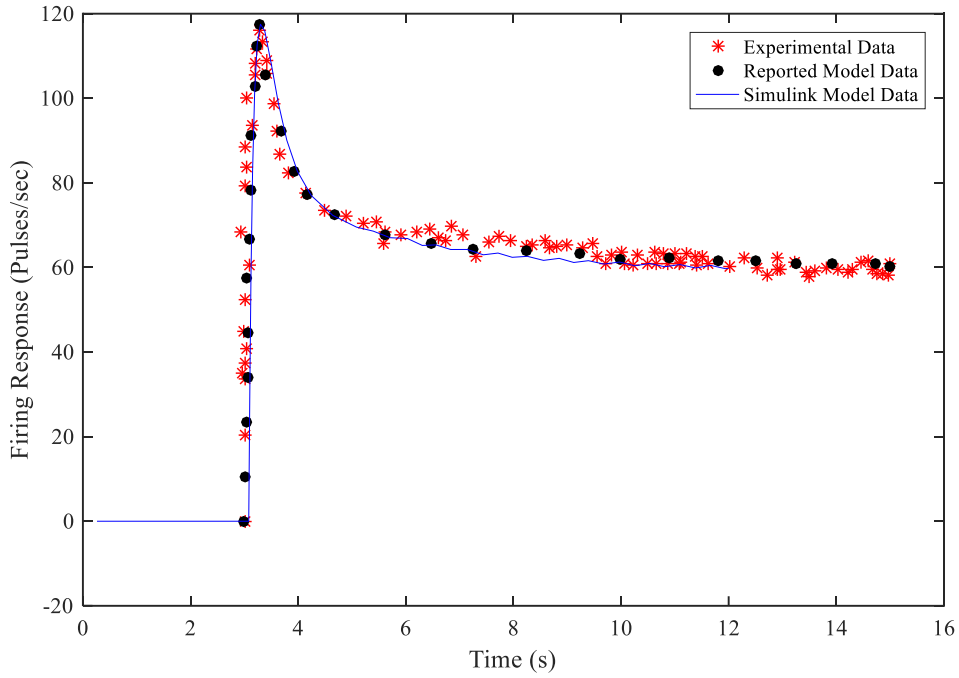

Figure 3.9: Comparison between firing responses simulated in this study, and published experimental and simulated data (Bugenhagen et al. [22]). Model parameters as in Table 3.3 (Optimised K_1)

3.4 Beard et al. Baroreceptor Model

3.4.1 Model Context

This model of the baroreceptor is based on how a changing pressure in a thin walled and compliant cylinder, affects the rate of change of strain in the vessel wall [14]. This model of the pressure-strain relationship is an alternative to the combined membrane strain (from static and dynamic strain elements), and includes a time constant for relaxation as well as factors for acute and chronic compliance in the vessel wall [14]. The firing of the baroreceptor is a function of how quickly the strain changes at the arterial wall, a saturating static non-linearity for that change, and how many baroreceptor afferent fibres are available for discharge [14]. This model is found to be more adept at handling experimental data from different species than the model from Srinivasen et al. or from Bugenhagen et al. Essentially, this model is an alternative to the techniques from Srinivasen et al [27]; Bugenhagen et al [22]; and Mahdi et al [2]. Parameterisation, initial conditions, and experimental test data are explicitly defined in the paper. This allows a more thorough analysis of the model behaviour.

3.4.2 Model Equations and Description

As shown in Eq. (3.18), the rate of change of the aortic volume (V_{Ao}) is a function of the aortic compliance (C_{Ao}) and the effective rate of change of the creep stress volume of the aorta ($\dot{V}_{sAo}$).

$$\dot{V}_{Ao} = C_{Ao}\dot{P}_{Ao} + \dot{V}_{sAo} \tag{3.18}$$

Eq. (3.19-3.20) show the creep mechanics for the creep stress aorta volume (V_{SAo}), as parameterised with a time constant of stress relaxation (τ_{CAo}) and a long-term/chronic creep stress volume ($V_{SAo}{}^{\infty}$). This long-term creep stress volume ($V_{SAo}{}^{\infty}$) is related to the aorta volume (V_{Ao}) by a factor (γ_{Ao}). This factor represents a ratio of the acute to the effective long-term compliance in the vessel.

$$\dot{V}_{sAo} = \frac{1}{\tau_{CAo}}(V_{sAo}{}^{\infty} - V_{sAo}) \tag{3.19}$$

$$\dot{V}_{sAo} = \frac{1}{\tau_{CAo}}(\gamma_{Ao}V_{Ao} - V_{sAo}) \tag{3.20}$$

The strain at the baroreceptor nerve ending (δ_{ε}) is related to the strain at the arterial wall (ε) as a function of the aortic volume (V_{Ao}), the unstressed volume (V_0), the average rate of change in that strain ($\dot{\bar{\varepsilon}}$) and an adjustable time constant (τ_s). These relationships are expressed in Eq. (3.21-3.23)

$$\dot{\varepsilon} = \frac{1}{2}\left(\frac{1}{\sqrt{V_{Ao}V_0}}\right) \tag{3.21}$$

$$\dot{\bar{\varepsilon}} = \frac{1}{\tau_s}(\varepsilon - \bar{\varepsilon}) \tag{3.22}$$

$$\delta_{\varepsilon} = \tau_s\dot{\bar{\varepsilon}} \tag{3.23}$$

The fraction of the baroreceptor afferent fibres (s), which are in an active state for discharge, is determined through the dynamic relationship between adjustable parameters (a and b) and the effective change in the membrane strain (δ_{ε}). The rate of change of that fraction. Eq. (3.24) is physiologically analogous to muscle fibre recruitment during exercise [14]. Eq. (3.25) shows how the baroreceptor firing response is therefore a function of the available baroreceptor afferent fibres, the changing membrane strain, and the existing firing rate.

$$\dot{s} = a(1 - s) - bs\left(\frac{\delta_{\varepsilon}}{\delta_{\varepsilon} + \delta_0}\right) \tag{3.24}$$

$$f_{BR} = f_0 s\left(\frac{\delta_{\varepsilon}}{\delta_{\varepsilon} + \delta_0}\right) \tag{3.25}$$

The subsystems in Figure 3.10 show the relationships between the model components.

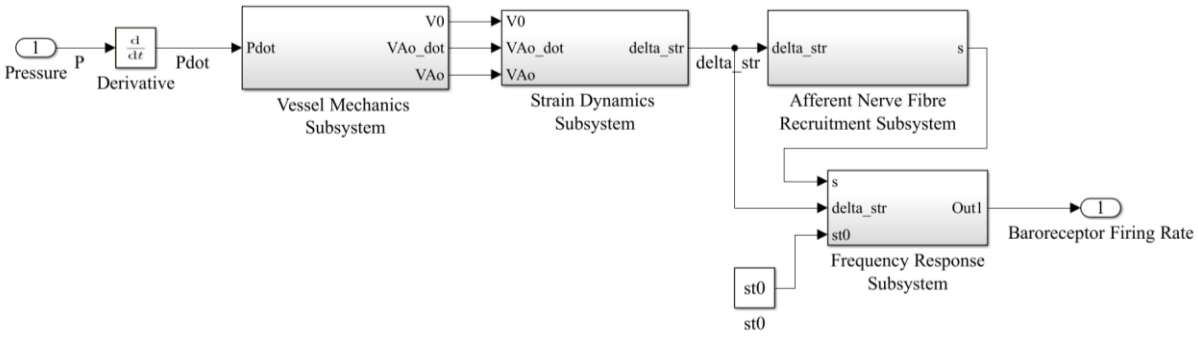

Figure 3.10: Beard et al. baroreceptor model with model components shown as subsystems [14]

The block diagram for the expanded subsections of the model is shown in Figure 3.11. The equations above are described with reference to the variables in Figure 3.11.

The block diagram for the implementation of the model components in Simulink, as per the subsystems shown in Figure 3.10 is in Appendix C, Figure C.7.5 to Figure C.7.8.

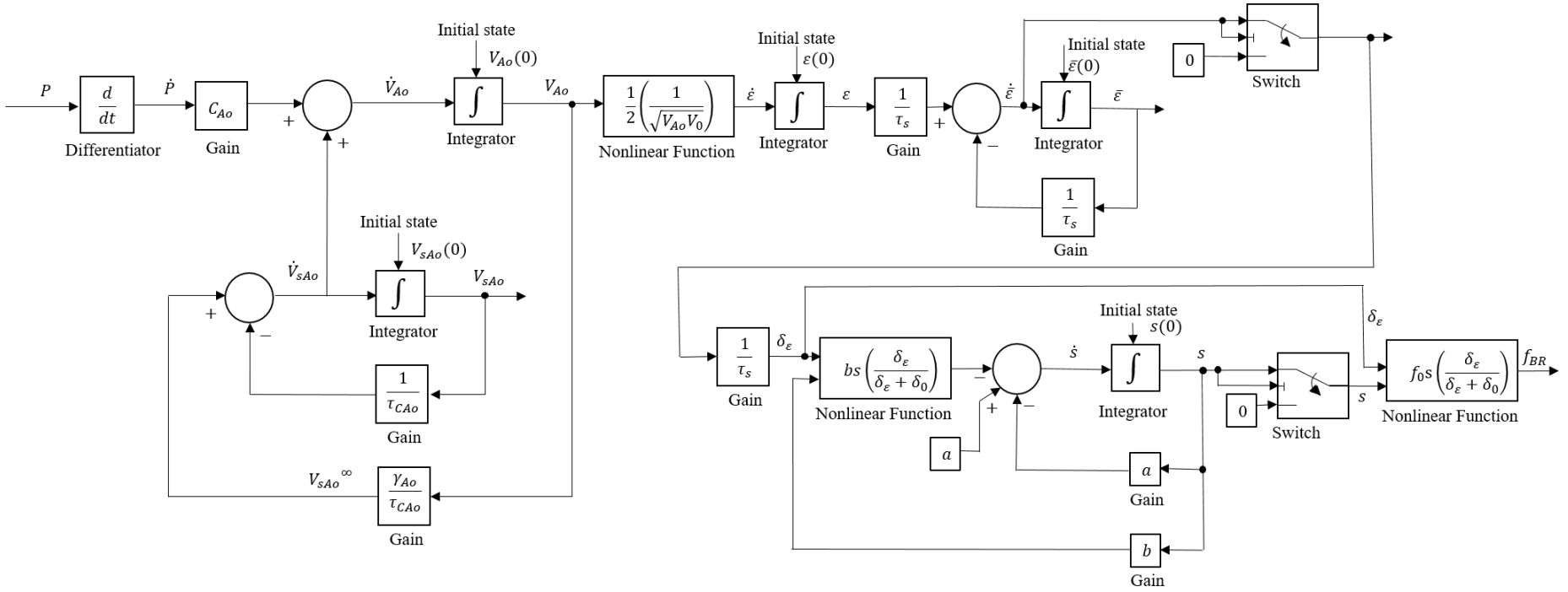

Figure 3.11: Conventional block diagram representing the Beard et al. baroreceptor model [14]

3.4.3 Model Behaviour Compared with Published Data

Beard et al. used many different experiments on different species to test and evaluate this model [14]. Initially, the large artery mechanics component was parameterised on dog aortic pulsatile pressure (for the pressure-radius relationship) [14]. Thereafter adjustable parameters were determined from non-pulsatile step input pressure experiments on dog carotid sinuses [43] and then again from in-vivo pulsatile ramp input pressure experiments on dog aortas [14], [44].

Beard et al. modelled the closed loop baroreflex in MATLAB, and made the source code available through 'https://zenodo.org/record/7126' [14]. In the current study, I have adapted the baroreceptor subsystems from Beard et al's closed-loop model to simulate an open-loop baroreceptor in Simulink.

I use the parameters shown in Table 3.4 to model the experiment, as reported by Chapleau et al. [43]. These parameters were reported by Beard et al., and were used for open-loop simulation in Simulink [14]. The parameters are slightly adjusted to compensate for Beard et al's MATLAB closed loop baroreflex model [14]. This experiment involved a step input pressure from 46 – 93 mmHg at a rate of 53 mmHg/s from 1s. I simulated the resting conditions in MATLAB to determine initial conditions, before running the Simulink model with experimental conditions. These are listed in Table 3.5.

Table 3.4: Parameters used to simulate the experiment of Chapleau et al. [14]

Parameter	Value	Units	Parameter	Value	Units
d_0	12.0000	mm	τ_s	251.5250	sec
L	30.0000	mm	a	0.0651	/sec
V_0	0.6875	ml	b	0.2004	/sec
C_{Ao}	0.0070	ml/mmHg	δ_0	0.4965	unitless
γ_{Ao}	0.4000	unitless	f_0	299.7511	/sec
τ_{CAo}	0.1200	sec			

Table 3.5: Initial conditions required to model the Chapleau et al experiment

Parameter	Value	Units	Comments
$V_{SAo_{initial}}$	0.1867	ml	Initial condition (calculated)
$V_{Ao_{initial}}$	0.4667	ml	Initial condition (calculated)
$\bar{\varepsilon}_{initial}$	0.8239	unitless	Initial condition (calculated)
$s_{initial}$	1.0000	unitless	Initial condition (assumed)

In the Chapleau experiment, the input variable is not pressure but the rate of change of pressure. Therefore my Simulink model is updated to use the rate of change of input pressure for this experiment. Beard et al made use of a stiff variable step solver in MATLAB (ode23s), which was matched in the Simulink model. Results of simulating the Chapleau experiment are shown in Figure 3.12 and Figure 3.13.

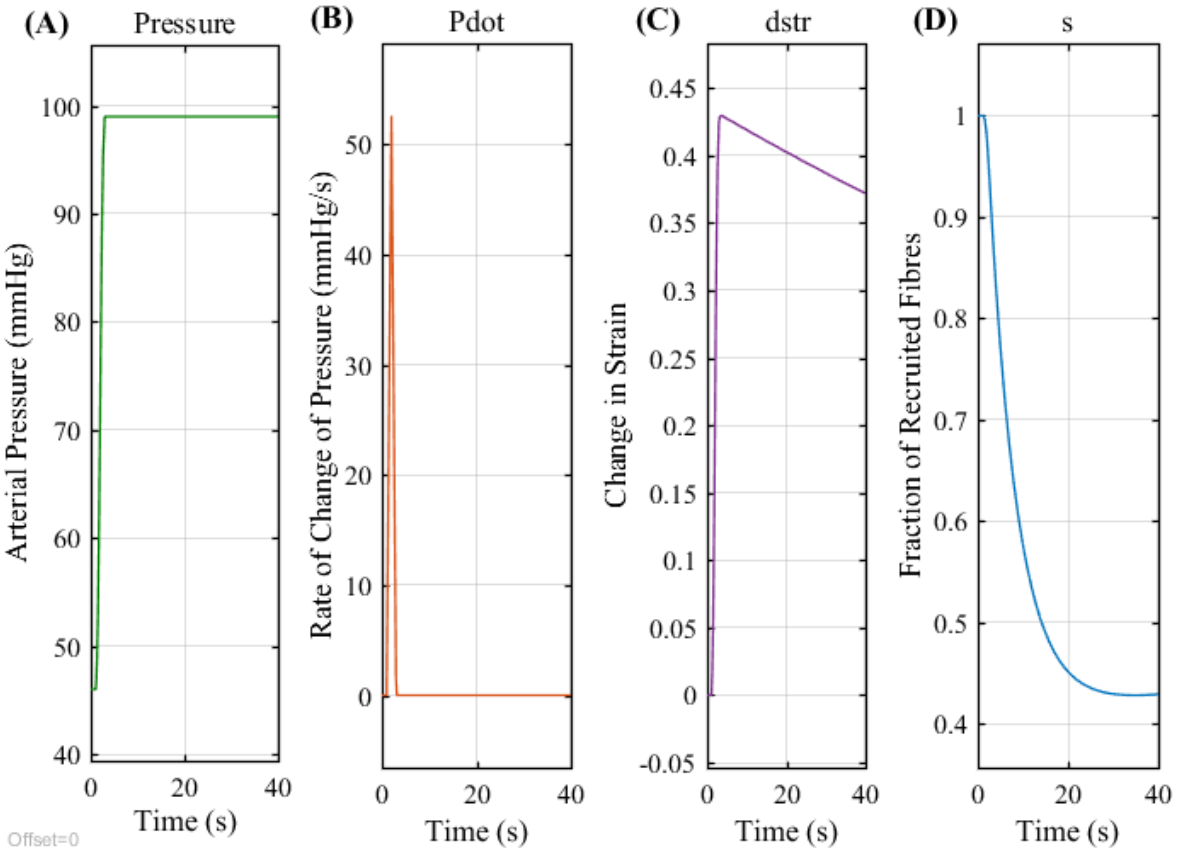

Figure 3.12: Simulink modelled states based on pressure (A), for differential input pressure (B), total membrane strain (C) and baroreceptor afferent fibre activity (D)

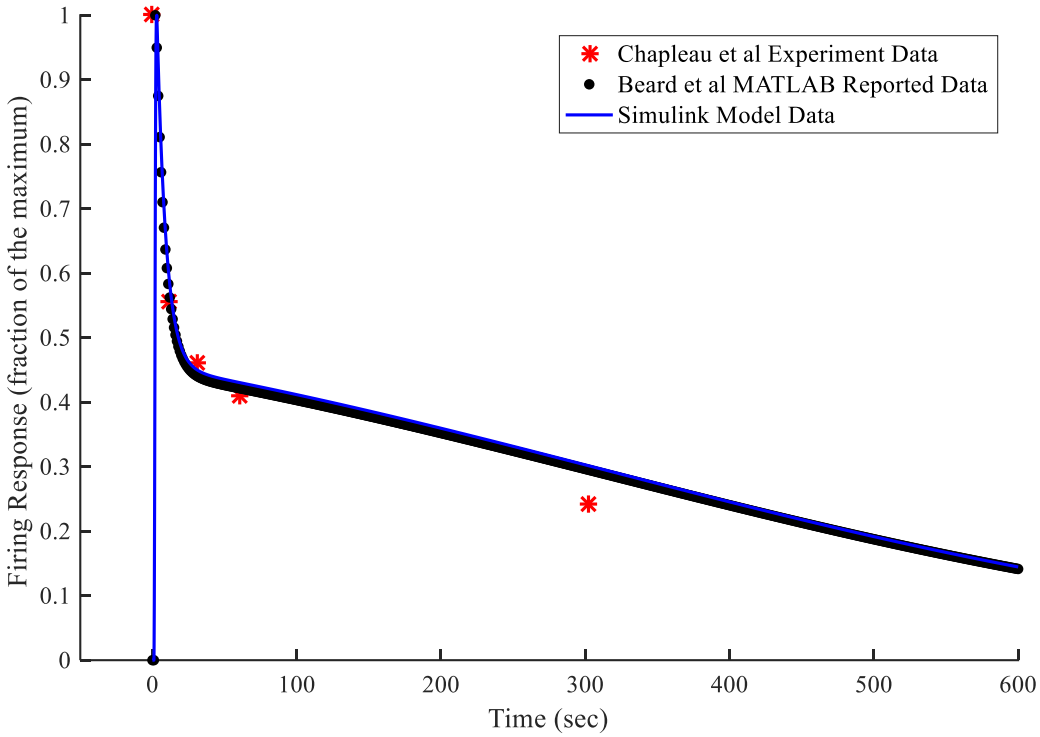

Figure 3.13: Comparison of experimental firing from Chapleau et al. [43], reported firing from Beard et al. [14] and simulated firing following a step change of pressure.

A step increase volume input for an in-vivo experiment was used to test the model by Beard et al., as shown in Figure 3.14. The results in Figure 3.15 highlight how well the open-loop Simulink model, when adjusted for a volume input, predicts the results from Beard's closed loop MATLAB model. Beard et al. use experimental results from Guyton and colleagues, in which large volumes of blood where infused into an anaesthetised dog's aorta for 5 min, followed by a recovery period of 30min [14].

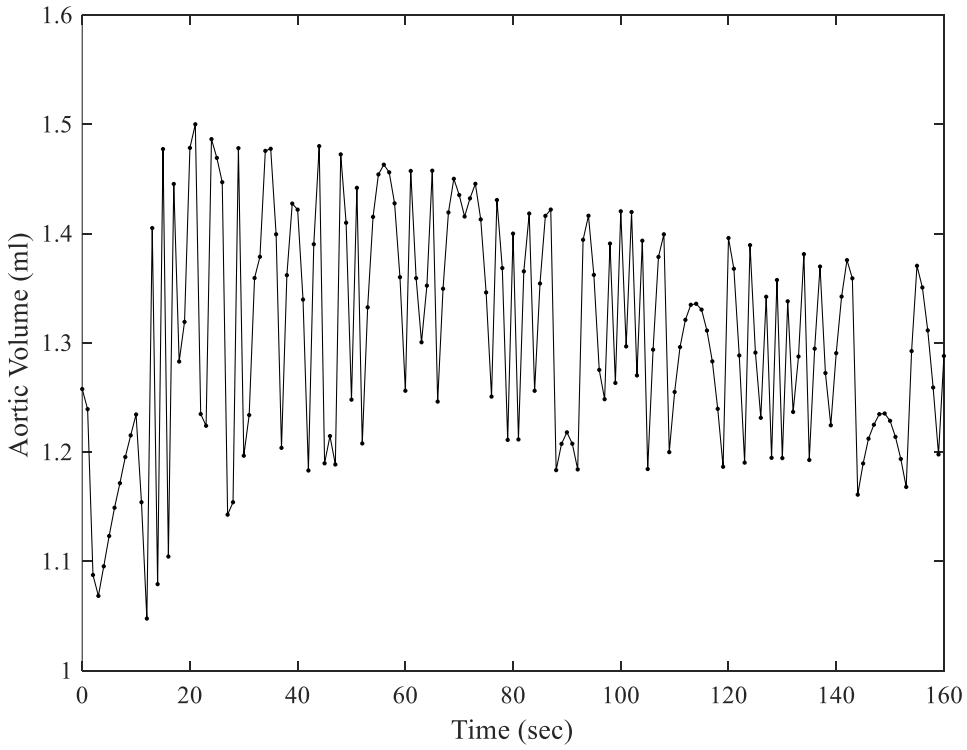

Figure 3.14: Aortic volume step infusion for Guyton et al. [45] experiment

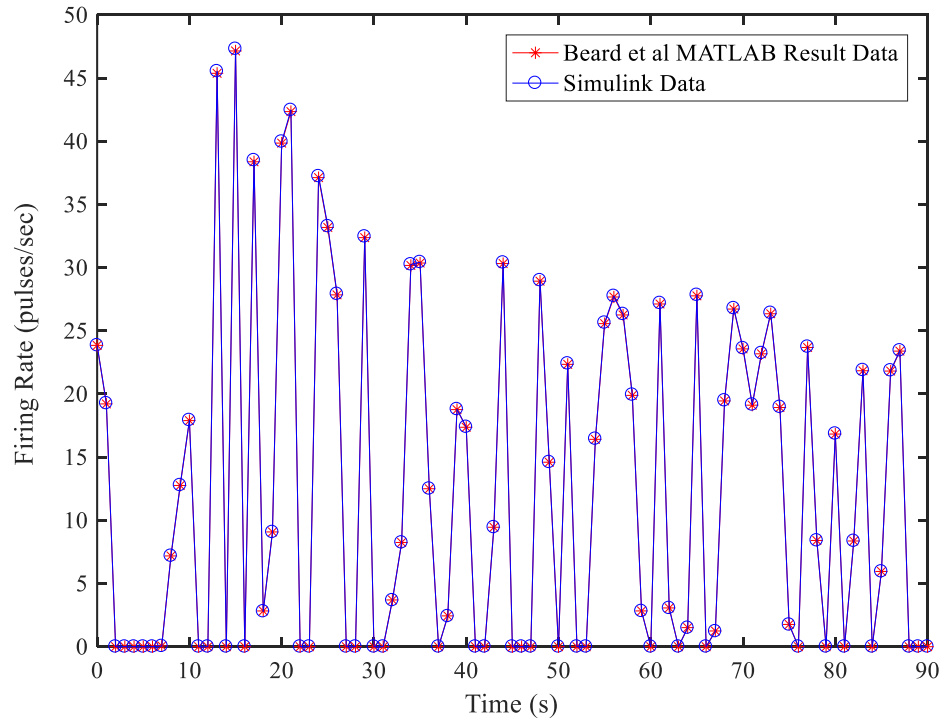

Figure 3.15 Firing Rates calculated by the Beard et al. MATLAB model and the Simulink model of the present study.

Beard et al. used their model to simulate the experiments of Quail et al. on rabbits [14]. The animals underwent a 17.5 min haemorrhage, starting at time t = 0, from a baseline MAP of 100 mmHg. Aortic volume measured during haemorrhage (shown in Figure 3.16 was used as model input. Simulated firing rates calculated by the closed-loop MATLAB model of Beard at al. and my open-loop Simulink model are shown in Figure 3.17. This simulation shows the model's ability to perform under pulsatile haemorrhage conditions.

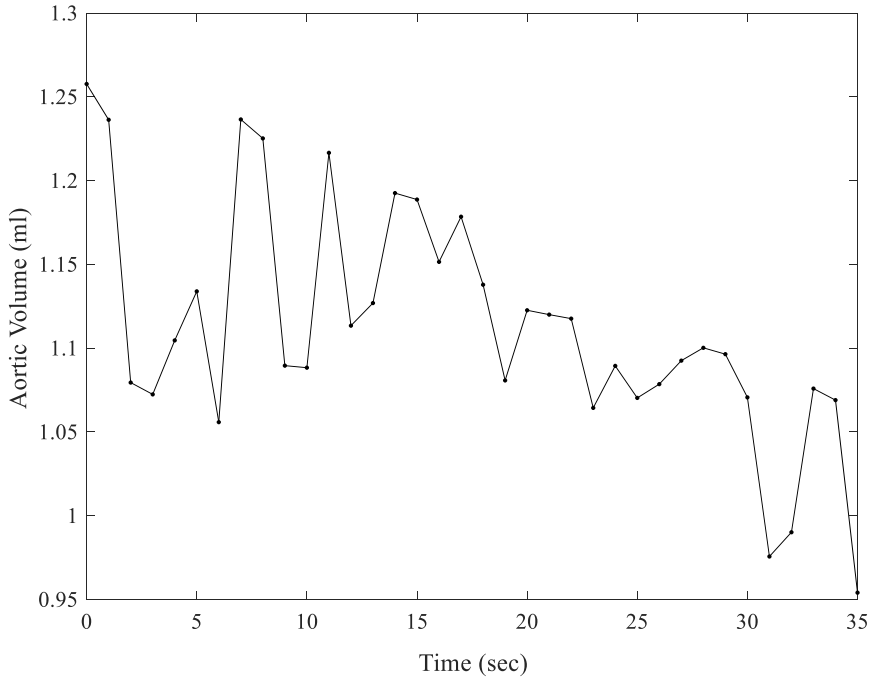

Figure 3.16: Aortic volume changes during the Quail et al. haemorrhage experiment [46]

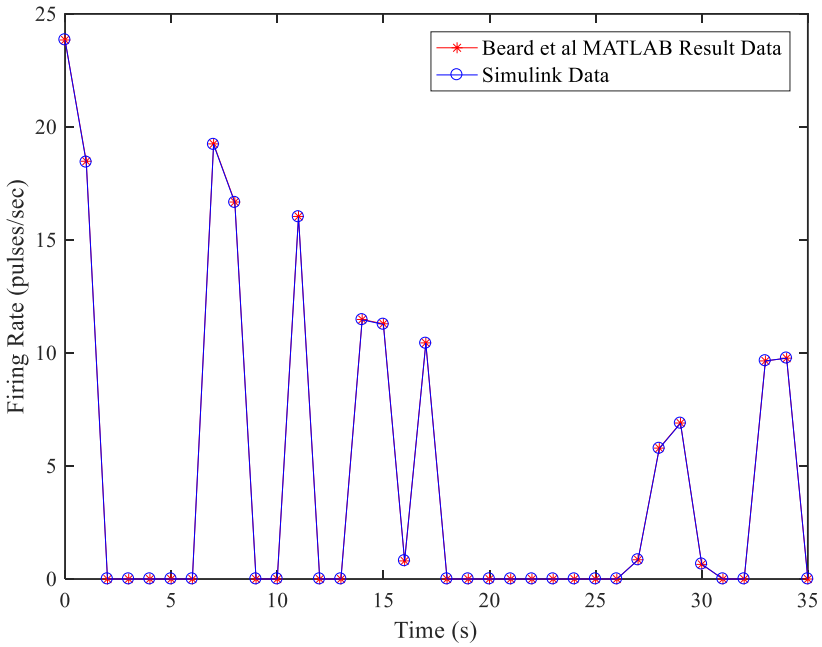

Figure 3.17: Firing Rates calculated by the Beard et al. MATLAB model and the Simulink model of the present study.

3.5 Mahdi et al. Baroreceptor Model

3.5.1 Model Context

Mahdi et al. present a number of different combinations for the composition of a baroreceptor model. They investigate different methods for modelling the arterial wall strain, the transmission of strain from the arterial wall to the baroreceptor nerve ending membrane, and for calculating the firing response from the transduced strain at the nerve ending. Their findings show that the combination of a non-linear elastic wall model for arterial wall deformation (W_{ne}), a two Voigt body model for mechanoreceptor stimulation (V_2), and a leaky integrate-and-fire model for the baroreceptor firing rate (N_{IF}), produces the best quantitative and qualitative response [2]. Two of the models presented by Mahdi et al. [2] are investigated in the present study: the simplified amplifier model ($W_{ne}V_2N_a$) and the integrate-and-fire model ($W_{ne}V_2N_{IF}$). These two models are made up of the same equations for arterial wall strain (W_{ne}) and Voigt body arterial wall mechanics (V_2), but differ in their equations for signal transmission and firing response. I compare both the simplified amplifier model and the integrate-and-fire model to the other researchers' model components for signal transmission and firing response (see section 4.1).

In context, the arterial wall deformation component in the integrate-and-fire model from Mahdi et al. aligns with similar techniques for modelling arterial wall deformation in the Srinivasen et al. and Bugenhagen et al. models [2], [22], [27]. The main difference being that parametrisation of the

pressure-radius curve in the Mahdi et al. model isn't species specific. The mechanoreceptor stimulation, associated with dynamic strain or transmission of stress across the membranes in the arterial wall, is modelled with two Voigt bodies instead of three as in the Bugenhagen et al. model. The leaky integrate-and-fire model of the baroreceptor firing response in the Mahdi et al. model is much more sophisticated than the version in the Srinivasen et al. model [2], [27]. This is apparent because in the Srinivasen et al. model, a polynomial needed to be fitted to match a certain expected firing response [27]. In the Bugenhagen et al. model the technique is similar to Mahdi's simplified amplifier model, where the sensitivity and gain are linearly applied to the strain at the baroreceptor membrane when it is above threshold [22]. Lastly, although the Beard et al. model uses a different technique for baroreceptor afferent fibre recruitment combined with a static non-linearity for a saturating response, it does not make use of any fitted functions and the parameterisation of the function is not species dependent [14].

3.5.2 Model Equations and Description

The Mahdi models discussed here are based on three main subsystems, the arterial wall subsystem; the strain dynamics subsystem; and the firing response subsystem [2]. The behaviour of both types of firing response models, the simplified amplifier and the integrate-and-fire, are discussed here.

Mahdi et al have selected a non-linear elastic model for the arterial wall strain component of their baroreceptor model. This non-linear elastic model (W_{ne}) is represented in Eq. (3.26) and Eq. (3.27) below, where the area of the artery (A) is a function of the unstressed area (A_0) and the maximum area (A_m). The area of the artery is also characterised by the saturation pressure (α) and the vessel distensibility (k) under pressure (p) [2].

$$A = (A_m - A_0)\frac{p^k}{\alpha^k + p^k} + A_0 \tag{3.26}$$

$$\varepsilon_w = 1 - \sqrt{\frac{A_0(\alpha^k + p^k)}{A_0\alpha^k + A_m p^k}} \tag{3.27}$$

Mahdi et al have also shown that two Voigt bodies are sufficient to capture the dynamics of the transmission through the connective tissue and baroreceptor membrane [2]. Based on this, their best model for the strain dynamics is represented with the coupling of strain through two spring-damper bodies (V_2). These spring damping bodies are modelled with elastic and viscous constants that are captured as nerve ending constants (α_1, α_2, and α_3) and nerve ending relaxation rates (β_1, β_2, and β_3) [2]. In this way, the strain at the nerve ending (ε_{ne}), will be the strain directly applied to the inner side of the wall (ε_w), less the strain encountered through the different tissues between the inner side of the wall and the outer-most side of the wall where the nerve ending rests (ε_1) [2]. The relationship between these different elements is captured in Eq. (3.28) to Eq. (3.30).

$$\dot{\varepsilon_1} = -(\alpha_1 + \alpha_2 + \beta_1)\varepsilon_1 + (\beta_1 - \beta_2)\varepsilon_2 + (\alpha_1 + \alpha_2)\varepsilon_w \tag{3.28}$$

$$\dot{\varepsilon_2} = -\alpha_2\varepsilon_1 - \beta_2\varepsilon_2 + \alpha_2\varepsilon_w \tag{3.29}$$

$$\varepsilon_{ne} = \varepsilon_w - \varepsilon_1 \tag{3.30}$$

The baroreceptor firing rate is modelled in two ways, one with a simplified amplifier (N_a – Eq. (3.31)) and the other with a 'leaky integrate-and-fire model' (N_{IF} – Eq. (3.32-3.34)). Mahdi et al show in their paper that the integrate-and-fire model has the best response for post-excitatory depression and for qualitative responses such as rectification, saturation, adaptation and asymmetry [2]. Both these models were simulated in Simulink and were used to compare different features of other models. The simplified amplifier model of the firing rate is later used to compare the dynamic strain of other models, whereas the integrate-and-fire model is used to extend the comparison of the firing rate responses of the other models.

The simple amplifier model relates the frequency of the baroreceptor (f_{N_a}) to the strain at the nerve ending (ε_{ne}) through one constant for a baroreceptor gain (s_1) and another for the baroreceptor shift (s_2).

$$f_{N_a} = s_1 \varepsilon_{ne} - s_2 \tag{3.31}$$

The integrate-and-fire model for baroreceptor is based on an analogy for a membrane which is electrically excitable, where the nerve action potential is modelled as the discharge of voltage through a capacitor circuit. This voltage discharge is based on whether the current generated from the strain at the nerve ending exceeds an expected threshold. Eq. (3.32-3.33) show that if the current generated exceeds the threshold ($g_{leak}V_{th}$), it is related to the strain in the nerve ending (ε_{ne}) through constants for gain and shift of the stimulus ($\bar{s_1}, \bar{s_2}$). The voltage in the membrane (V_m), is a function of the generated current (I_{ne}), based on model parameters such as capacitance (C_m) and leakage conductance (g_{leak}) of the membrane. In this way, the firing rate of the action potential ($f_{N_{IF}}$) is calculated from the time taken for the membrane voltage to discharge and to recover (t_{ref}) before another discharge is possible. For a more extensive explanation, please see the model description in the research from Mahdi et al [2].

$$I_{ne} = \bar{s_1}\varepsilon_{ne} + \bar{s_2} \tag{3.32}$$

$$\dot{V_m} = \frac{1}{C_m}(I_{ne} - g_{leak}V_m) \tag{3.33}$$

$$f_{N_{IF}} = \begin{cases} \left[\frac{C_m}{g_{leak}}\left[ln\left(\frac{I_{ne} - g_{leak}V_{th}}{I_{ne}}\right)\right] + t_{ref}\right]^{-1} & if\ I_{ne} > g_{leak}V_{th} \\ 0 & otherwise \end{cases} \tag{3.34}$$

The subsystems shown below in Figure 3.18 show the relationships between the Mahdi et al. model components, along with the two alternate firing response models as separate subsystems. The block diagram for the expanded subsections of the model is shown in Figure 3.19, in which the colours highlight the separate subsystems. The equations above are described with reference to the variables in Figure 3.19. The block diagram for the implementation of the model components in Simulink, as per the subsystems shown in Figure 3.18 are available in Appendix C, Figure C.7.9 to Figure C.7.12.

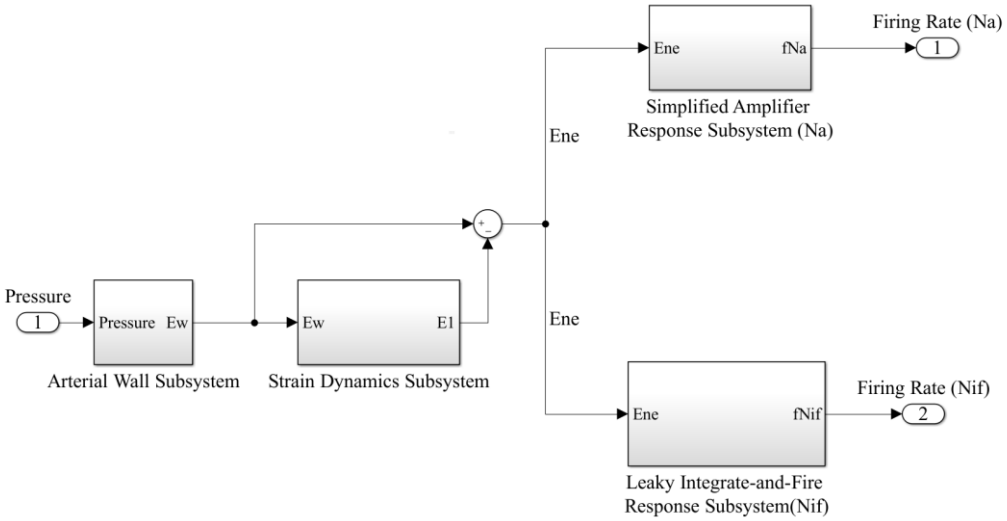

Figure 3.18: Mahdi et al. baroreceptor model with model components shown as subsystems [2].

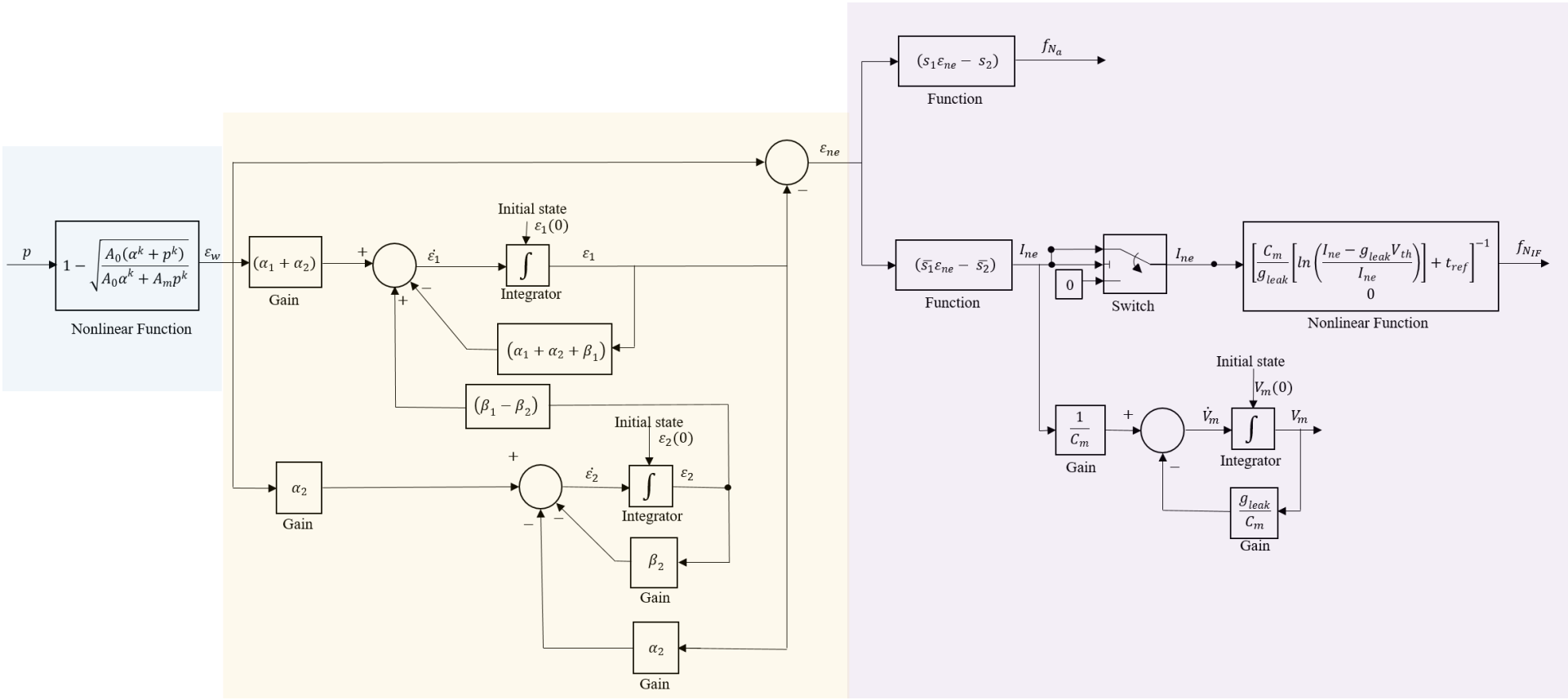

Figure 3.19: Conventional block diagram representing the Mahdi et al. baroreceptor model [2].

3.5.3 Model Behaviour Compared with Published Data

The analysis performed by Mahdi et al. shows that the integrate-and-fire model for the baroreceptor is the best model for capturing all the dynamics associated with their qualitative tests [2]. However, inconsistencies with the results reported by Mahdi et al., based on the parameters reportedly used and experimental inputs defined, are not explained. The comparative study by Mahdi and colleagues, are for a wide range of experiments for a selection of different models. In their paper, they do not report the parameter values used to confirm the qualitative responses for the simplified amplifier model ($W_{ne}V_2N_a$) or the integrate and fire model ($W_{ne}V_2N_{IF}$) [2].

Subsequently, the parameters used to produce the experimental results in Figure 10 of their paper [2], which shows an array of outputs of the integrate-and-fire model ($W_{ne}V_2N_{IF}$) under different stimuli (sinusoidal, step-increase, ramp-increase and triangular inputs) were not available to me. This means that I could not simulate an experiment to successfully reproduce the reported results.

However, output data and parameters for their step input experiment on an elastic arterial wall, two Voigt body, simple amplifier model (based on Figure 8 of their paper for $W_eV_2N_a$) is available [2]. The parameters I used are shown below in Table 3.6, with the direct comparison of the simulated results shown in Figure 3.20. For comparisons of how this model performed to step and step-pulsatile inputs with its integrate-and-fire counterpart, and with the other models, please see sections 4.1.2 and 4.1.3.

Table 3.6: Parameters as per Table 6 for Figure 8 of the Mahdi et al. paper [2].

Parameter	Value	Units
alpha1	0.4490	mm
alpha2	0.3666	mm
beta1	0.4850	ml
beta2	1.9226	ml/mmHg
s1	1041.5000	unitless
s2	342.4934	sec

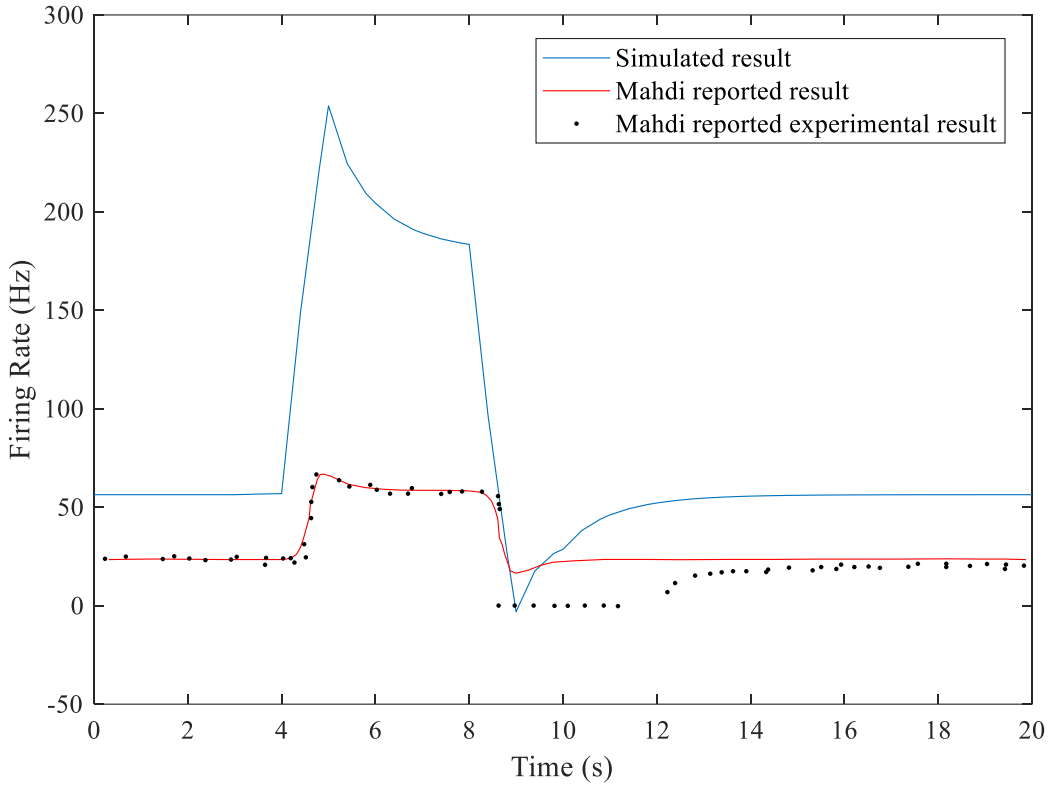

Figure 3.20: Firing response results for the square pulse input experiment for Mahdi et al. simplified-amplifier model.

Based on the discrepancies in the Simulink results and the Mahdi et al. results, for the $W_eV_2N_a$ model, I have low confidence in the parametric values presented by Mahdi et al. Parameters for the models of interest in this research, ($W_{ne}V_2N_a$ and $W_{ne}V_2N_{IF}$), were reported by Mahdi et al. for the same experimental input (square-pulse input), but the output of the model experiments using these parameters were not presented.

Based on the unexplained discrepancies between parameters provided and experimental results provided, the following summary outlines the limitations of the model-parameter results:

- Square-pulse experiment for $W_eV_2N_a$
    - Parameters available
    - Output experimental data available
    - Simulated results don't match reported results without a scaled and shifted firing response (as shown in Figure 3.20 and Figure 3.21)
- Square-pulse experiment $W_{ne}V_2N_a$/$W_{ne}V_2N_{IF}$:
    - Parameters available

    - No output experimental data
- Qualitative experiments $W_{ne}V_2N_a/W_{ne}V_2N_{IF}$:
    - Parameters unavailable
    - input and output experimental data is available

Based on the lack of output experimental data for the square-pulse experiments for the models of interest in this research ($W_{ne}V_2N_a$ and $W_{ne}V_2N_{IF}$), it was not possible to compare the simulated results using available parameter values.

Without the actual parameters required for these models of interest, or the initial conditions required to get the same response, none of my parameter estimation or optimisation techniques were able to find parameters which would approximate the results reported by Mahdi et al. for the qualitative tests.

However, to qualify whether the shape of the firing response in the Simulink model compared well with the Mahdi et al. reported results I scaled the simulated results against Mahdi et al.'s reported experimental results. To do this, I followed these steps:

1. Found the Simulated Firing Rate as a fraction of the peak Simulink Firing Rate value
2. Found the product of this fractioned Firing Rate with the peak Firing Rate value from the Mahdi experimental data

The scaled simulated result is shown in Figure 3.21 below.

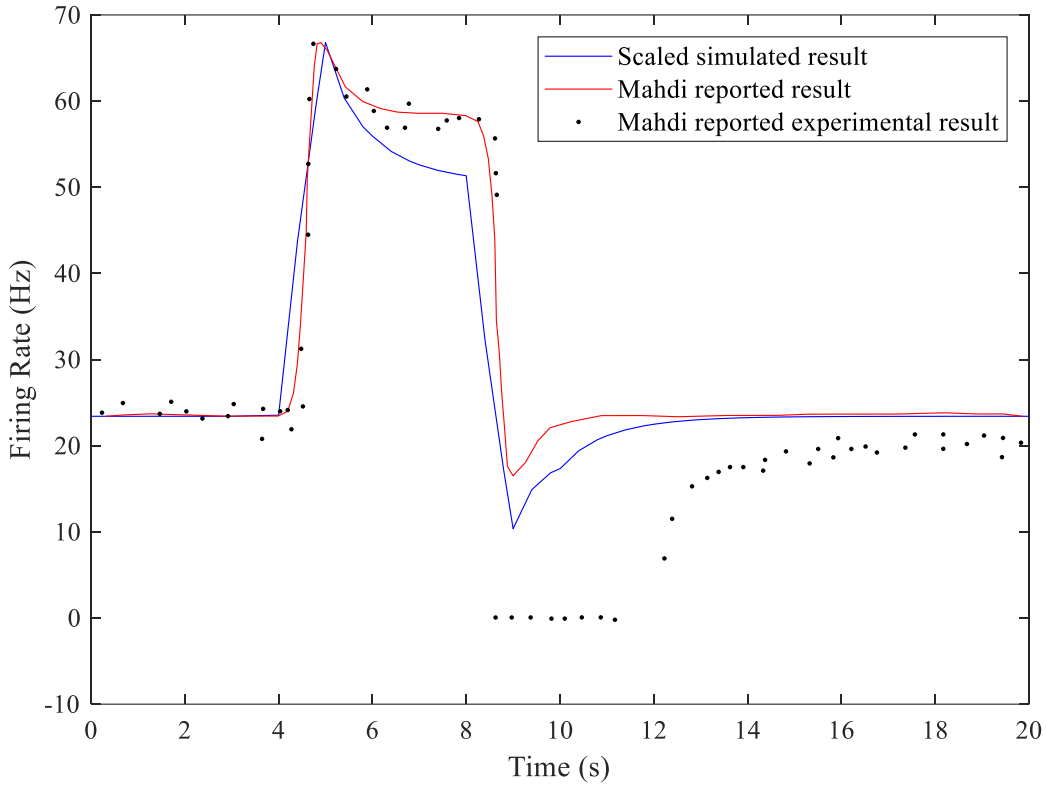

Figure 3.21: Scaled and shifted firing response results for the square pulse input experiment for Mahdi et al. simplified-amplifier model.

These discrepancies limit my ability to further critically analyse how these models behave under long-term inputs, and so have not been tested for long-term dynamics. These models do show valuable responses to different qualitative inputs, and so are compared to the other models investigated here. The parameter values used for those analysis are the parameters listed by Mahdi et al. for the square-pulse experiment [2]. This is possible because all comparative results from the other models' firing responses are shifted and scaled to align with the experimental data. This is explained in more detail in section 4.1.

4 Critical Comparison of Models

4.1 Model Feature Comparison

4.1.1 Arterial Wall Strain

For this component of the baroreceptor model, it is clear that the Srinivasen et al. mathematical function for the arterial wall strain (Langevin function for non-linear elastomeric properties) [27] will have more generic results across different species and at different ages than the Bugenhagen et al. fitted experimental function (based on rat aortas of rats at a certain age) [22]. In this way the approach of King and Srinivasen is better suited for modelling baroreceptor sensor characteristics across different species, and for modelling how those characteristics change with age. This is significant for the purpose of understanding how adaptation of sensor characteristics in the long term can affect hypertension.

King tested his model for strain on data from Human aortas, and showed that the calculated values for pressure-volume relationships compare well with experimental values for all ages [24]. Although they compare well, King notes that the age parameter (A) and the factor for the unconstrained twisting of the molecular chains at the periphery of the wall (β) had to be adjusted to fit the curves, and that the function was considerably sensitive to β [24]. Srinivasen et al. tested their model for strain on the arterial wall using Landgren's experimental data from cat carotid sinuses and from Clarke's experimental data from dog carotid sinuses [27]. One major limitation in the Srinivasen et al. model is that the model parameters need to be fitted optimally in order to match the experimental data, which means that there is no single set of optimised parameter values which will give the correct response at different input pressures. Another limitation is that their model was only tested on steady-state stepped pressure inputs and not on pulsatile pressure inputs [27]. Bugenhagen et al. tested their model for strain at the arterial wall against experimental results from rat aortas, and showed that both their linearised and non-linearised models (with fitted parameter values) compare well to the experimental data [22]. The non-linear model compares better to the experimental data in the extreme pressure ranges [22]. In order to compare how the different models respond to the same pressure input, I have simulated the different Simulink models with the same input pressure, as shown below in Figure 4.1 and Figure 4.2. Note that because the model parameters used by the researchers were fitted to different species (cat carotid sinuses and rat aortas), the strain values do not compare. This is based on the different radii for the differently sized vessels. The figures are presented only to show how the different models behave under the same conditions. The results show that the Bugenhagen et al. model has a slower response for high frequency changes, and that the Srinivasen et al. model is a better approximation given that it is more generic across vessel types and more descriptive for effects from age [22], [27]. Furthermore, the three different ways of modelling arterial wall strain which were

analysed by Mahdi et al. are also presented [2]. These models are the elastic (W_e), visco-elastic (W_{ve}), and non-linear elastic (W_{ne}) arterial wall models from Mahdi et al. [2]. The model from Beard et al. is not compared here because their dynamic arterial wall strain model is not directly comparable to these static wall strain models [14]. This is because the Beard et al. model does not have separated components for the arterial wall and the arterial membrane [14].

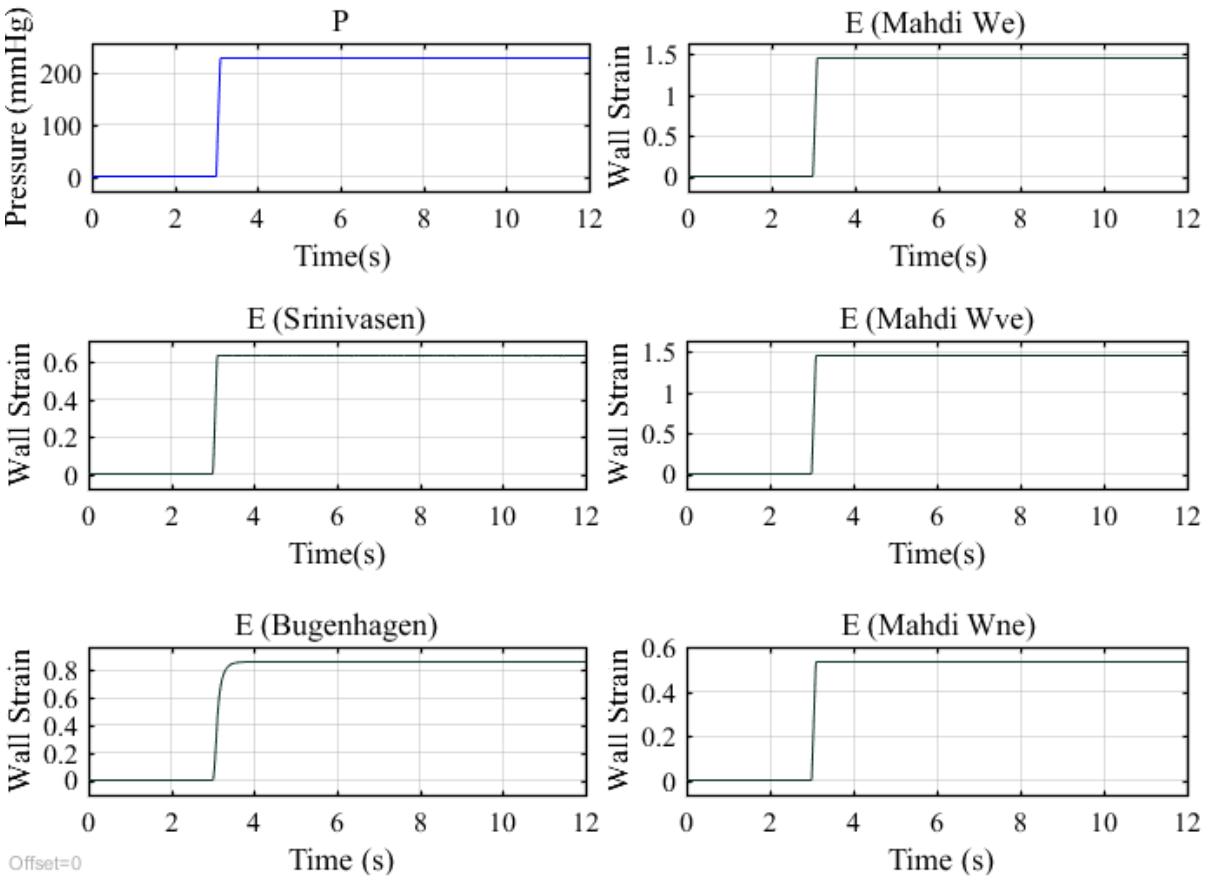

Figure 4.1: Comparison of static wall strain model responses for a non-pulsatile step input pressure

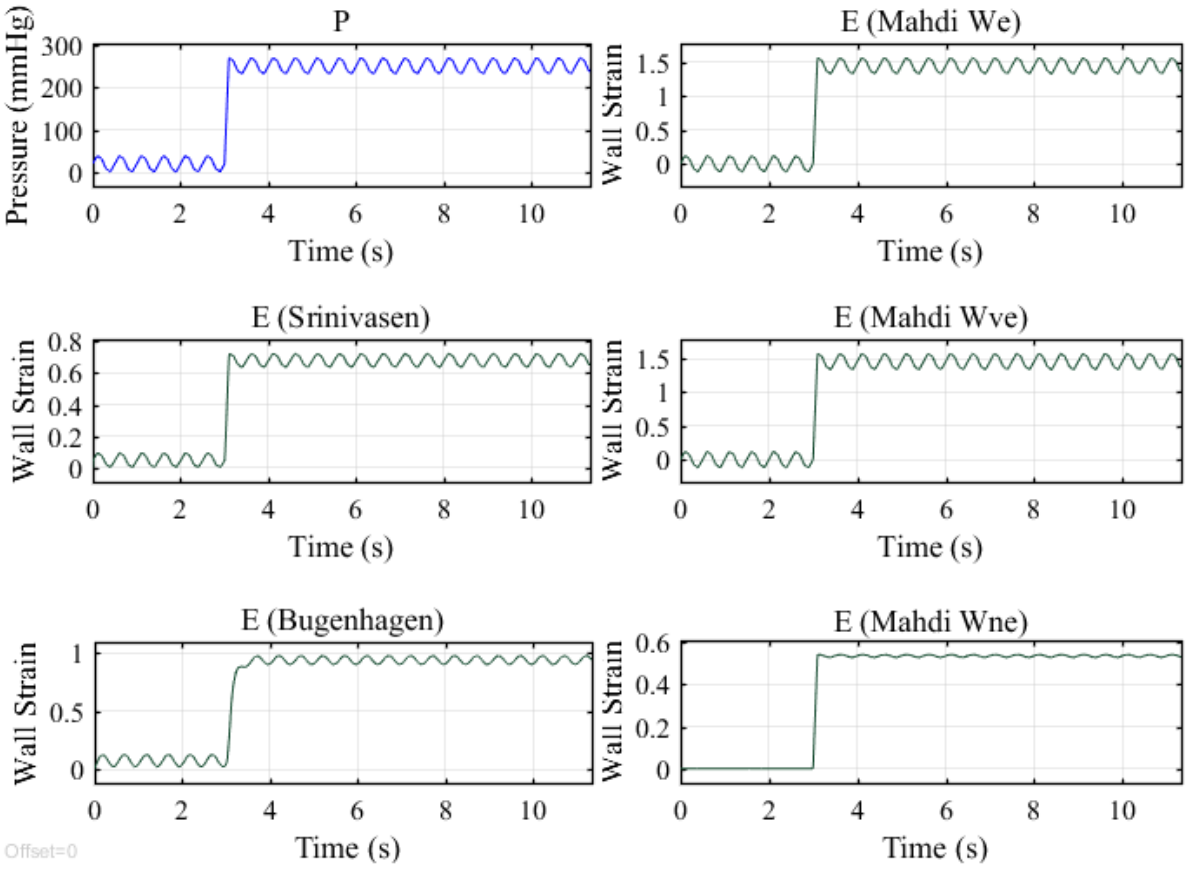

Figure 4.2: Comparison of static wall strain model responses for a pulsatile step input pressure

4.1.2 Voigt Body Arterial Wall Mechanics

In the Srinivasen et al. model, the dynamic strain is modelled using a single Voigt body [27]. According to Srinivasen et al., this is sufficient to model pressure responses at low pressures but inadequate at the non-linear high pressure range [27]. Subsequently, many researchers have shown that a single Voigt body is unable to capture the full response with a first order differential equation [2], [22].

Bugenhagen et al. have extended the dynamic strain model from the Srinivasen et al. single Voigt body representation to a three Voigt body representation [22], [27]. Similarly Mahdi et al. modelled baroreceptor behaviour with a different number of Voigt bodies, and came to the conclusion that two Voigt bodies are sufficient to capture all the dynamic characteristics of the strain transmission through the arterial wall [2]. The response differences between models which contain a different number of Voigt bodies for modelling the dynamic strain, are not discussed here as this investigation has been captured adequately by Mahdi et al [2].

There are two different trends displayed in the subset of models simulated in this research, one where strain dynamics are modelled using Voigt-bodies (Srinivasen et al., Bugenhagen et al., Mahdi et al.) and one where strain dynamics are a function of creep volume changes [2], [14], [22], [27]. Two comparisons are made, based on the same simulated experiment. The first is a comparison between the Srinivasen et al. model (single Voigt-body) and the Bugenhagen et al. model (two Voigt-body) [22], [27]. The second comparison is with the non-linear elastic wall strain and two-Voigt body model (from Mahdi et al.) against the creep volume to strain model (from Beard et al.) [2], [14]. I have implemented all these models in Simulink with the same pulsatile step pressure input from 20 to 250 mmHg, with a 20 mmHg pulsatile pressure amplitude. The pulsatile pressure amplitude was selected as 20 mmHg based on the aortic pulsatile experimental tests used by Beard et al. [14] based on the Coleridge experiments on dog aortas. The pressure step increase of 230 mmHg was selected based on the experimental data from the Bugenhagen et al. [22] results, which are used in section 4.1.3 to highlight models which perform best.

The way Mahdi et al. model the baroreceptor strain through coupling between visco-elastic layers of the arterial wall and membranes is also implemented by Srinivasen et al and Bugenhagen et al. [2], [22], [27]. Strain results are shown for the Srinivasen et al. and Bugenhagen et al. models in Figure 4.3 and Figure 4.4 respectively [22], [27]. These results highlight the differences between their models, and show that the Langevin function used by Srinivasen et al. to model the non-linearity of the arterial wall introduces a false artefact for exponential decrease of strain sensitivity as strain becomes static [27]. The Bugenhagen et al. model has a more reliable response for the long term adaptation of a prolonged strain, but is limited by the linearised model for the pressure-area relationship he used for the operating range of the rat aortic arch.

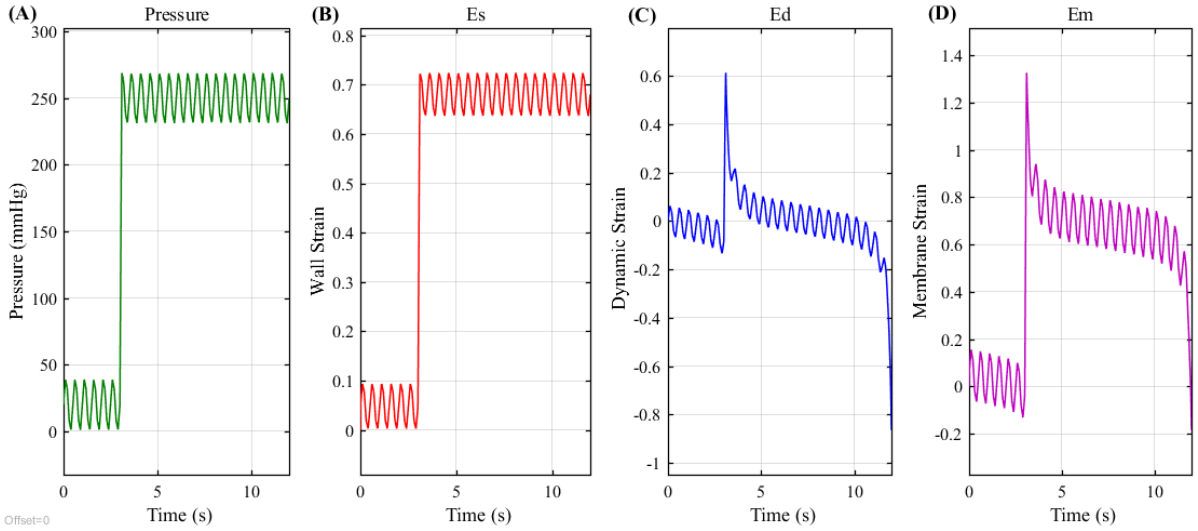

Figure 4.3: Simulink results for the Srinivasen et al. strain model, based on a 230 mmHg step input Pressure (A), Static strain (B), Dynamic strain (C) and total strain at baroreceptor membrane (D).

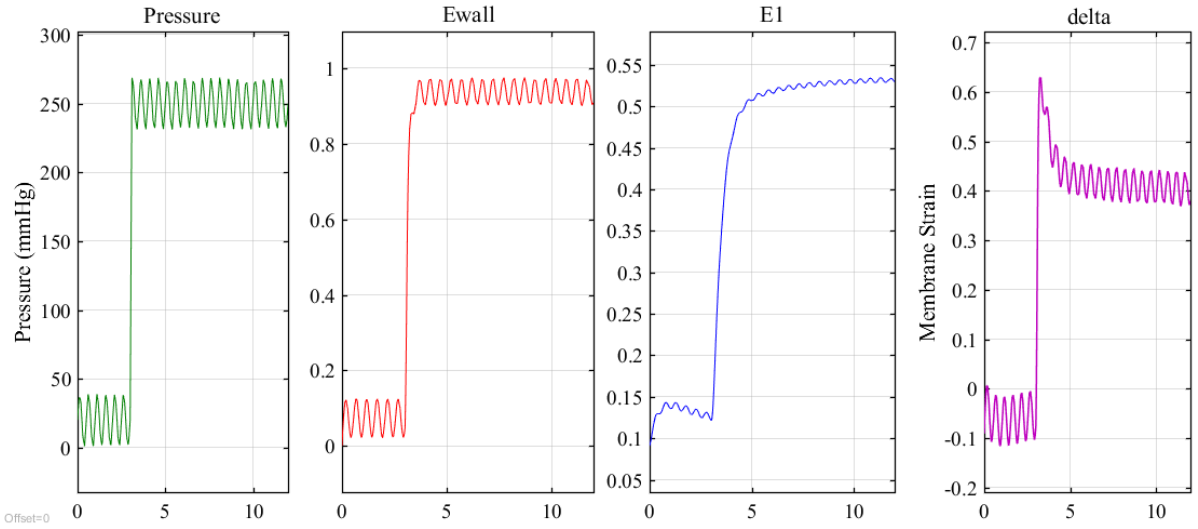

Figure 4.4: Simulink results for the Bugenhagen et al. strain model, based on a 230 mmHg step input Pressure (A), Static wall strain (B), Dynamic strain (C) and total strain at baroreceptor membrane (D).

Figure 4.5 and Figure 4.6 below show the different model responses between the Beard et al. model and the Mahdi et al. WneV2Na model [2], [14]. I needed to include the firing rate components in order

to compare the dynamic strain models, because the Beard et al. model for strain has an extra feature for baroreceptor afferent nerve activity [14] which is not modelled in the other researchers' models. The Mahdi et al. simplified amplifier model was chosen to compare with the Beard et al. model because the simplified amplifier model highlights the non-linear wall strain and strain dynamic behaviour best [2], [14]. Note that the firing rates differ significantly quantitatively because the models are parameterised for different species and for different initial conditions.

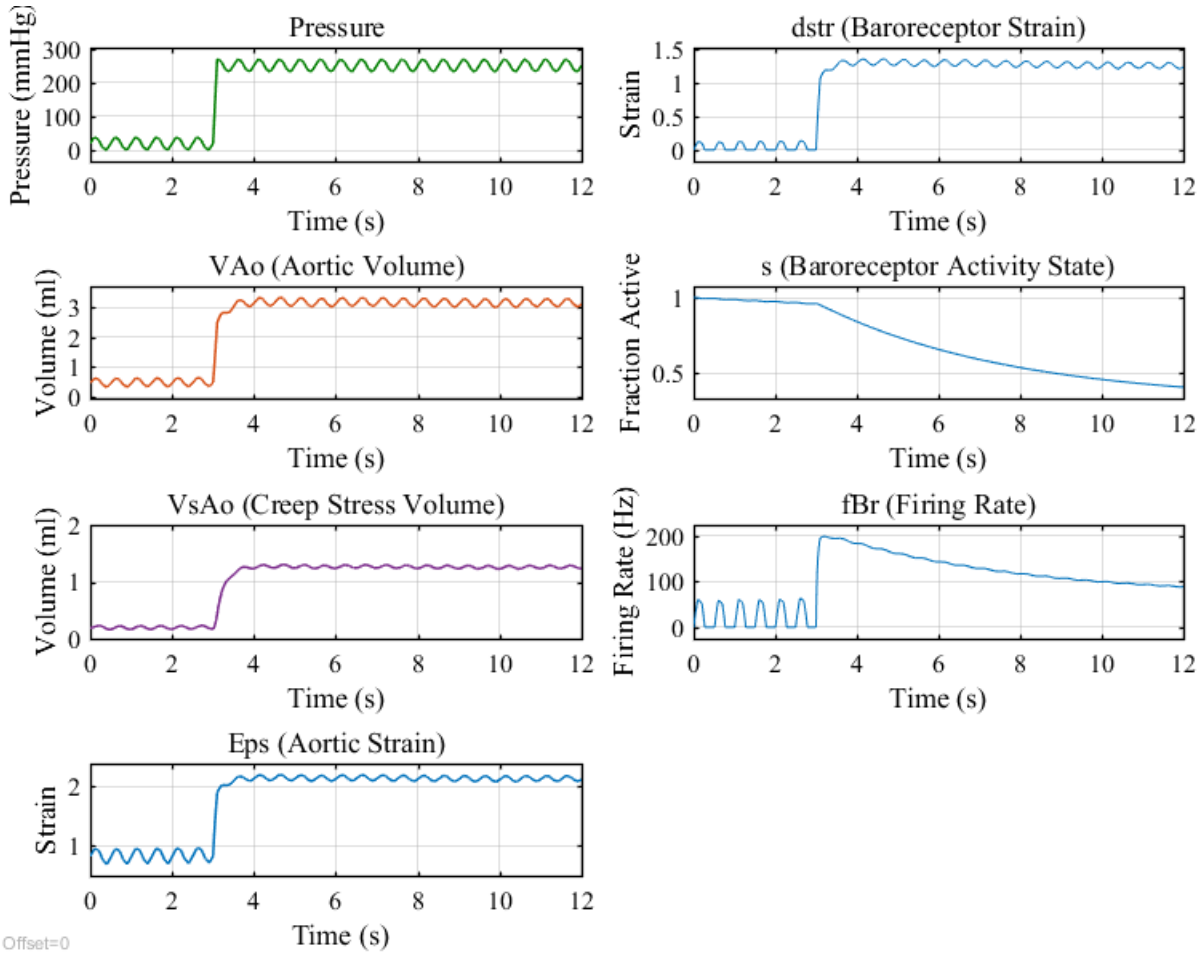

Figure 4.5: Results from simulation of the Beard et al baroreceptor model, based on a pulsatile step input pressure.

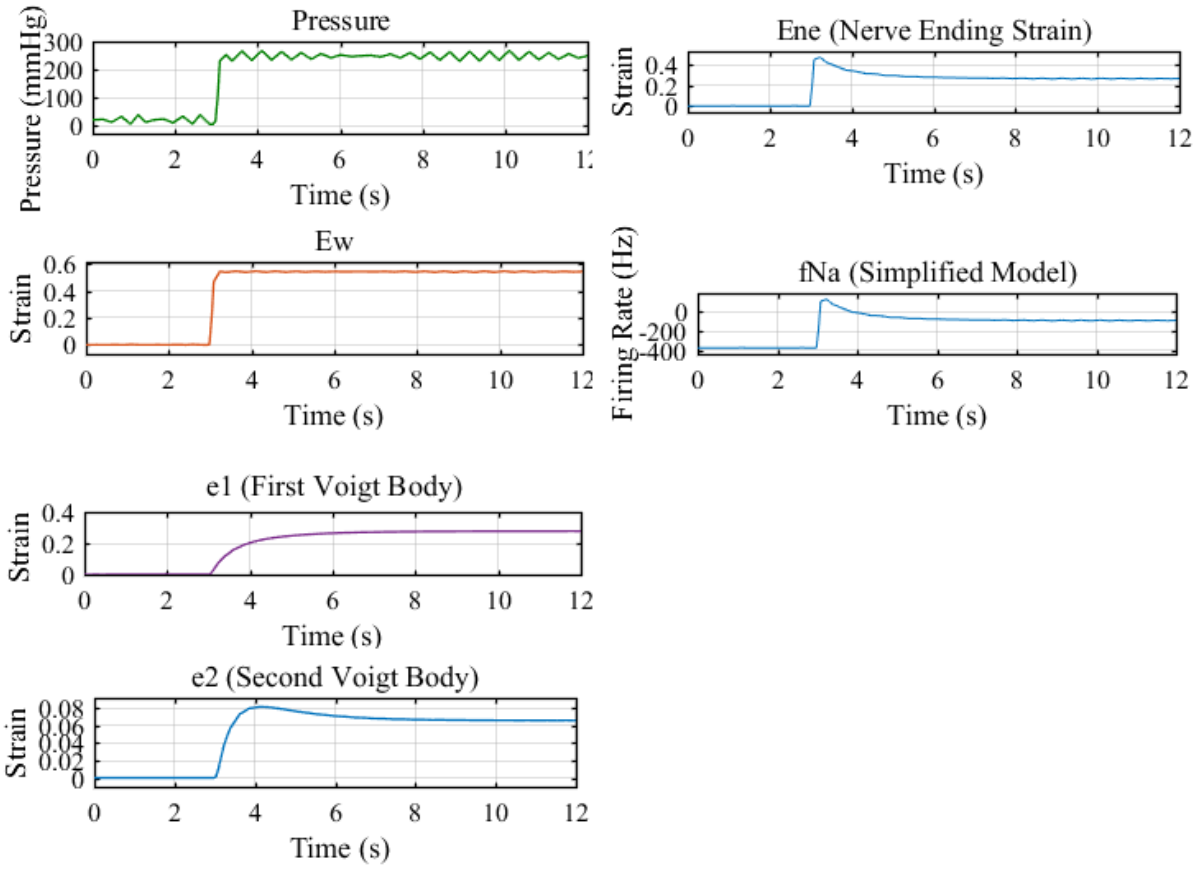

Figure 4.6: Results from simulation of the Mahdi et al baroreceptor model, based on a pulsatile step input pressure.

It can be seen from these results that the Beard et al. model is more adept at capturing dynamic variations in pressure [14], but that the firing rate is found to reset far more slowly than the firing rate from the Mahdi et al. model [2]. It is clear that the Beard et al. model does not capture any resetting of the strain at the arterial wall or at the nerve ending, and rather uses the state of activity of the baroreceptor afferent fibres (s) to model the resetting behaviour of the baroreceptor firing rate [14]. In the Mahdi et al. model, the strain at the nerve ending is found to already show resetting behaviour before the baroreceptor transmits the strain signal as an afferent firing rate [2].

Interestingly, the Mahdi et al. model is not sensitive to the pulsatility of the input whereas the Beard et al. model reflects the pulsatility of the input even when the MAP is constant [2], [14]. The behaviour of these different models and their firing rate responses will be discussed in further detail in the next section.

Overall, modelling the coupling between different layers between the arterial wall and the nerve ending shows that the resetting behaviour is an inherent property of the coupling between the

baroreceptor and the arterial wall. This way of modelling the arterial wall mechanics has been used in most of the models investigated here (Srinivasen et al, Bugenhagen et al, and Mahdi et al) [2], [22], [27]. Although these authors have modelled the baroreceptor this way, the Beard et al. model introduces a different technique (using the baroreceptor active state) which may provide more insight into the behaviour of the baroreceptor itself [14]. In order to investigate the performance of these models further, the firing rate responses are compared in the following section.

4.1.3 Signal Transmission and Firing Response

I have compared all models in this section, for their ability to interpret the same pulsatile step input. I compare the following five models that are summarised as follows:

- Srinivasen et al. used a simplified integrate-and-fire model for the baroreceptor firing rate, which is triggered if the membrane strain exceeds a threshold [27]
- Bugenhagen et al. used a linear sensitivity scaling and jump frequency shift for the membrane strain to model the baroreceptor firing rate [22]
- Beard et al. used a combination of afferent fibre recruitment and the changing membrane strain to model the baroreceptor firing rate [14]
- Mahdi et al. initially used a simplified amplifier model which scales and shifts the membrane strain directly to model the baroreceptor firing rate [2]
- Mahdi et al. also used a leaky integrate-and-fire model which is based on a gradual ‘charging up’ of the membrane voltage until it reaches a threshold which then discharges the membrane and models an action potential of a baroreceptor afferent fibre [2]

Each model is compared in its entirety, including wall strain and strain dynamics, because the arterial wall and the layers between it and the baroreceptor afferent fibre are all part of the sensor function of the baroreceptor. This reasoning is based on the principle that states that the material which a sensor is attached to forms part of that sensor itself. An example of this is the piezo-resistive effect in certain semiconductor materials or in a strain gauge, where the sensed strain is directly related to the strain characteristics of the material within the sensor [47].

The models from Bugenhagen et al. and the simplified amplifier model from Mahdi et al. are similar in that they both use Voigt bodies to model the strain dynamics in the layers of the arterial wall, and use scaling or amplification of the strain signal to produce a firing rate [2], [22]. These two models differ in the modelling of the static arterial wall strain, where Mahdi et al. use a non-linear elastic model while Bugenhagen et al. used a linearised elastic model [2], [22].

Figure 4.7 and Figure 4.8 show the comparable firing rate outputs of the different models, simulated with a step input pressure and a pulsatile step input pressure respectively. The step input highlights the

model responses to known experimental results, and the pulsatile step input exercises the models for their higher frequency dynamics. Figure 4.9 has extra points plotted to show how the expected experimental results compare to the model responses for a step input. The experimental secondary data was retrieved from the analysis presented by Bugenhagen et al. based on the similar experiments performed by Brown et al. on rats [22], [37] for a non-pulsatile step response in the range of 0-230 mmHg. The experimental data curve has been scaled to compare with the maximum firing rate output from each model. This was done to compare all the different modelled firing responses, which are parameterised differently, to the experimental results.

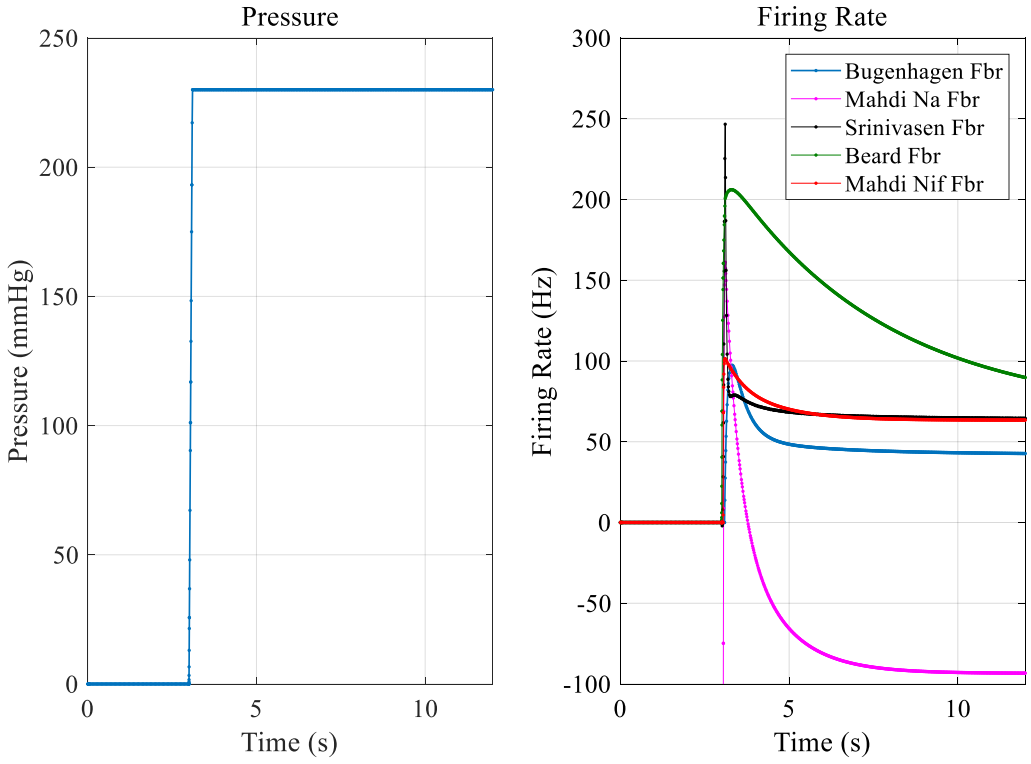

Figure 4.7: Step input firing rates for different baroreceptor modelling techniques

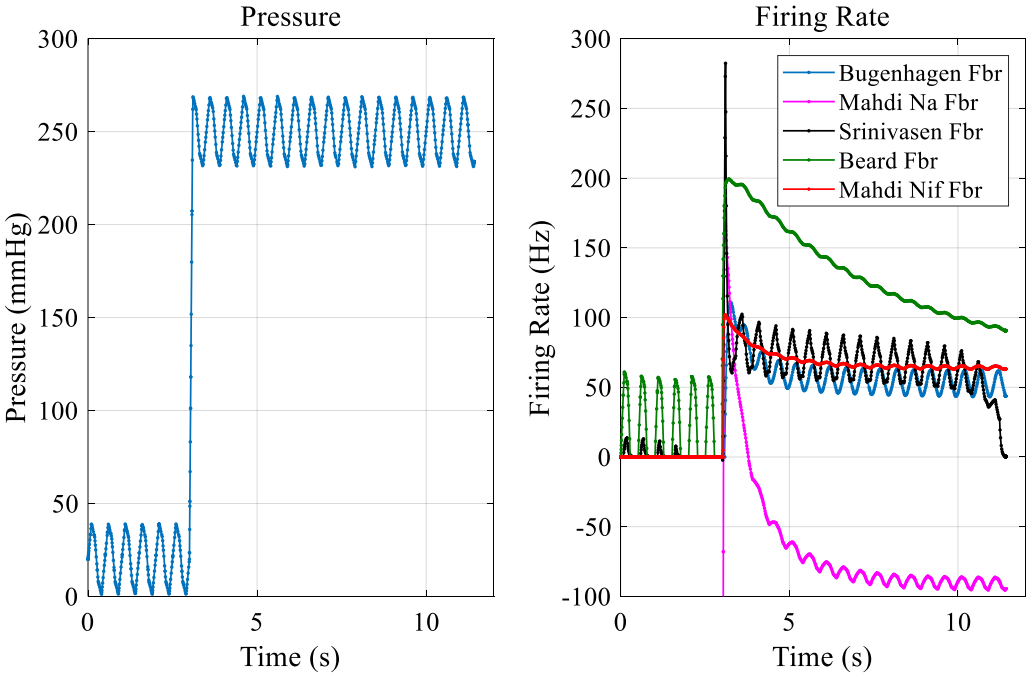

Figure 4.8: Pulsatile step input firing rates for different baroreceptor modelling techniques

Comparing the model responses in Figure 4.8 and Figure 4.9, the Bugenhagen model and the Mahdi integrate-and-fire models have similar responses. The Mahdi simplified amplifier model (Mahdi Na Fbr) is incorrectly scaled to accommodate the range of the input, and indicates a negative firing rate which is not physiologically possible. The Srinivasen et al. and Beard et al. models firing responses are different from the responses of Bugenhagen et al. and Mahdi et al. The Srinivasen model has an extremely fast decay of firing rate after the initial stimulus and where the Beard model has a much slower decay of firing rate. The Srinivasen and Beard models also have a non-zero firing response before the step increase.

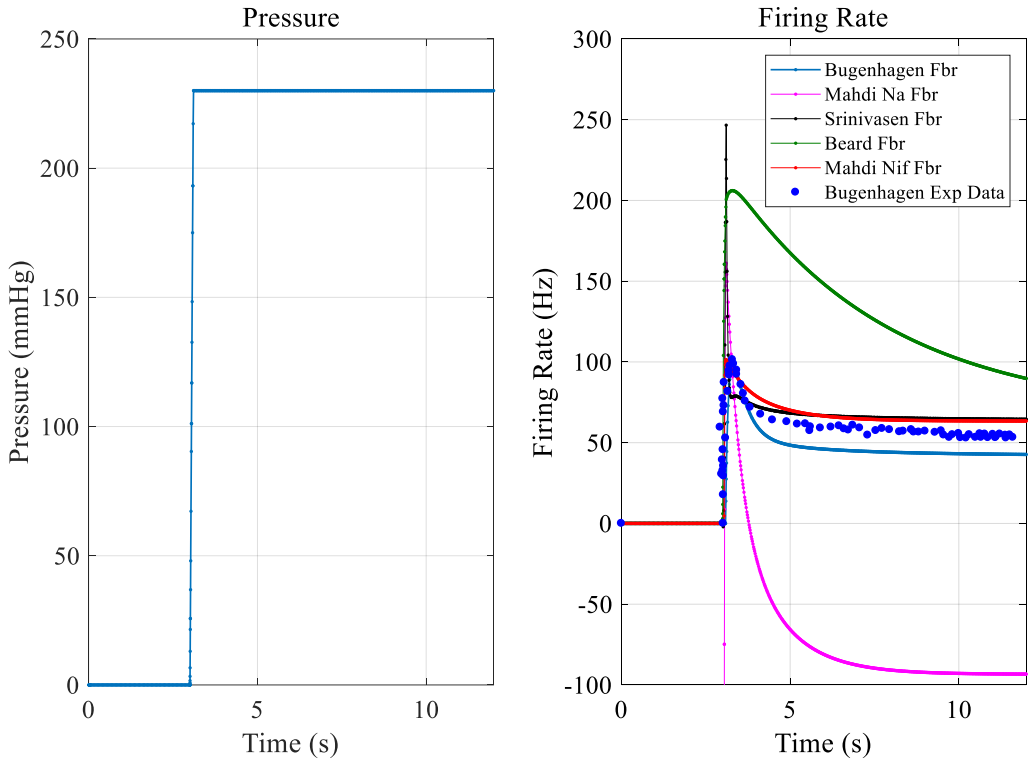

Figure 4.9: Step input firing rates for different baroreceptor modelling techniques, as compared with experimental data from Bugenhagen et al. [22]

The results in Figure 4.9 show that the Mahdi et al. leaky integrate-and-fire model (NIF) model matches the expected experimental data best, followed by the Bugenhagen et al. and the Beard et al. models [2], [14], [22]. This indicates that the integrate-and-fire (NIF) model characterises the expected behaviour best, but that using a simplified amplifier model (NA) such as used by Bugenhagen et al. will approximate the response well [22]. The pulsatile step responses also show that the NIF model performs the best. This statement is based on the fact that the NIF firing rate is not pulsatile before stimulus and does not mimic the pulsatility of the pressure input after stimulus. This validates the

known physiology where the firing rate of the baroreceptor will increase as the pressure increases and decreases as the pressure decreases, but not with every pulsatile heart cycle [7]. Similarly, the major strength of the Mahdi et al. model is that the difference in response to step input stimulus compared to pulsatile step stimulus is not significantly different, as would be expected from the biological system which inherently has a pulsatile environment [20].

However, although the Mahdi et al. NIF model behaves the best under these conditions I have low confidence in the parametrisation defined for the modelling experiments in the Mahdi et al. paper [2]. To expand on the frequency response of the Mahdi et al. model, more information on the parameterisation of the model is required. For more detail on the inconsistencies discovered in the reported model results for the parameters described, please see section 3.5.3

4.2 Frequency Response

The comparative results in section 4.1 highlight how the different model components contribute to the characteristics of the firing response. In order to evaluate the dynamic sensor characteristics of the baroreceptor, I investigate the frequency response of the two most reliable models (as identified in section 4.1) in Simulink. This investigation is based on frequency response tests, where I linearise over certain operating points in the frequency range in order to estimate the whole frequency range of a non-linear system.

4.2.1 Model Selection

I conduct the experimental tests for frequency response using simulations of the Beard et al. and Bugenhagen et al. Simulink models. These models have been shown to model experimental data well for input pressure that undergoes short-term changes, for a wide range of different experimental conditions. In order to study how the baroreceptor behaves under long-term pressure changes, these high frequency models are extrapolated to lower frequencies. This allows for some insight on how these baroreceptor models behave under long-term inputs, and draw conclusions on what the baroreceptor frequency response might look like. In this way, it is possible to experiment on the baroreceptor models for changes in pressure over a much longer time frame than would have been physically feasible in an in-vitro or in-vivo experimental test.

The models used to test frequency responses for the baroreceptor were selected based on their ability to match experimental data and their contrasting ways of modelling the baroreceptor. In this way, the Beard et al. model of the baroreceptor is used for its characterisation of stress mechanics in the aorta and of baroreceptor afferent fibre recruitment for firing rate [48]. The Beard et al. model also is very clearly parameterised and presented with clear model results for a wide range of experiments. This allows for a high level of confidence in my Simulink representation of the model, because my

simulated results match the presented results and the experimental results. However the Beard et al. model only has an input for the rate of change of pressure, and not for the absolute level of pressure [48]. This introduces a differentiating characteristic into the model dynamics, leading to a very low sensitivity (or zero gain) at low frequencies (for long periods). In order to investigate whether this behaviour is an inherent property of the baroreceptor, a second model with a different modelling technique was investigated. The Bugenhagen et al. model was selected based on its simplicity and my confidence in the simulation results based on the reported results for the many experiments used to parameterise it [22].

The Bugenhagen et al. model is very similar to the Mahdi et al. simplified amplifier baroreceptor model [2], [22]. The Mahdi et al. reported model parameterisation for their presented results were found to be inconsistent, and could not be reproduced or optimised in my Simulink simulations. For more information on the reported inconsistencies, please refer to section 3.5.3. Based on these inconsistencies with experimental data for validating the Mahdi et al. models in the short-term, these models were not selected for testing frequency response in the long-term.

4.2.2 Simulation Methodology

To determine the frequency response of the non-linear baroreceptor models, it is necessary to linearise the models over a broad range of frequencies. To do this, each model is simulated with a sinusoidal input of a specific frequency. For each of these frequencies, I analyse the output to determine the gain and phase shift of that sinusoidal input.

The frequency range used for the ‘simulated experiments’ is from 10 Hz to 0.000001 Hz. This corresponds to sinusoidal inputs which have periods that range from 0.1 s to 10 days. My approach is to test the output firing response with an input sinusoidal pressure, based on a 100 mmHg operating point with a 1 mmHg peak amplitude. The operating point was selected based on an average mean blood pressure in humans. The peak amplitude was chosen to be 1mmHg to keep the pulsatile properties of an arterial signal, but greatly reduced from the human peak amplitude of 20 mmHg due to the need for long term simulation of frequency response (which would result in a simulated step increase of 20 mmHg over short periods). I vary the frequency of the sinusoidal input at logarithmic points within the frequency range of interest. See Figure 4.10 for an example of the inputs used.

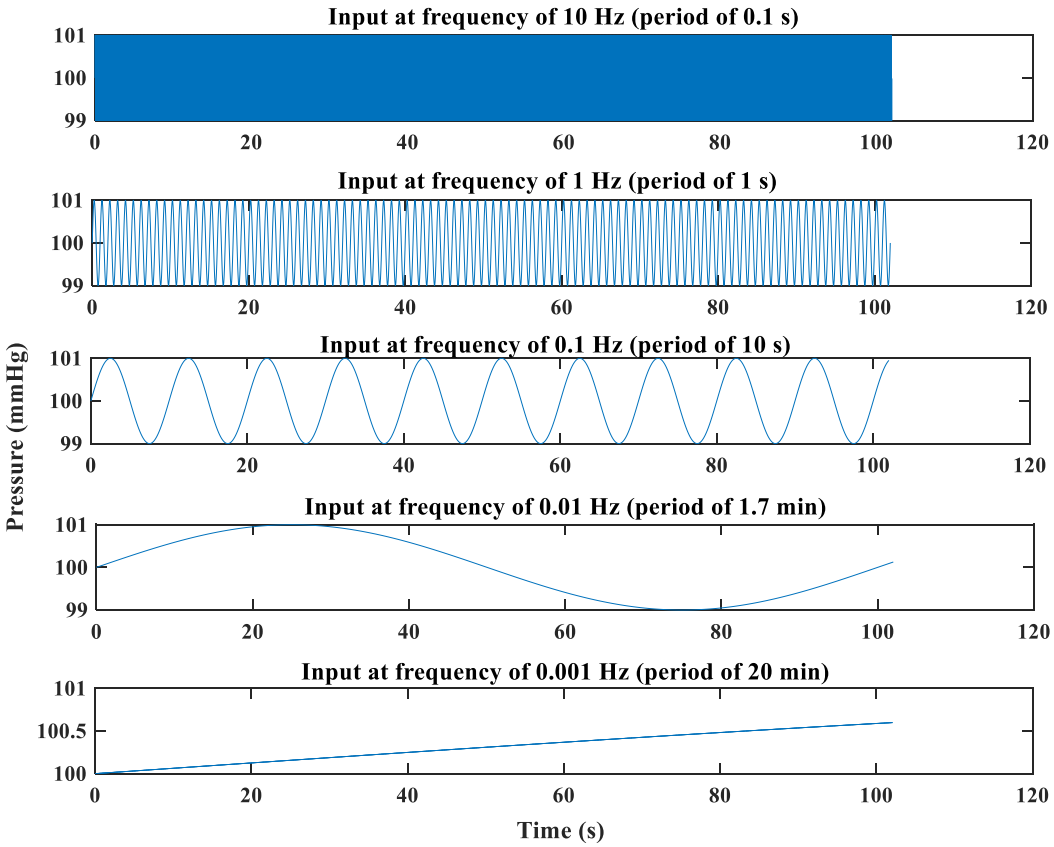

Figure 4.10: Example of input sinusoidal pressure used to test frequency response

The input sinusoids were sampled at a frequency which was always well above the required Nyquist sampling rate [21]. I thoroughly checked this sampling rate for every simulation in order to prevent aliasing effects into the recorded frequency response. Each model was always run for a much longer settling time than the period of the sinusoidal input, until the output reflected the input without any transient disturbances.

The methodology used to test each model, at each frequency of interest is as follows:

1. Prepare sinusoidal input for frequency of interest
    a. Check sampling frequency and settling time doesn't cause too many or too few data points (for simulation in Simulink)
2. Inspect sinusoidal input to validate sufficient sampling
3. Run the Simulink model with this input, under the same parameterisation and solver as the model validation tests
4. Inspect the simulated outputs for transient behaviour. The output sinusoid must not reflect any change in the base line, especially near the end of the settling time.

5. Check that the period of the output is constant (must be a whole number of cycles)
6. Check that the sample times of the input and output sinusoids match
7. Check that the output sinusoid periods are constant
8. Calculate the Gain of the output sinusoid
    a. Output sinusoid less the output mean, divided by the Input sinusoid less the input mean
9. Calculate the Phase Difference of the output sinusoid
    a. Time for last peak of the input sinusoid less the time for the last peak of the output sinusoid
    b. 360° x test frequency x time difference

An example of the input and output results is shown below in Figure 4.11.

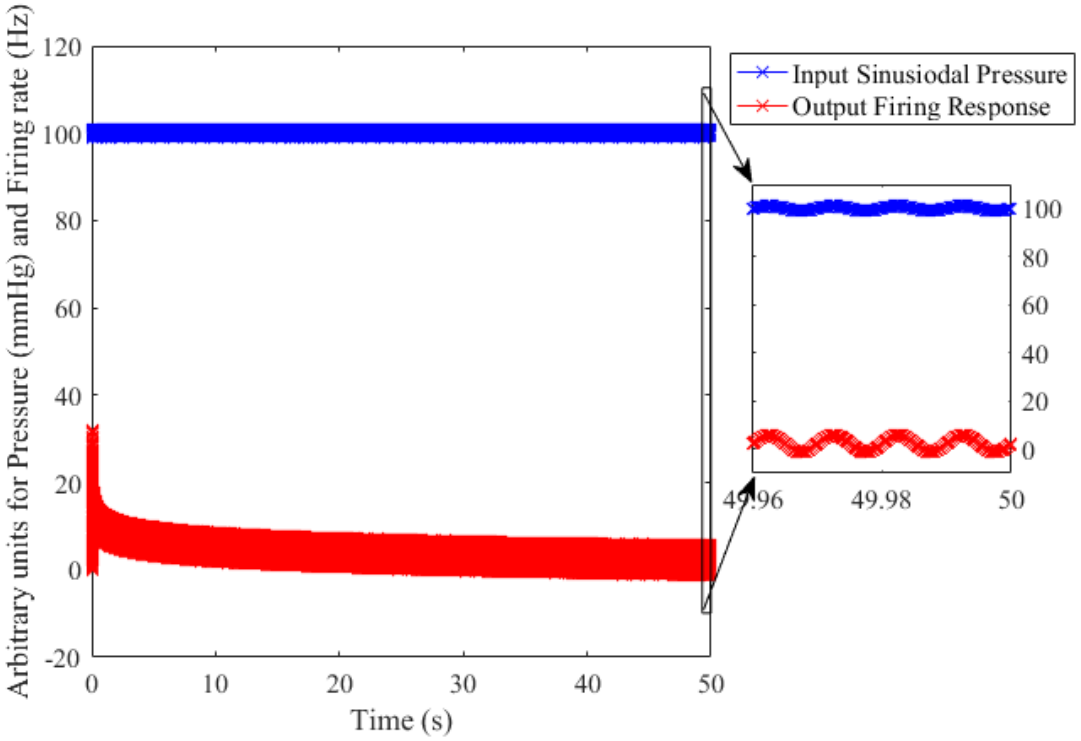

Figure 4.11: Input to Output Comparison for the Beard et al. model at Test Frequency 100 Hz, with portion of the last 0.04 s of the signals highlighted to show their sinusoidal nature

4.2.3 Simulation Test Results

The gain is measured as the change in amplitude from the input sinusoid to the output sinusoid. The units of such a gain (for firing rate based on pressure) are arbitrary, as in this case they would be

Hz.$mmHg^{-1}$. The gain is used to indicate how the sensitivity of the firing rate changes as the frequency of the input changes. The phase is the fraction of the output wave cycle which has elapsed relative to the input wave cycle (sinusoid). This phase difference is represented in degrees, and represents the cyclical shift of the output based on the frequency of the two waves (input and output) and the difference in time between two identical points along each wave [21]. Using phase difference as a metric for frequency response is valuable because it indicates how the input is translated through the arterial wall and membranes in time. The frequency response of the Beard et al. model and the Bugenhagen et al. model, are reflected in Figure 4.12 and Figure 4.13 respectively. Each frequency response figure shows a gain (sensitivity) and phase difference (distortion in time).

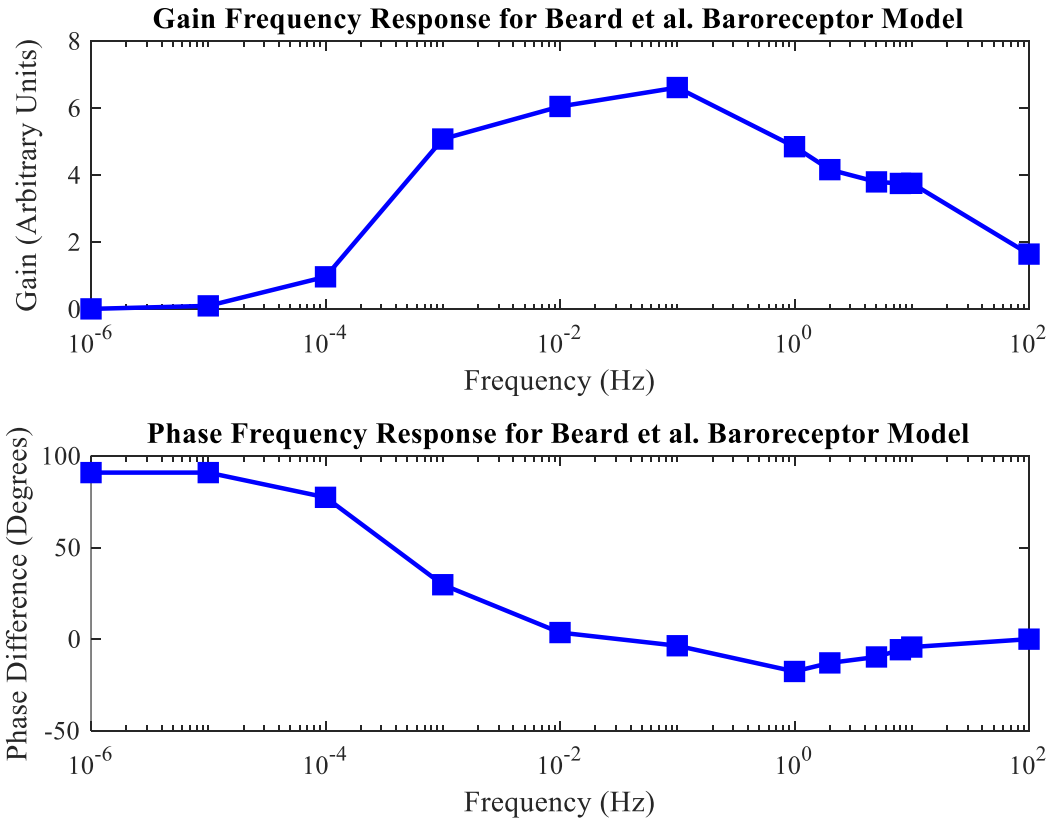

Figure 4.12: Frequency Response for the Beard et al. Baroreceptor Model [14].

The frequency response simulated from the Beard et al. implementation has characteristics which distinguish it as a high pass filter [21]. This is based on the very low gain at low frequencies, which increase at higher frequencies. The gain (or sensitivity) of the baroreceptor for this model reaches a maximum around 0.1 Hz, and immediately begins slowly decreasing. The gain across this frequency range is as physiologically expected for a baroreceptor, which would have very low sensitivity at very low frequencies (approximating zero gain under DC conditions) with a non-infinite band of higher sensitivity at higher frequencies. The response shows that the sensitivity significantly decreases at

frequencies between 1 Hz and 10 Hz (1 s to 0.1s) which is realistic for a practical sensor which cannot translate changes in pressure that happen infinitely fast. The phase difference from the Beard et al. model is in line with expected high-pass filter and band-pass filter responses, and is expected to occur based on the differentiating nature of the input, where the only input is the rate of change of pressure which immediately shifts the phase of any input outside its frequency band of positive sensitivity by 90° [21].

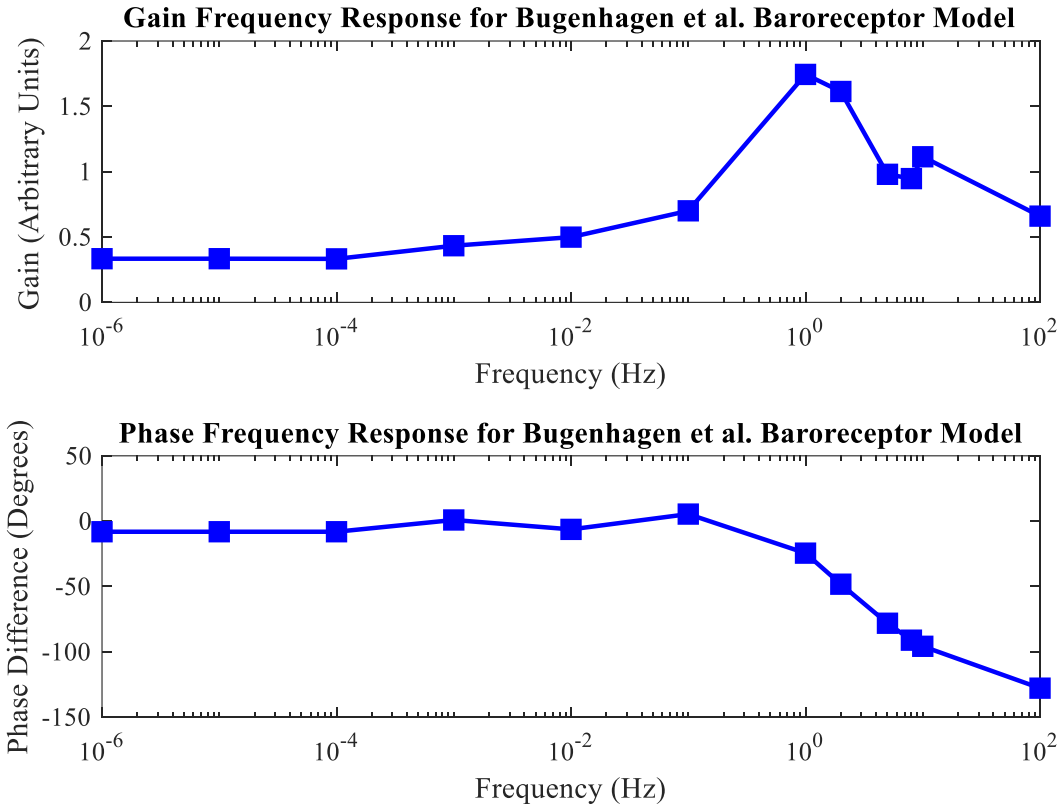

Figure 4.13: Frequency Response for the Bugenhagen et al. Baroreceptor Model [22]

The sensitivity frequency response for the Bugenhagen et al. model of the baroreceptor is similar to the model from Beard et al. The sensitivity is shown to be significantly lower in the lower frequency range, and unchanging in the range from 1e-6 Hz to 1e-4 Hz. Thereafter the sensitivity increases to a maximum sensitivity at 1 Hz, where it then immediately begins to decrease. Regarding the phase shift, the Bugenhagen et al. model also experiences a 90° phase shift over the frequency range, but here the shift occurs between 1e-1 Hz and 1 Hz.

In both model frequency responses, it is evident that the maximum sensitivity of the baroreceptor lies in the frequency range from 0.01 Hz to 1 Hz, and that the phase difference is zero in the frequency range between 0.01 Hz to 0.1 Hz. In both models the baroreceptor sensitivity is shown to decrease significantly at the lower frequency ranges. In both models the sensitivity decreases after 1Hz, this

supports the physiology because the baroreceptor would become less sensitive to changes that occur faster than 0.1s.

The Bugenhagen et al. model has a narrower band of sensitivity than the Beard et al. This is reflected by both the gain and the phase difference results. Furthermore, the Beard et al. model response shows a zero gain at very low frequencies whereas the Bugenhagen model response clearly shows an unchanging non-zero gain at these frequencies. The reason behind these differences are most likely based in the differentiating component of the Beard model, which is more pronounced than the Bugenhagen model because its input is really the rate of change of pressure and not the pressure itself.

Both models show band pass dynamics for different sections of the same frequency band. A possible reason for this is that each of these models were parameterised for different experiments, for different species. Beard et al. used dog and rabbit aortic baroreceptors, while Bugenhagen et al. used rat aortic baroreceptors. Such parametric differences introduce an interesting question to this simulated data, which is whether the differences in the frequency response of the models is due to the modelling technique or due to the different size/lifespan of the species which parameterised the model. Such species specific parameterisation may affect the time constants of the arterial wall mechanics, which although used in the models in different ways, produce the same effect.

5 Key Findings and Considerations for the Role of the Baroreceptor

5.1 Key Findings for the Role of the Baroreceptor

The contentious debate around the ability of the baroreflex to act as a long-term controller of blood pressure, has resulted in many experiments trying to find the operating range that the baroreceptor can detect changes in blood pressure. These experiments are limited in their ability to draw conclusions on the long-term behaviour of the baroreceptor, due to the sensitive and limited time constraints on very sensitive tissues and very interconnected physiological systems. Based on this challenge, many researchers have produced mathematical models to prove that their interpretation of the baroreceptor's behaviour is valid. All their research aims to elucidate the static and dynamic characteristics of the baroreceptor, so that they may better understand the role the baroreceptor plays in the baroreflex and better understand how the baroreflex can act as a controller of blood pressure.

The key findings of this research are as follows:

- A subset of baroreceptor mathematical models have been implemented in Simulink and simulated results validate experimental data for short-term changes in blood pressure.
    - Each model is shown to translate the rate of change of arterial pressure as a rate of change in strain at the arterial wall
    - The adaptation characteristics of the baroreceptor occur due to the decay of a dynamic strain across the visco-elastic layers of the arterial wall
    - Each model has a consistent response, even though parameterised for different baroreceptor types, from different experimental conditions and from different species
- The best performing models have been simulated to an extrapolated range of frequencies, testing how baroreceptors behave under inputs that have different rates of change.
    - Both models are found to have high sensitivity to changes that occur over a timeframe between 1s and 1min 36s
    - Both models are found to have very low sensitivity to changes that occur over a timeframe longer than 16 min 36s
    - Both models highlight the role of the visco-elastic layer model components in producing 'low-pass' frequency responses.

The outcome of the critical analysis of the baroreceptor, for modelling and simulating a long-term frequency response, is a new approach to solving many experimental and theoretical questions around the physiology of blood pressure regulation. These findings have presented two baroreceptor models which are good candidates for further modelling and improvements. These findings have highlighted

that the short-term range of the baroreceptor as a sensor, means that the baroreflex cannot have an impact on long-term blood pressure regulation.

5.2 Further Considerations for the Role of the Baroreceptor

Based on the frequency response results, it is clear that these baroreceptor models do not have infinite gain, and could not directly influence long-term blood pressure control. However, in an effort to clear up some misconceptions about how the baroreceptor could influence long-term control two subjects of debate are discussed. The first is the carotid sinus distensibility, which could directly influence the sensitivity of the baroreceptor through the peripheral baroreflex arc (sympathetic response to arterial walls) by dilating the carotid sinus and changing the strain transduction properties of the wall [2]. The second is the effect that age has on the elasticity of the arterial walls, and whether the variation in strain sensitivity over time to a less elastic vessel can influence the baroreceptor sensor characteristics [24].

5.2.1 Carotid Sinus Distensibility

An artery experiences pressure on the surface of its vessels. In the models included in this study, all of these vessels are cylindrical. The force exerted on the arterial wall (tension in the wall), is modelled as a pressure on the surface area of the wall. The radius and thickness of the wall are directly related to the pressure. King modelled this pressure-strain relationship as a force which is exerted on the surface of the arterial wall by a cylindrical mesh of molecular chains, which changes radius to accommodate the pressure under the visco-elastic properties of the arterial wall [24].

This model is part of the general theory of elastomers [24], and describes how the force exerted at right angles to a surface yz $(i.e. F_x)$, by a mesh of molecular chains, which has an unstrained wall thickness of e_0, an unstrained undistorted area $y_0 z_0$, will be described by

$$F_x = B_x y_0 z_0 \mathcal{L}^{-1}(k_x x) \tag{5.1}$$

Where B_x is a coefficient which is directly proportional to the absolute pressure, and k_x is a property that depends inversely on the maximum length of the molecular chains [24].

The first topic for consideration, is that the distensibility of the carotid sinus may be able to directly change the sensitivity of the carotid sinus baroreceptors. By distending the radius of the arterial wall the carotid sinus experiences decreased wall thickness and increased tension in the wall [24]. Under these conditions the visco-elastic properties of the arterial wall still contribute to the change in radius, but under a different geometrical relationship than for a cylindrical vessel. This may affect the pressure-strain transduced across the arterial wall and baroreceptor membrane, and allow for different information about transient pressure to be conveyed through the baroreceptors.

It is also unclear from the physiology whether the baroreceptor afferent firing rate could directly change the distensibility of the carotid sinus at high pressures. The possibility of such an elasticity feedback feature, or the increased sensitivity to pressure in the carotid sinus, has not been discussed thoroughly in the literature.

Further investigation is required in order to fully understand how the physiology adapts to an increased pressure at the carotid sinus, and whether the baroreceptors there would be able to give a more complex translation of absolute and relative pressure levels to the brainstem. Such an investigation would give a clearer indication as to whether the baroreceptor is capable of influencing long-term control of blood pressure through this pathway. In order to extend this investigation, the baroreceptor model from Srinivasen et al. or Bugenhagen et al. should be adapted and parameterised for a bulbous carotid sinus with an enlarged resting radius from the aortic arch cylindrical model [22], [27]. This would require a new adaptation from King's mathematical model for arterial wall strain in an elastomeric cylindrical vessel [24]. The Mahdi et al. model could be adapted for the non-linear elastic strain based on the increased area of a dilated elastomeric cylindrical vessel, but the model would not translate the increased surface area of sinus in the vessel as well as the updated geometrical model from King et al. would [2], [24]. The Beard et al. model would not be as easily adapted, because their model is parameterised for volume and creep stresses in the aortic arch [48].

5.2.2 Age-Related Effects

In the second case, the age of the subject is known to influence the visco-elastic properties of the arterial wall, as demonstrated by King [24]. As mentioned by Pettersen et al. the adaptation of the baroreceptor firing rate in essential hypertension may be the result of the brainstem reacting to the baroreceptor's interpretation of strain in a less elastic arterial wall [15]. The age related effects of the visco-elastic properties of the arterial wall are expected to shift the frequency response of the baroreceptor. This is expected to be due to a new relationship between pressure at the wall to strain detected at the baroreceptor membrane.

From the equations in Srinivasen's model, as described in section 3.2.2, it can be seen that the membrane strain is a function of parameters A, β and r_0. These parameters are all shown to vary with age [24], as shown in 3.1.2. In this way, it is clear that the strain threshold at the membrane must also change, to allow the adapted elastomeric properties to transduce a stain and cause a firing response. Munch et al. show that a prolonged shift to MAP changes the threshold point that initiates a firing response [4].

In order to conclusively model the effect of age on the baroreceptor firing rate, more experimental data is required in order to adapt the baroreceptor model to reflect the elastomeric properties of the arterial wall as parameters that are functions of time. When the membrane threshold and the elastomeric

parameters are functions of time, the model can be exercised across a longer time span, to highlight how the baroreceptor sensitivity changes over a lifetime.

6 Discussion and Conclusion

I have outlined the contentious debate surrounding the ability of the baroreflex to act as a long-term controller, through the critical review of existing models and experiments in chapter 2. Although many researchers have modelled the baroreceptor in order to investigate the baroreflex, the purpose behind their investigations is not the same. Some researchers have argued that because the baroreceptor is capable of resetting, it cannot effect long-term control [13], [45]. While others argue that because the baroreceptor firing rate can influence other physiological systems through the baroreflex it must be acting as a controller [5], [32], [48]. The purpose of this investigation is not to make a conclusive study on the baroreflex, and how it might be capable of effecting different physiological systems to control blood pressure in the long-term, but rather to investigate the baroreceptor's sensor role in the control feedback system, and identify the full extent of its behaviour over time to different kinds of stimuli.

The static characteristics of the BR with respect to long-term control of BP, are described by the mathematical models which interpret BR behaviour. The models which characterise the baroreceptor sensor behaviour best are made up of three model components for strain at the arterial wall, dynamic strain in the arterial wall and firing response. In each of these components, different researchers' modelling techniques have been compared. The best performing models have a non-linear elastomeric strain model for the arterial wall, with two or more Voigt bodies to model the visco-elastic mechanics within the arterial wall, and a firing response based on either nerve fibre recruitment or on a leaky integrate-and-fire model.

I have implemented the mathematical models from Srinivasen et al., Bugenhagen et al., Beard et al., and Mahdi et al. in Simulink and validated them against reported experimental data [2], [22], [27], [48]. All the models, which have been compared, show that the firing response to a step input will decay primarily due to the visco-elastic mechanical properties in the arterial wall. This means that all baroreceptors, as modelled here for aortic and carotid sinus baroreceptors, will only be able to transmit signals based on short term changes to strain. This is because prolonged strain signals are reduced over time in the different visco-elastic layers between the surface of the arterial wall and the inner membrane surrounding the baroreceptor nerve ending, which is embedded in the arterial wall. It is important to note that these dynamics in the different layers of the arterial wall are inherently the dynamics of the baroreceptor itself, and not a separate property of the baroreceptors environment.

The experiments and models presented by many of the researchers analysed in chapter 3, suggest that the baroreceptor interprets a signal based on strain. Whether this strain is a function of pressure, volume, chronic changes to the compliance of the arterial wall, or due to a creep stress change in volume, the strain in the tissue of the arterial wall is a fundamental component of the baroreceptor

which cannot be ignored. Assumptions and conclusions made by many of the researchers presented, aim to deduce the role the baroreceptor plays in the baroreflex, and more importantly how that role changes under chronically elevated arterial pressure conditions.

Based on my study, it is clear that although there is much debate on the ability of the baroreceptor to influence blood pressure control, there is an agreement that the baroreceptor transduces strain at the arterial wall. In addition, although the purpose of experimental studies and modelling techniques may differ, the components of models for the baroreceptor are generally similar. Although this may seem trivial, none of the baroreceptor models presented here have components which model an inherent ability of the baroreceptor nerve to adapt the signal detected for a different response based on the rate of change of the signal. If we reflect on how well the models predict actual results for short term experiments, and if we extrapolate that those models will behave in the same way in the long-term, then the models show that the baroreceptor is not be capable of resetting its own threshold for a different response.

My comparative analysis in section 4, for different dominant models in the literature, show that the adaptation characteristics of the baroreceptor occur due to the decay of a dynamic strain across the visco-elastic layers of the arterial wall. All the baroreceptor models investigated show that the baroreceptor transduces a strain based on pressure, into a firing rate. It is clear then, that the adaptation of the baroreceptor firing rate does not occur at the brainstem, but rather as an inherent property of the layers between the arterial wall and the sensor nerve ending. The visco-elastic properties of the arterial wall will remove all low frequency components from the strain transduced at the nerve ending, meaning that any long term pressure changes will not be transduced to the BR nerve ending.

Guyton also argued that total peripheral resistance, as potentially modulated through the baroreflex, does not play a role in regulating arterial pressure [9]. This is further expressed by Guyton and Cowley's statements that the primary controller of chronic blood pressure levels is only through kidney function or through fluid balance [9], [13]. Other researchers have shown that the SNS can shift the renal function curve, and such a shift can be based on the baroreflex. This implies causality, on the basis that because the BR can affect the renal curve through the SNS, and the renal curve regulates BP, then the BR indirectly regulates BP. However Guyton and Cowley's arguments still hold, because the shift of the renal curve (as the primary regulator) only occurs under long-term changes to SNS, which may be affected by the baroreflex but which is also affected by other sensors and control mechanisms which contribute to blood pressure regulation.

This reiterates statements from other researchers, and from this analysis, that the baroreceptor acts as a sensor which contributes to a control mechanism to regulate blood pressure (BRX) in the short-term, but does not necessarily constitute the whole control feedback mechanism (SNS) in the long term.

The dynamic characteristics of the BR with respect to long-term control of BP are described by the frequency response tests on the BR models. The frequency response tests which I conducted on the baroreceptor models show a high sensitivity to inputs within the frequency range from 0.01 Hz to 1 Hz, and a very low sensitivity for frequencies below 0.001 Hz. This means that the baroreceptor is most sensitive to changes in pressure which occur within the period of 1 s to 1 min 36 s, and are not sensitive to changes in pressure with a period greater than 16 min 36. These frequency sensitivities suggest that the baroreceptor has approximately zero gain (change in sensitivity) at DC conditions (i.e. for frequencies which approximate steady state). Such a frequency response characteristic suggests that the baroreceptor cannot give the brainstem any information on changes that occur slower than 20 min. Even if all the baroreceptor afferent fibres had different thresholds and their signals are superimposed at the brainstem, they will all be influenced by the visco-elastic properties of an elastomeric arterial wall. Based on this, this research suggests that it is unlikely that the baroreflex is capable of acting as a long-term controller of blood pressure.

The implication suggested by authors, such as Guyton and Cowley, is that the limited response of the baroreceptor over longer time periods means that it can't play a direct role in long-term blood pressure control [9], [13]. This is plausible because my simulation tests used to extrapolate baroreceptor model behaviour for inputs of a wide range of frequencies show that these baroreceptor models do not have an infinite bandwidth for high sensitivity. The models used to show the frequency response were validated against their authors' reported results as well as to experimental data. Although these models were parameterised for a specific species of animal, at a specific region in the arterial vessel, and for a specific type of fibre, comparisons between the models show that the parameterisation doesn't significantly change the shape of the firing response or change the sensitivity of the frequency response. Furthermore, the Beard et al. model has been extensively tested on a range of experimental data from dog carotid sinuses, dog aortas and rabbits, and so its frequency response should translate to all these species.

Other researchers argue that the baroreflex can act as a long-term controller because baroreceptor afferents can be of different types; have different thresholds and sensitivities; and may reset at different rates to absolute and relative pressure changes. In addition the baroreceptor afferents for these different types may terminate in different regions of the brainstem, causing a wide range of subtle effects to other physiological systems.

All of these arguments are possible, but as outlined by Cowley, solving these questions with experimentation is very difficult [13]. The critical review of the baroreceptor characteristics in this study show that although this is possible, it is highly unlikely. An example of this is the significant

drop off in sensitivity of the baroreceptor for changes in pressure over longer durations, as shown for both the Beard et al. and Bugenhagen et al. models (which are parameterised for different vessel types and different thresholds) in section 4.2.3.

This study shows that the sensitivity approaches zero in the Beard et al. model, and has an unchanging low sensitivity in the Bugenhagen et al. model. The sensitivities shown for the frequency response in both models indicate that there is a significant drop in sensitivity for inputs which have periods longer than 2.78 hours (0.0001 Hz).

Based on these results, even if a small number of fibres which had a different threshold were able to send signals to the brainstem, and the termination of those fibres were in a location which allowed for some alternate response, the baroreflex would still not be primarily responsible for regulating pressure in the system.

Furthermore, all baroreceptor fibre types measure strain. An example of this is in Beard's model, where regardless of all the different fibre types available, they must all act on some change to the strain, which is based on physical mechanical properties for the elasticity of the vessel wall. These mechanical properties are based on the elastomeric material of the physical vessel wall, which are not infinitely elastic, and so the strain signal must eventually reset.

Another common argument which has linked much of the research on this topic, has been the experimental results which show that electrically stimulated baroreceptors don't reset, and will decrease SNS levels through the baroreflex to reduce a hypertensive arterial pressure [34]. These results have been used as evidence that even when the baroreceptor firing response is very low they do influence the SNS, and can be used as a long-term controller [5].

In response to this, it should be clarified that an electrically stimulated baroreceptor has actually had its sensor function bypassed, so that the electrical signal is directly transmitted through the baroreceptor afferent nerve fibre to the brainstem [15]. Here, the response to electrical stimulation of the baroreceptor gives us no information about the baroreceptor. It only shows that by bypassing the sensor the brainstem is sent false information about the state of the blood pressure, and that it adjusts its physiological response to counteract the change in the signal received.

The blood pressure in essential hypertensive patients who undergo this treatment is known to decrease to normal levels while they undergo electrical stimulation of their baroreceptors on one set of carotid sinus baroreceptors [34]. Their short-term baroreflex control for pressure changes around their new operating pressure continues as normal [34]. This makes sense because as long as the electrical signal is maintained on one set of BRs for one of the carotid sinuses, the brainstem will recognise the prolonged firing response as a new corresponding absolute pressure signal. While this takes place, the

baroreceptor signals from the carotid sinus on the other side and the aortic arch can continue to transduce short-term pressure changes around the operating pressure.

It is suspected that the pathology of essential hypertension and a non-responsive baroreflex are not due to any pathology of the baroreceptor per se, but rather a misinterpretation of strain signals from a less elastic baroreceptor environment. This is not in contradiction of the experimental studies that show arterial blood pressure returns to normal from a chronic hypertensive state when electrically stimulated, but rather that the electrical stimulation bypasses the sensor function of the baroreceptor for interpreting the strain through a less elastic arterial wall.

Lastly, one of the final arguments which suggest the baroreceptor may be able to control pressure in the long term is that different fibres may have different feedback mechanisms at the brainstem.

The baroreceptor system is non-linear, because the threshold differential pressure which initiates a firing response can change over time. The analysis in this study for the frequency response of the baroreceptor is based on models which have been linearised for a specific threshold. If the baroreceptor was able to update its own thresholds in the short term, then the firing rate wouldn't reset. Whether the threshold can reset in the long term is outside the scope of this investigation, and I can only suggest that if such behaviour were true then the models wouldn't tie so closely to such a wide range of experiments. In addition, Cowley also reported that although this could be possible, he found no evidence of such behaviour [13].

Further considerations for the role of the baroreceptor in long-term control of blood pressure have been suggested in this study, with regards to the effect that carotid sinus dilatation or age would affect the frequency response of the baroreceptor. Possible future work in this regard include an adaptation to existing geometry models for the carotid sinus to include a dilatation in the cylindrical surface area of the arterial wall, and to investigate the subsequent effect on the baroreceptor sensitivity to absolute and relative pressure changes. The other modelling enhancement is to evaluate the frequency response of a baroreceptor model which has parameters for visco-elastic properties as functions of time. This will allow for further extrapolation to the frequency response of the baroreceptor as the subject ages and the properties of the arterial wall compliance change.

Published mathematical models of baroreceptors have been reviewed in order to understand how different researchers interpret the relationship between the baroreceptor and long term blood pressure control. A subset of them have been investigated in MATLAB and Simulink, for their mechanism of resetting. The four simulated models are from Srinivasen et al.[26], Bugenhagen et al.[22], Beard et al.[48] and Mahdi et al [2]. The performance of these models have been evaluated using available data in the literature, and further compared to each other under the same input and experimental data (0-230 mmHg step input over 12 s).

Similarities between the different techniques for modelling the components of baroreceptor behaviour have been identified, which highlight the role of visco-elastic coupling in the arterial wall mechanics and how it leads to baroreceptor resetting. The baroreceptor models were also tested with the same inputs, to highlight the differences in their modelling techniques. By investigating two of the models that performed well under short-term experiments (the Beard et al.[48] and Bugenhagen et al[22] models), these baroreceptor models' responses to long-term inputs have been investigated with sinusoidal inputs which have periods that range from 0.1 s to 10 days and have a 100 mmHg operating point with a 1 mmHg peak amplit

Through the critical analysis of a range of baroreceptor models, in the short-term and the long-term, insights on the ability of the baroreceptor to affect long-term blood pressure regulation have been discussed. The mathematical modelling presented and validated by other researchers has been extended to simulate their frequency response. This is a new approach to critically analysing the mathematical models and interpreting the dynamic characteristics of the baroreceptor. Key findings show that baroreceptor resetting is a function of the strain detected at the arterial wall and the visco-elastic properties of the arterial wall. This suggests that baroreceptor sensitivity is closely tied to the elasticity of the arterial wall, and would thus not be able to inform the brainstem on long-term changes to MAP.

7 References

[1] M. J. Joyner and J. K. Limberg, “Blood pressure regulation: every adaptation is an integration?,” *Eur. J. Appl. Physiol.*, vol. 114, no. 3, pp. 445–450, 2014.

[2] A. Mahdi, J. Sturdy, J. T. Ottesen, and M. S. Olufsen, “Modeling the Afferent Dynamics of the Baroreflex Control System,” *PLoS Comput. Biol.*, vol. 9, no. 12, Dec. 2013.

[3] L. Sherwood, Fundamentals of Physiology: A Human Perspective, chapter 10, pp.304-307. Cengage Learning, 2005.

[4] P. A. Munch, M. C. Andresen, and A. M. Brown, “Rapid resetting of aortic baroreceptors in vitro,” *Am. J. Physiol.*, vol. 244, no. 5, pp. H672-680, May 1983.

[5] C. J. Barrett, “Problems, possibilities, and pitfalls in studying the arterial baroreflexes’ influence over long-term control of blood pressure,” *AJP Regul. Integr. Comp. Physiol.*, vol. 288, no. 4, pp. R837–R845, Dec. 2004.

[6] W. Landgren, “On the Excitation Mechanism of the Carotid Baroceptors,” *Acta Physiol. Scand.*, vol. 26, no. 1, pp. 1–34, Jan. 1952.

[7] W. B. Clarke, *Static and dynamic characteristics of carotid sinus baroreceptors*. University of Rochester, 1968.

[8] E. M. Krieger, “Time course of baroreceptor resetting in acute hypertension,” *Am. J. Physiol. -- Leg. Content*, vol. 218, no. 2, pp. 486–490, Feb. 1970.

[9] A C Guyton, T G Coleman, and and H. J. Granger, “Circulation: Overall Regulation,” *Annu. Rev. Physiol.*, vol. 34, no. 1, pp. 13–44, 1972.

[10] A. M. Brown, W. R. Saum, and S. Yasui, “Baroreceptor dynamics and their relationship to afferent fiber type and hypertension,” *Circ Res*, vol. 42, no. 5, pp. 694–702, 1978.

[11] H. M. Coleridge, J. C. Coleridge, M. P. Kaufman, and A. Dangel, “Operational sensitivity and acute resetting of aortic baroreceptors in dogs.,” *Circ. Res.*, vol. 48, no. 5, pp. 676–684, May 1981.

[12] H. M. Horsman, K. C. Peebles, D. C. Galletly, and Y.-C. Tzeng, “Cardiac baroreflex gain is frequency dependent: insights from repeated sit-to-stand maneuvers and the

modified Oxford method," *Appl. Physiol. Nutr. Metab.*, vol. 38, no. 7, pp. 753–759, Jul. 2013.

[13] A. W. Cowley, "Long-term control of arterial blood pressure," *Physiol. Rev.*, vol. 72, no. 1, pp. 231–300, Jan. 1992.

[14] D. A. Beard, K. H. Pettersen, B. E. Carlson, S. W. Omholt, and S. M. Bugenhagen, "A computational analysis of the long-term regulation of arterial pressure," *F1000Research*, Dec. 2013.

[15] K. H. Pettersen, S. M. Bugenhagen, J. Nauman, D. A. Beard, and S. W. Omholt, "Arterial Stiffening Provides Sufficient Explanation for Primary Hypertension," *PLoS Comput Biol*, vol. 10, no. 5, p. e1003634, May 2014.

[16] R. Klabunde, "CV Physiology: Neurohumoral Mechanisms." [Online]. Available: http://www.cvphysiology.com/Blood%20Pressure/BP007.htm. [Accessed: 03-Jul-2016].

[17] R. Freeman and M. W. Chapleau, "Chapter 7 - Testing the autonomic nervous system," in *Handbook of Clinical Neurology*, vol. 115, G. S. and C. Krarup, Ed. Elsevier, 2013, pp. 115–136.

[18] J. T. Ottesen and M. Danielsen, *Mathematical Modelling in Medicine*. Page 121-135: IOS Press, 2000.

[19] Y. Hirooka, "Importance of Neural Arc for Baroreflex Resetting in Hypertension," *Circ. J.*, vol. 79, no. 3, 2015.

[20] L. Sherwood, *Human Physiology: From Cells to Systems*. Cengage Learning, 2015.

[21] B. P. Lathi, *Linear Systems and Signals*, 2nd ed. Oxford, UK: Oxford University Press, 2009.

[22] S. M. Bugenhagen, A. W. Cowley, and D. A. Beard, "Identifying physiological origins of baroreflex dysfunction in salt-sensitive hypertension in the Dahl SS rat," *Physiol. Genomics*, vol. 42, no. 1, pp. 23–41, Jun. 2010.

[23] K. Heusser *et al.*, "Carotid baroreceptor stimulation, sympathetic activity, baroreflex function, and blood pressure in hypertensive patients," *Hypertension*, vol. 55, no. 3, pp. 619–626, Mar. 2010.

[24] A. L. King, “Pressure-Volume Relation for Cylindrical Tubes with Elastomeric Walls: The Human Aorta,” *J. Appl. Phys.*, vol. 17, no. 6, pp. 501–505, Jun. 1946.

[25] B. W. Knight, “Dynamics of Encoding in a Population of Neurons,” *J. Gen. Physiol.*, vol. 59, no. 6, pp. 734–766, Jun. 1972.

[26] R. Srinivasan and H. B. Nudelman, “Modeling the carotid sinus baroreceptor,” *Biophys. J.*, vol. 12, no. 9, pp. 1171–1182, Sep. 1972.

[27] R. Srinivasan and H. Nudelman, “Theoretical studies on the behavior of carotid sinus baroreceptors,” *Kybernetik*, vol. 13, no. 3, pp. 144–150, Sep. 1973.

[28] A. C. Guyton, “The surprising kidney-fluid mechanism for pressure control--its infinite gain!,” *Hypertension*, vol. 16, no. 6, pp. 725–730, Dec. 1990.

[29] J. E. Hall, A. C. Guyton, and M. W. Brands, “Pressure-volume regulation in hypertension.,” *Kidney Int.*, vol. 49, 1996.

[30] M. Ursino, “A mathematical model of the carotid baroregulation in pulsating conditions,” *IEEE Trans. Biomed. Eng.*, vol. 46, no. 4, pp. 382–392, Apr. 1999.

[31] G. A. Head, E. V. Lukoshkova, S. L. Burke, S. C. Malpas, E. A. Lambert, and B. J. A. Janssen, “Comparing spectral and invasive estimates of baroreflex gain,” *IEEE Eng. Med. Biol. Mag.*, vol. 20, no. 2, pp. 43–52, Mar. 2001.

[32] E. Petiot, C. Barrès, B. Chapuis, and C. Julien, “Frequency response of renal sympathetic nervous activity to aortic depressor nerve stimulation in the anaesthetized rat,” *J. Physiol.*, vol. 537, no. Pt 3, pp. 949–959, Dec. 2001.

[33] J. W. Osborn, F. Jacob, and P. Guzman, “A neural set point for the long-term control of arterial pressure: beyond the arterial baroreceptor reflex,” *Am. J. Physiol. - Regul. Integr. Comp. Physiol.*, vol. 288, no. 4, pp. R846–R855, Apr. 2005.

[34] T. E. Lohmeier and R. Iliescu, “The Baroreflex as a Long-Term Controller of Arterial Pressure,” *Physiology*, vol. 30, no. 2, pp. 148–158, Mar. 2015.

[35] A. Mahdi, N. Meshkat, and S. Sullivant, “Structural Identifiability of Viscoelastic Mechanical Systems,” *PLOS ONE*, vol. 9, no. 2, p. e86411, Feb. 2014.

[36] G. N. Franz, A. M. Scher, and C. S. Ito, “Small signal characteristics of carotid sinus baroreceptors of rabbits.,” *J. Appl. Physiol.*, vol. 30, no. 4, pp. 527–535, Apr. 1971.

[37] A. M. Brown, W. R. Saum, and F. H. Tuley, “A comparison of aortic baroreceptor discharge in normotensive and spontaneously hypertensive rats.,” *Circ. Res.*, vol. 39, no. 4, pp. 488–496, Oct. 1976.

[38] T. Sato *et al.*, “Dynamic transduction properties of in situ baroreceptors of rabbit aortic depressor nerve,” *Am. J. Physiol. - Heart Circ. Physiol.*, vol. 274, no. 1, pp. H358–H365, Jan. 1998.

[39] “Physiological Origins of Baroreceptor Firing Patterns: Mechanical and Electrophysiological Features. - NCSU Digital Repository.” [Online]. Available: http://repository.lib.ncsu.edu/ir/handle/1840.16/9918. [Accessed: 15-Apr-2016].

[40] S. A. Smith *et al.*, “Comparison of aortic and carotid baroreflex stimulus–response characteristics in humans,” *Auton. Neurosci.*, vol. 88, no. 1–2, pp. 74–85, Apr. 2001.

[41] V. A. Averina, H. G. Othmer, G. D. Fink, and J. W. Osborn, “A new conceptual paradigm for the haemodynamics of salt-sensitive hypertension: a mathematical modelling approach,” *J. Physiol.*, vol. 590, no. 23, pp. 5975–5992, Dec. 2012.

[42] M. C. Andresen, “Short- and long-term determinants of baroreceptor function in aged normotensive and spontaneously hypertensive rats.,” *Circ. Res.*, vol. 54, no. 6, pp. 750–759, Jun. 1984.

[43] M. W. Chapleau, J. Lu, G. Hajduczok, and F. M. Abboud, “Mechanism of baroreceptor adaptation in dogs: attenuation of adaptation by the K+ channel blocker 4-aminopyridine.,” *J. Physiol.*, vol. 462, pp. 291–306, Mar. 1993.

[44] H. M. Coleridge, J. C. Coleridge, E. R. Poore, A. M. Roberts, and H. D. Schultz, “Aortic wall properties and baroreceptor behaviour at normal arterial pressure and in acute hypertensive resetting in dogs.,” *J. Physiol.*, vol. 350, pp. 309–326, May 1984.

[45] A. C. Guyton, *Arterial Pressure and Hypertension*. Saunders W B Co, 1980.

[46] A. W. Quail, R. L. Woods, and P. I. Korner, “Cardiac and arterial baroreceptor influences in release of vasopressin and renin during hemorrhage,” *Am. J. Physiol. - Heart Circ. Physiol.*, vol. 252, no. 6, pp. H1120–H1126, Jun. 1987.

[47] D. Sheingold, *Data Conversion Handbook*, Third. Elsevier, 2004.

[48] D. A. Beard, J. B. Bassingthwaighte, and A. S. Greene, “Computational modeling of physiological systems,” *Physiol. Genomics*, vol. 23, no. 1, p. 1–3; discussion 4, Sep. 2005.

A. Appendix A

Table A.1: Historical Overview of Baroreceptor Research

Year	Authors	Title	Description	Species	Experiment/ Model	
1945	A.L King	Pressure-Volume Relation for Cylindrical Tubes with Elastomeric Walls: The Human Aorta	Theory for elastomeric walls of aortas used in Srinivasen's model	Human aortas	Pressure-strain relationships of elastomeric walls	[24]
1952	S. Landgren	On the Excitation Mechanism of the Carotid Baroreceptors	Experimentation for different sizes of baroreceptor fibres in order to analyse operating behaviour	Cat carotid sinuses	Single fibre in-vivo baroreceptor firing response (for different nerve fibre sizes). These are based on impulse, step, square and steady state sinusoidal inputs. Actual values of firing rates range from 250 impulses/sec (large fibre) to 50 impulses/sec (small fibre).	[6]

1968	W.B. Clarke	Static and Dynamic Characteristics of Carotid Sinus Baroreceptors	Modelling the behaviour of the baroreceptor through experimentation and comparison with other models	Dog carotid sinuses	Experimental responses of single fibre baroreceptors are determined with positive and negative step inputs, ramp inputs, triangular waveforms as well as recurrent triangular waveforms.	[7]
1970	E.M. Krieger	Time Course of baroreceptor resetting in acute hypertension	Experimenting with the resetting behaviour of the aortic baroreceptor based on pulsatile changes in pressure. Findings are consistent with Munch et al. [4]	Rat aortas	Multi-fibre Aortic pulsatile perfusion and constriction for in-vivo study of the resetting behaviour of the baroreceptor during hypertension.	[8]
1972	B.W. Knight	Dynamics of Encoding in a Population of Neurons.	Theory for neuron encoding firing patterns based on the input stimulus	Horse-shoe crab limulus eccentric cell (visual neurons)	Comparisons between a deterministic impulse encoding model, a ‘forgetful integrate-and-fire’ model and a probabilistic encoder model	[25]
1972	A.C. Guyton	Circulation: Overall Regulation	An overview of an extensive circulatory regulation system model which aims to use systems analysis to define the principles which govern circulatory	Many		[9]

			physiology. Also an overview of existing studies which experiment with circulatory regulation.			
1972	R. Srinivasan and H.B. Nudelman	Modelling the Carotid Sinus	Overview of modelling components for intra-sinus pressure to carotid sinus baroreceptor firing response	Cat and Dog carotid sinuses	Mathematical modelling of the baroreceptor based on fitting one set of parameters for the model to Landgren's data [6] and Clarke's data [7].	[26]
1973	R.Srinivasan and H.B. Nudelman	Theoretical Studies on the Behaviour of Carotid Sinus Baroreceptors	Extended description of the modelling components for intra-sinus pressure to carotid sinus baroreceptor firing response	Dog carotid sinuses	Mathematical modelling of the baroreceptor based on fitting a set of parameters for the model to the authors' data and to Clarke's data [7].	[27]
1978	A.M. Brown, W.R. Saum, S. Yasui	Baroreceptor Dynamics and Their Relationship to Afferent Fiber Type and Hypertension	Frequency response experimentation for baroreceptors for myelinated/un-myelinated types and for normotensive/hypertensive rats. Hysteresis and short-term resetting discussed as due to visco-elastic wall characteristics.	Rat aortic-arch nerve	In-vitro, pressure steps and pulsatile pressure. Flat frequency response found within the frequency range of 0.1 – 20 Hz	[10]

1980	H.M. Coleridge, J.C. Coleridge, M.P. Kaufman and A. Dangel	Operational Sensitivity and Acute Resetting of Aortic Baroreceptors in Dogs	Hysteresis in the firing rate of the baroreceptors show that it increases as pressure increases and decreases when pressure decreases (but not at the same rate).	Dog aortic nerve, single fibres	In-vivo experimentation with extreme levels of MAP, both below and above normal.	[11]
1983	P.A Munch, M.C. Andresen and A.M. Brown	Rapid Resetting of Aortic Baroreceptors In Vitro	Analysis and comparison of the resetting time and curve shift of the baroreceptor under different MAP	Rat aortic-arch nerve, single fibres	In-vitro experimentation with ramp increases in pressure at different resting MAP levels.	[4]
1990	A.C. Guyton	The Surprising Kidney-Fluid Mechanism for Pressure Control – Its Infinite Gain!	Discussion surrounding the findings from simulations with the Overall Circulation model, which surmises that kidney-fluid control of blood pressure has infinite gain.		Model simulations show that increased total peripheral resistance does cause hypertension, but blood pressure regulates back to normal after a few days.	[28]
1992	A.W Cowley Jr	Long-Term Control of Arterial Blood Pressure	A comprehensive summary of a number of experiments and conclusions surrounding the	Dogs, Rabbits, Rats, Humans	Wide range of experiments are discussed.	[13]

			controversy around long term control of blood pressure.			
1996	J.E. Hall, A.C. Guyton, M.W. Brands	Pressure-Volume Regulation in Hypertension	A review of experiments carried out to understand the role of pressure natriuresis in essential hypertension. Their aim is to discuss whether pressure-natriuresis is secondary to hypertension or a primary cause of hypertension.	Dog, rat and human kidneys	Wide range of experiments aimed to test the pressure-natriuresis curve under chronic hypertension, under hormones angiotensin, vasopressin, and norepinephrine.	[29]
1999	M. Ursino	A Mathematical Model of the Carotid Baroregulation in pulsating conditions	The pressure-nerve activity for the carotid sinus is described as having a sigmoidal shape in non-pulsatile conditions, and a less sensitive ”quasilinear” shape in pulsatile conditions	Dog carotid sinus nerve (Vagotomised subjects)	Mathematical model of nerve activity of the carotid sinus nerve after pressure changes (both pulsatile and non-pulatile) is corroborated by the experimental data from Chapleau and Abboud.	[30]
2001	G.A. Head, E.V. Lukoshkova, S.L. Burke, S.C. Malpas,	Comparing Spectral and Invasive Estimates of Baroreflex Gain	Different baroreflex gain estimation techniques are tested on rabbits under different experimental conditions. The baroreflex gain is defined as the	Rabbits	In-vivo experimentation on normal and SAD subjects, for normotensive and hypertensive subjects, under phenylephrine and nitroprusside, under balloon constriction, and under infusion of	[31]

	E.A. Lambert and B.J. Janssen		sensitivity based on a BP input and a HR output. In this way this paper discusses the short-comings and strengths of estimating the baroreflex gain in different ways. Results show that spectral or traditional estimation methods are best depending on the situation.		angiotensin. Comparison of spectral and invasive methods of estimating baroreflex gain.	
2001	E. Petiot, C. Barres, B. Chapuis and C. Julien	Frequency Response of Renal Sympathetic Nervous Activity to Aortic Depressor Nerve Stimulation in the Anaesthetized Rat	The frequency response of the baroreceptor gain shows high-pass characteristics with increasing gain for frequencies between 0.03 Hz – 1 Hz, Thereafter the gain is shown to decrease (but stay above the static gain) for frequencies below 12Hz.	Rat aortic depressor nerve, multi-fibre	In-vivo experimentation with sinusoidal stimulation of the aortic depressor nerve in a frequency range from 0.03 Hz to 20 Hz.	[32]
2004	C.J. Barret, S.C. Malpas	Problems, possibilities, and pitfalls in studying the arterial baroreflexes' influence over long-term control of blood pressure.	A review of studies done on the baroreceptor characteristics in the past.			[5]

2005	J.W. Osborn, F. Jacob, and P. Guzan	A neural set point for the long-term control of arterial pressure: beyond the arterial baroreceptor reflex	An invited review of studies and hypotheses surrounding the contention around long-term control of blood pressure. Examples of experiments are used to show that the baroreflex can affect systems and cause hypertension, but that the set-point for arterial pressure regulation is maintained in the CNS and is independent of "arterial baroreceptor reflex" [33].	Overview of experiments on rats, rabbits, dogs and baboons.	Experimental results for the level of SNA in SAD animals show that rat levels return to normal (for both indirect and direct assessment) but that in baboons the SNA levels remain elevated (even after 3 weeks of monitoring).	[33]
2010	S.M. Bugenhagen, A.W. Cowley Jr, D.A. Beard	Identifying physiological origins of baroreflex dysfunction in salt-sensitive hypertension in the Dahl SS rat.	A mathematical model of the baroreflex is described, and used to investigate baroreflex dysfunction based on experimental results with salt-sensitive hypertension in the Dahl rat.	Salt-sensitive and non salt-sensitive rats, aortic arch		[22]
2013	D.A. Beard, K.H. Pettersen, B.E.	A Computational Analysis of the Long-	A mathematical model is presented in order to describe the regulation of blood pressure. The	Dog aortic baroreceptors and	Model tested on data from experiments with dog in-vivo pulsatile aortic ramp pressure inputs, dog in-vivo non-pulsatile	[14]

	Carlson, S.W. Omholt, S.M. Bugenhagen	term Regulation of Arterial Pressure	model is presented as a description of physiological responses, along with the data used to test the model behaviour. The developed and tested model shows that long-term control of arterial blood pressure is possible through both the baroreflex arc and the angiotensin system.	rabbit cardiac and arterial barorecept ors.	carotid sinus step pressure inputs, as well as with hemorrhage on rabbits.	
2013	A. Mahdi, J. Sturdy, J. Ottesen, M. Olufsen	Modelling the Afferent Dynamics of the Baroreflex Control System	Systematic evaluation of different combinations of models, which describe the baroreceptor, and their ability to successfully exhibit the behavioural properties for rectification; threshold; saturation; overshoot; post-excitatory depression (PED); adaptation as well as asymmetry.	Tested on experimen tal data for rat aortic barorecept ors	Model tested on experimental data from sinusoidal and step input stimuli as well as artificial stimuli of different types (sinusoidal, step, square, ramp and triangle). Model parameters are optimised for closest fit to the experimental data (quantitative analysis) and then investigated for behavioural properties of the output firing rate under artificial stimuli (qualitative analysis).	[2]
2014	H.M. Horsman, K.C. Peebles, D.C.	Cardiac baroreflex gain is frequency dependent: insights	Experiments on heart rate changes to blood pressure, considering how the rate of change on blood	Human sit-stand manoeuvr	Experiments where subjects perform the sit-stand manoeuvre at different frequencies (0.03 Hz, 0.05 Hz, 0.07 Hz and 0.1 Hz)	[12]

	Galletly, Y.C. Tzeng	from repeated sit-to-stand manoeuvres and the modified Oxford method	pressure affects the estimated gain of the baroreflex. Gain estimation of the baroreflex is based on the reflex alteration in heart rate based on changing input blood pressure.	es and the modified Oxford method	show that the gain changes at different frequencies of oscillation for the input blood pressure, which validates the non-linearity of the baroreflex. In addition, gain estimates from the oxford method do not align with the sit-stand manoeuvre results, which challenges convention that baroreceptor sensitivity is constant across different experimental techniques.	
2014	K.H. Pettersen, S.M. Bugenhagen, J. Nauman, D.A. Beard, S.W. Omholt	Arterial Stiffening Provides Sufficient Explanation for Primary Hypertension.	A new model based on a combination of models from King, Bugenhagen and Smith, is used to highlight how the baroreceptor may be able cause age-related hypertension due to less compliant vessels, and subsequently affect the pressure-natriuresis regulation of blood pressure.	Tested on experimental data for rats.	Model parameterised using age-related data for arterial distensibility, investigated under Valsalva conditions, and tested against experimental data from normotensive and spontaneously hypertensive rats.	[15]

B. Appendix B

List of Equations

Srinivasen et al. Model Equations

$$\mathcal{L}(z) = \coth z - \frac{1}{z} \tag{3.1}$$

$$\dot{\varepsilon} = \frac{P}{C} - \frac{A}{C\sqrt{(\varepsilon+1)}}\left[\frac{\mathcal{L}^{-1}\{\beta(\varepsilon-1)\}}{\mathcal{L}^{-1}(\beta)} - \frac{1}{\varepsilon+1}\right] \tag{3.2}$$

$$\dot{\varepsilon}_d = \frac{\sigma}{C_D}\left|\dot{P}\right| - \frac{1}{C_D}(\varepsilon_d)^2 \tag{3.3}$$

$$\delta = \varepsilon + \varepsilon_d \tag{3.4}$$

$$x = \begin{cases} 0 \; if \; \delta < \delta_{th} \\ \delta \; if \; \delta \geq \delta_{th} \end{cases} \tag{3.5}$$

$$if \; y > \; y_{th}, \tag{3.6}$$

$$then \int_{t_i}^{t_{i+1}} y(t)dt = A_r$$

$$\tau\dot{y} + y = g(x, \dot{x}) \tag{3.7}$$

$$g(x, \dot{x}) = x + h(x)\dot{x} \tag{3.8}$$

$$h(x) = \; w_1 + w_2 x \tag{3.9}$$

Bugenhagen et al. Model Equations

$$A = \; \pi(R_0 + \; C_{wall}P)^2 \tag{3.10}$$

$$\dot{A} = \left(\frac{-\sqrt{\frac{A}{\pi}} + R_0}{B_{wall}C_{wall}}\right) + \frac{P}{B_{wall}} \tag{3.11}$$

$$\varepsilon_{wall} = \frac{\sqrt{\frac{A}{\pi}} - \; R_0}{R_0} \tag{3.12}$$

$$\dot{\varepsilon_1} = \left(\frac{K_{ne}}{B_1}\right)\varepsilon_{wall} - \left(\frac{K_{ne}+K_1}{B_1}\right)\varepsilon_1 + \frac{K_1}{B_1}\varepsilon_2 + \dot{\varepsilon_2} \tag{3.13}$$

$$\dot{\varepsilon_2} = \left(\frac{K_1}{B_1+B_2}\right)\varepsilon_1 - \left(\frac{K_1+K_2}{B_1+B_2}\right)\varepsilon_2 + \left(\frac{K_2}{B_1+B_2}\right)\varepsilon_3 + \left(\frac{B_1}{B_1+B_2}\right)\dot{\varepsilon_1} + \left(\frac{B_2}{B_1+B_2}\right)\dot{\varepsilon_3} \tag{3.14}$$

$$\dot{\varepsilon_3} = \left(\frac{K_2}{B_2+B_3}\right)\varepsilon_2 - \left(\frac{K_2+K_3}{B_2+B_3}\right)\varepsilon_3 + \left(\frac{B_2}{B_2+B_3}\right)\dot{\varepsilon_2} \tag{3.15}$$

$$\delta = \varepsilon_{wall} - \varepsilon_1 \tag{3.16}$$

$$n = \begin{cases} 0\,, if\ \delta < \delta_{th} \\ S(\delta - \zeta\delta_{th})\,, if\ \delta \geq\ \delta_{th} \end{cases} \tag{3.17}$$

Beard et al. Model Equations

$$\dot{V}_{Ao} = C_{Ao}\dot{P}_{Ao} + \dot{V}_{sAo} \tag{3.18}$$

$$\dot{V}_{sAo} = \frac{1}{\tau_{CAo}}(V_{sAo}{}^{\infty} - V_{sAo}) \tag{3.19}$$

$$\dot{V}_{sAo} = \frac{1}{\tau_{CAo}}(\gamma_{Ao}V_{Ao} - V_{sAo}) \tag{3.20}$$

$$\dot{\varepsilon} = \frac{1}{2}\left(\frac{1}{\sqrt{V_{Ao}V_0}}\right) \tag{3.21}$$

$$\dot{\bar{\varepsilon}} = \frac{1}{\tau_s}(\varepsilon - \bar{\varepsilon}) \tag{3.22}$$

$$\delta_\varepsilon = \tau_s\dot{\bar{\varepsilon}} \tag{3.23}$$

$$\dot{s} = a(1-s) - bs\left(\frac{\delta_\varepsilon}{\delta_\varepsilon + \delta_0}\right) \tag{3.24}$$

$$f_{BR} = f_0 s\left(\frac{\delta_\varepsilon}{\delta_\varepsilon + \delta_0}\right) \tag{3.25}$$

Mahdi et al. Model Equations

$$A = (A_m - A_0)\frac{p^k}{\alpha^k + p^k} + A_0 \tag{3.26}$$

$$\varepsilon_w = 1 - \sqrt{\frac{A_0(\alpha^k + p^k)}{A_0\alpha^k + A_m p^k}} \tag{3.27}$$

$$\dot{\varepsilon_1} = -(\alpha_1 + \alpha_2 + \beta_1)\varepsilon_1 + (\beta_1 - \beta_2)\varepsilon_2 + (\alpha_1 + \alpha_2)\varepsilon_w \quad (3.28)$$

$$\dot{\varepsilon_2} = -\alpha_2\varepsilon_1 - \beta_2\varepsilon_2 + \alpha_2\varepsilon_w \quad (3.29)$$

$$\varepsilon_{ne} = \varepsilon_w - \varepsilon_1 \quad (3.30)$$

$$f_{N_a} = s_1\varepsilon_{ne} - s_2 \quad (3.31)$$

$$I_{ne} = \bar{s_1}\varepsilon_{ne} + \bar{s_2} \quad (3.32)$$

$$\dot{V_m} = \frac{1}{C_m}(I_{ne} - g_{leak}V_m) \quad (3.33)$$

$$f_{N_{IF}} = \begin{cases} \left[\frac{C_m}{g_{leak}}\left[ln\left(\frac{I_{ne} - g_{leak}V_{th}}{I_{ne}}\right)\right] + t_{ref}\right]^{-1} & if\ I_{ne} > g_{leak}V_{th} \\ 0 & otherwise \end{cases} \quad (3.34)$$

C. Appendix C

1. Srinivasen et al Model of the Baroreceptor

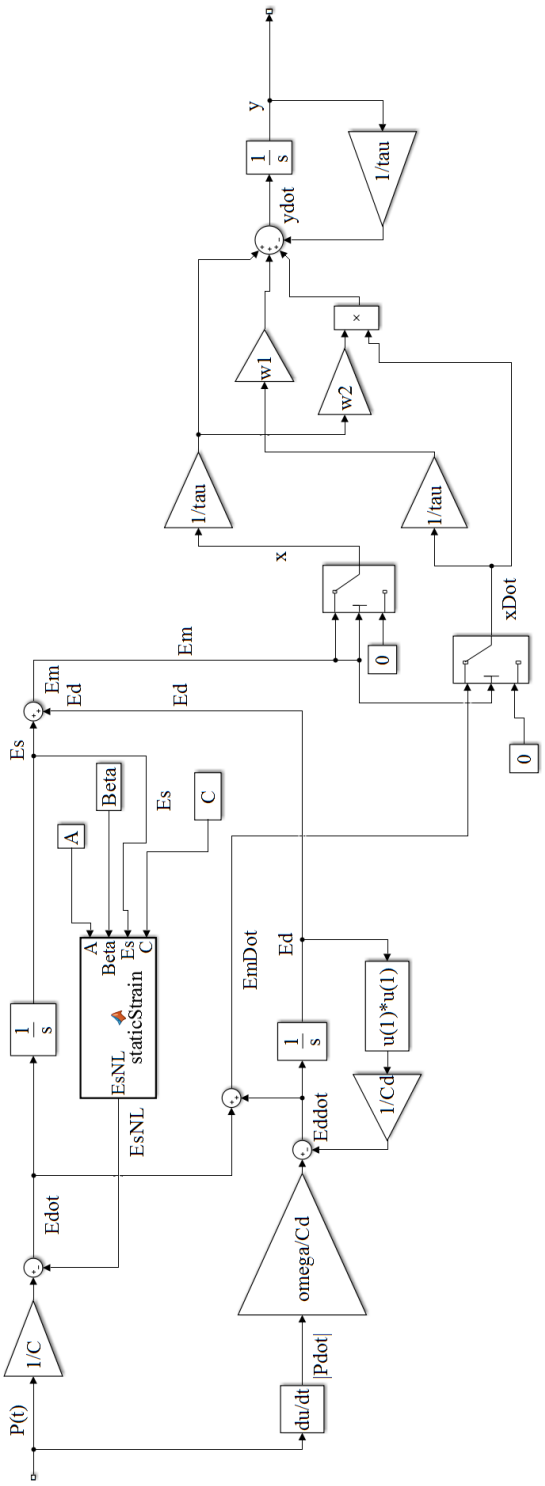

Figure C.7.1: Simulink block diagram representing Srinivasen et al Baroreceptor Model.

2. Bugenhagen et al Model of the Baroreceptor

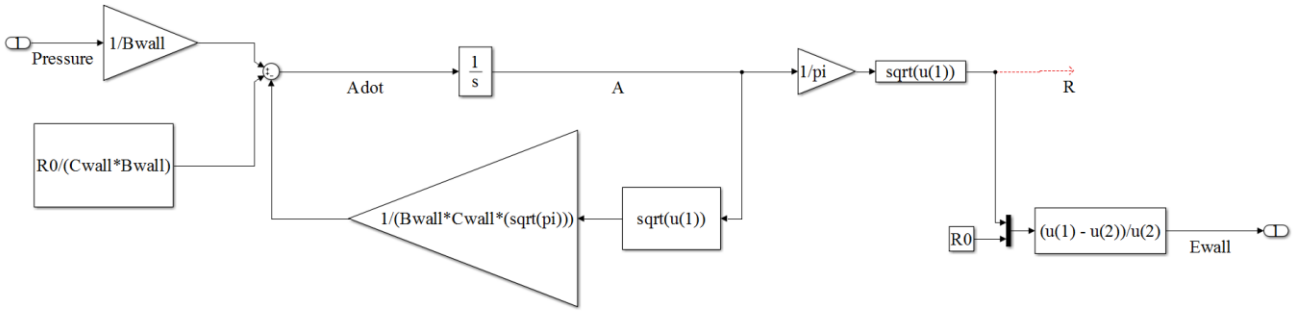

Figure C.7.2: Simulink block diagram representing Bugenhagen et al arterial wall strain model.

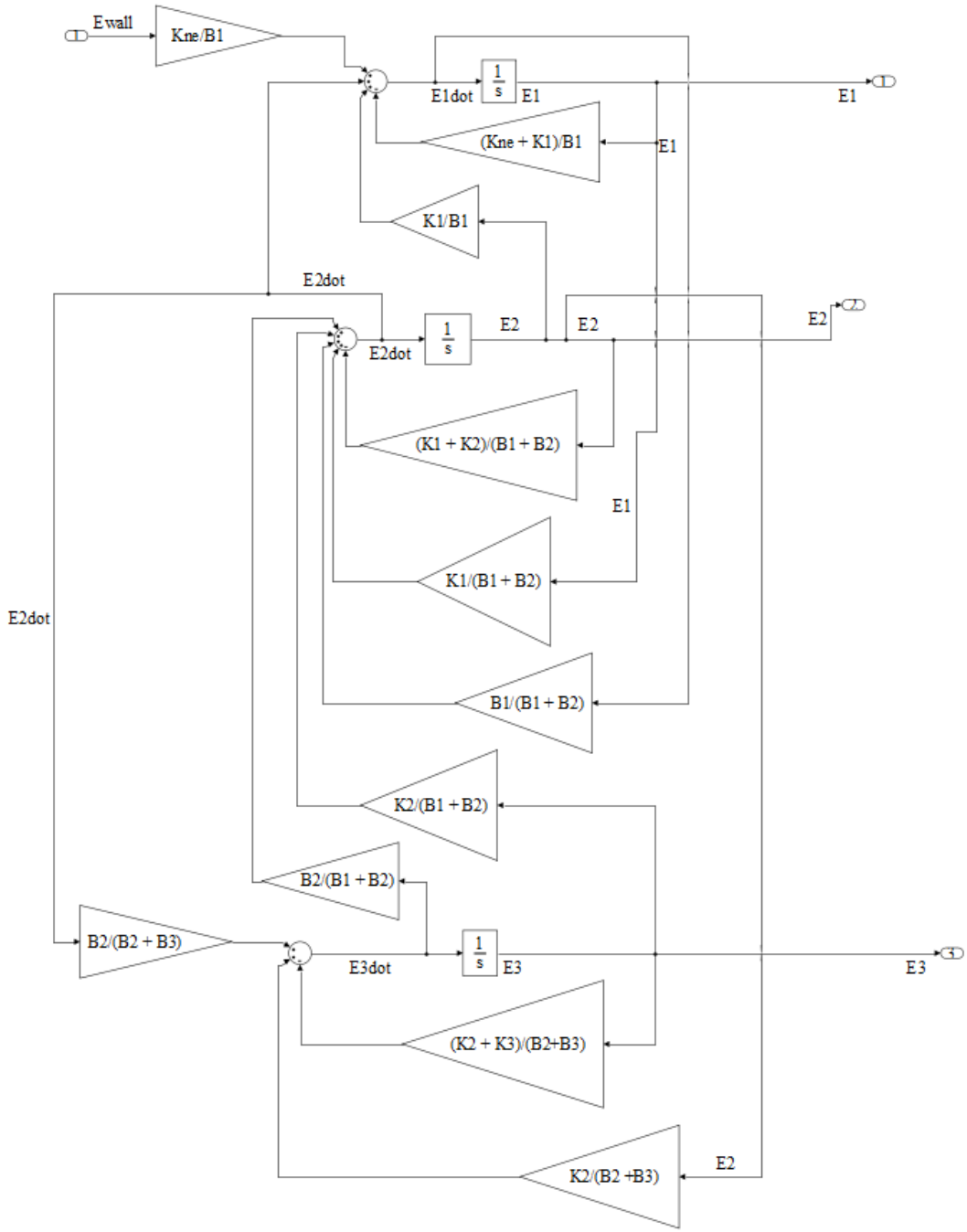

Figure C.7.3: Simulink block diagram representing Bugenhagen et al dynamic strain model.

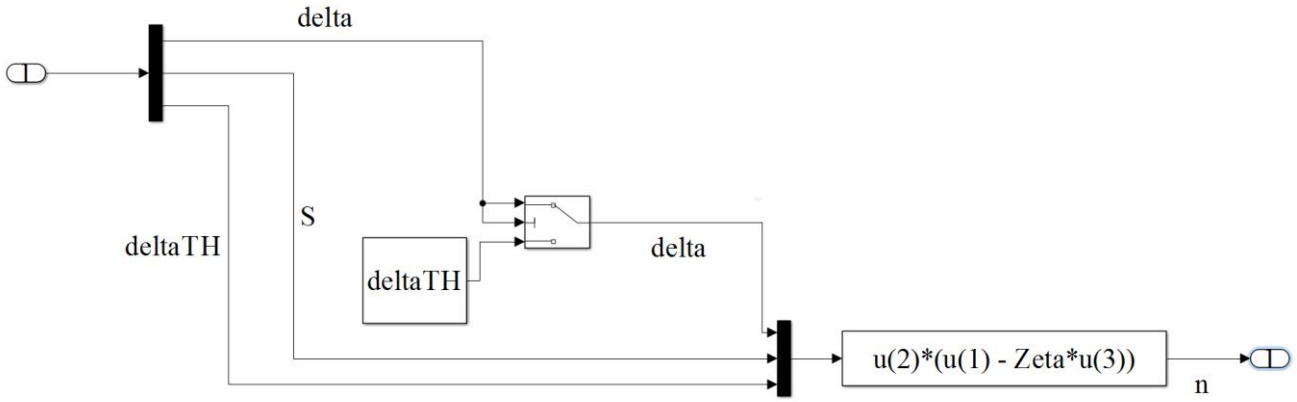

Figure C.7.4: Simulink block diagram representing Bugenhagen et al simplified integrate-and-fire model.

3. Beard et al Model of the Baroreceptor

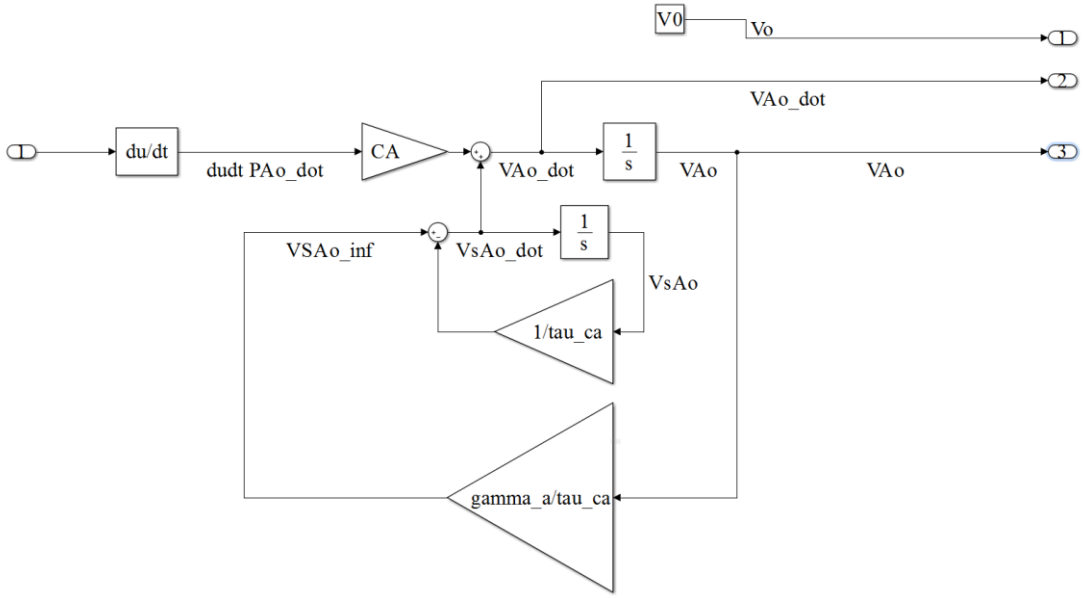

Figure C.7.5: Simulink block diagram representing Vessel Mechanics Subsystem for the Beard et al Baroreceptor Model.

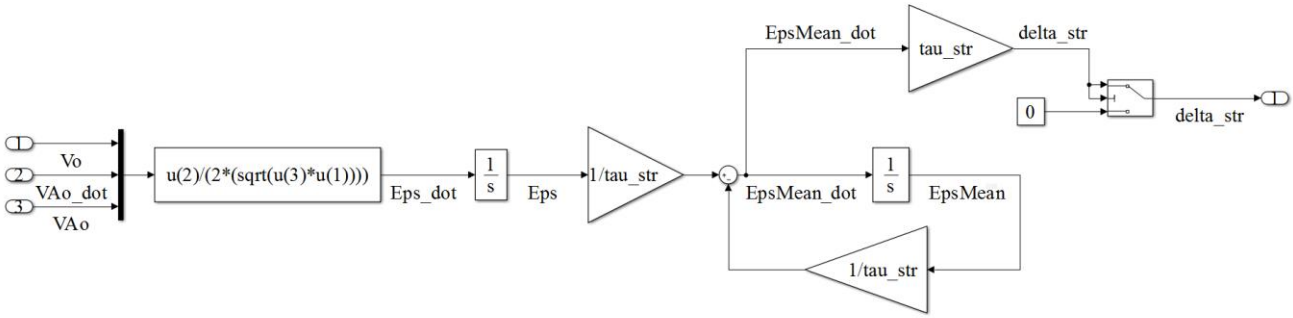

Figure C.7.6: Simulink block diagram representing Strain Dynamics Subsystem for the Beard et al Baroreceptor Model.

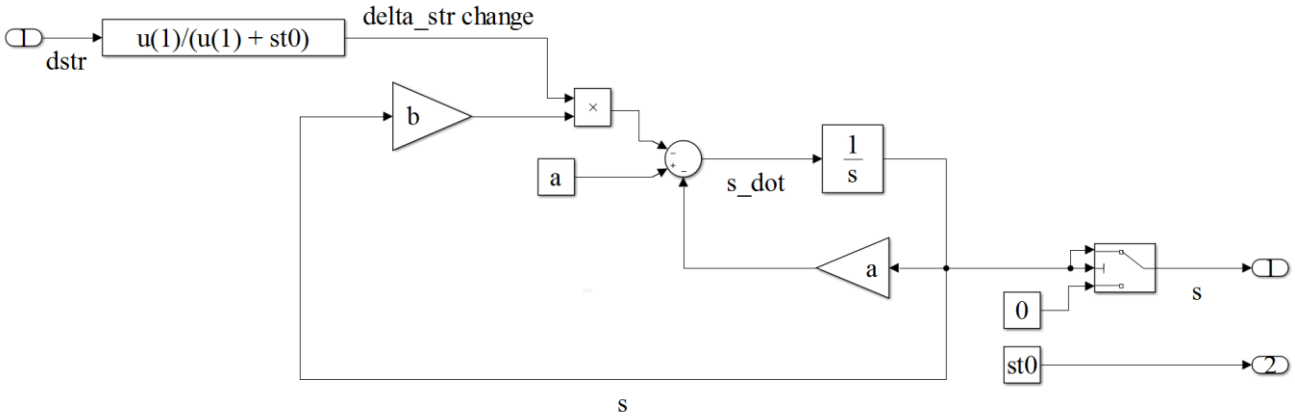

Figure C.7.7: Simulink block diagram representing Afferent Nerve Fibre Recruitment Subsystem for the Beard et al Baroreceptor Model.

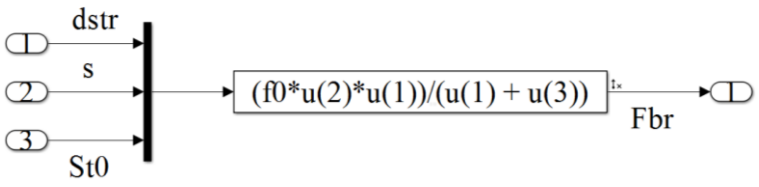

Figure C.7.8: Simulink block diagram representing Firing Response Subsystem for the Beard et al Baroreceptor Model.

4. Mahdi et al Model of the Baroreceptor

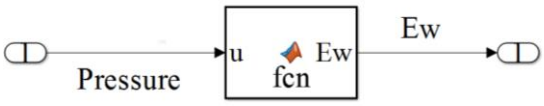

Figure C.7.9: Simulink Block Diagram representing Arterial Wall Subsystem for the Mahdi et al. Baroreceptor Model.

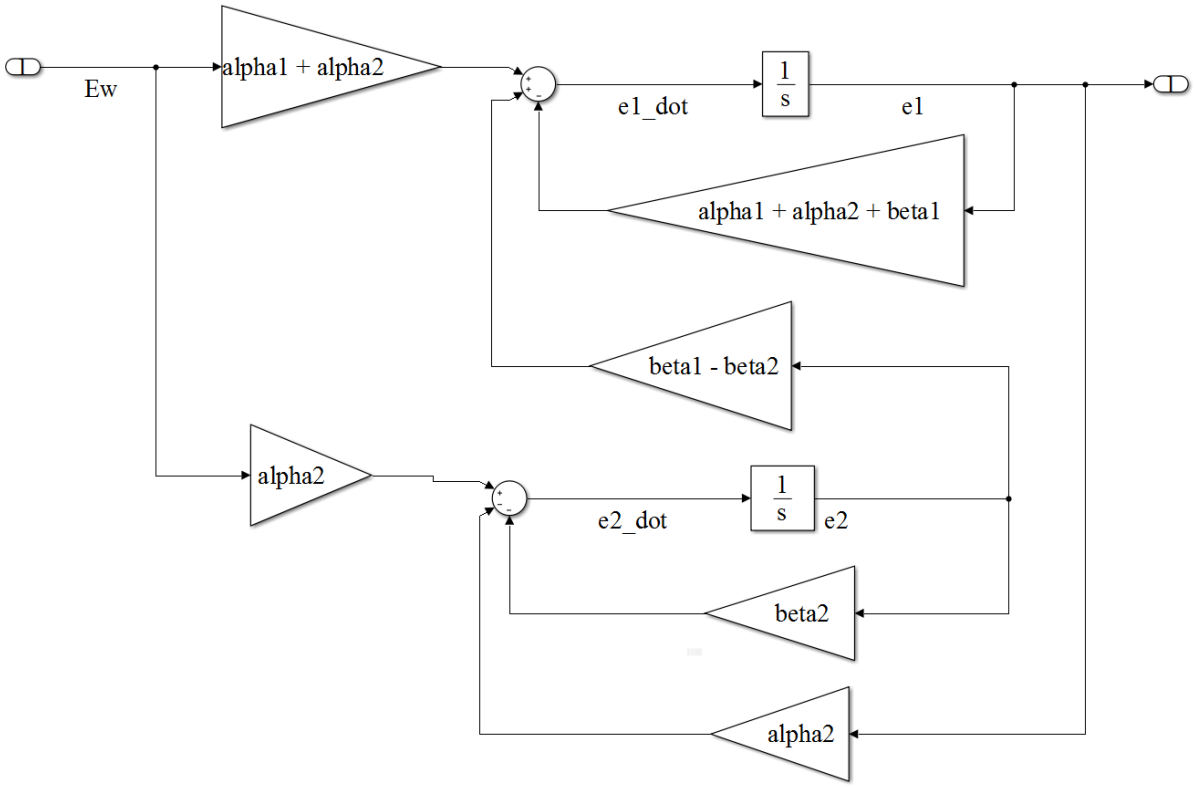

Figure C.7.10: Simulink Block Diagram representing Strain Dynamics Subsystem for the Mahdi et al. Baroreceptor Model.

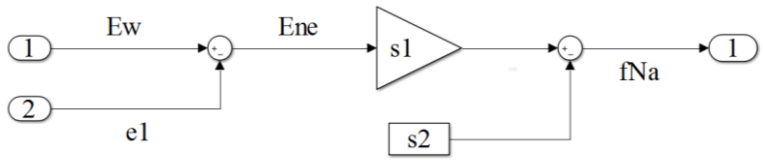

Figure C.7.11: Simulink Block Diagram representing Simplified Amplifier Response Subsystem for the Mahdi et al. Baroreceptor Model.

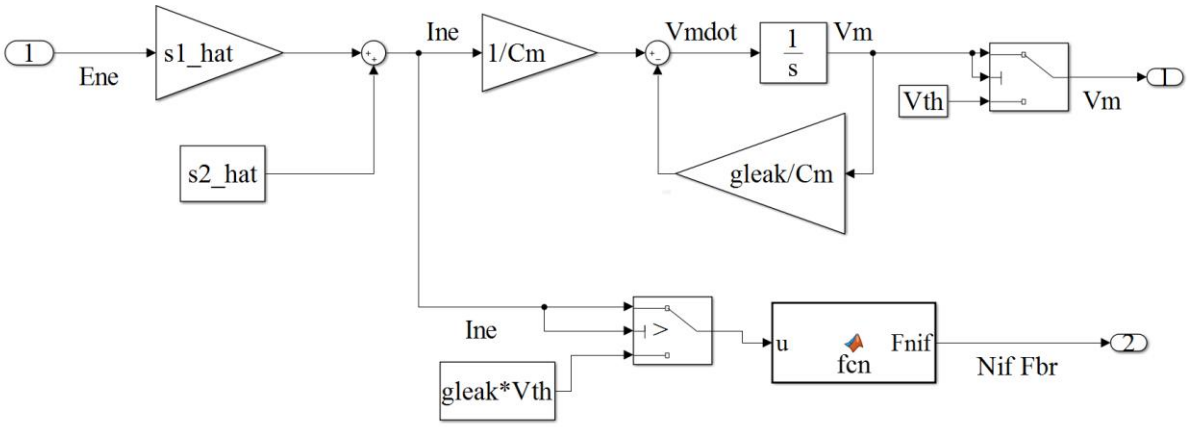

Figure C.7.12: Simulink Block Diagram representing Leaky Integrate-and-Fire Response Subsystem for the Mahdi et al. Baroreceptor Model.